Polymer Scaffold Approaches to Enhance Monitoring and Treatment of Type 1 Diabetes

by

Jessica Lynn King

A dissertation submitted in partial fulfillment
of the requirements for the degree of
Doctor of Philosophy
(Biomedical Engineering)
in the University of Michigan
2025

Doctoral Committee:

Professor Lonnie D. Shea, Chair
Associate Professor Sriram Chandrasekaran
Associate Professor Scott Soleimanpour
Professor Jason Spence

Jessica L. King

kingjl@umich.edu

ORCID iD: 0000-0002-2642-5977

© Jessica L. King 2025

Dedication

This dissertation is dedicated to Virginia A. King, Ed.D., who inspired my love for education.

.

Acknowledgements

I want to thank all of my family, friends, mentors, and lab mates who supported me through my Ph.D. and made the completion of this work possible. I am grateful to everyone who helped me along this path, whether that be answering protocol questions or listening to me lament my fate of having a desk in hearing distance of a ping pong table.

To my family, thank you for supporting me through all stages of my academic journey. My Michigan friends, Theo, Lauren, Monica, Ian, Rebecca, Elena, and Laila, thank you for bringing levity and moments of fun to the long and arduous process of grad school. To everyone in the Shea lab, thank you for the collaboration and camaraderie. You made the lab a fun place to work, and I always valued the insight and feedback I got from the group. Kelly and Liz, my projects would not be where they are today without you. Your support with all things cell culture truly made this work possible, and you inspire me with your dedication and willingness to help others.

I would also like to thank Lonnie for your mentorship and support. You have given me the opportunity to pursue research that interests me, while providing the support and direction I have needed to meet my project goals. To my committee, Sriram Chandrasekaran, Scott Soleimanpour, and Jason Spence, thank you for your feedback and support. Your insights throughout my training, from crafting my research projects in the qualifying exam, to preparing my final dissertation, have been invaluable in the completion of this work.

To Kevin and Benothy, thank you for all your love and support. Your confidence in me bolstered me in my most stressful times, and there is no one I would rather celebrate with as I meet this milestone.

Table of Contents

Dedication ii

Acknowledgements iii

List of Tables xi

List of Figures xii

Abstract xx

Chapter 1 Introduction 1

Chapter 2 Integration of Islet/Beta-Cell Transplants with Host Tissue Using Biomaterial Platforms 3

2.1 Authors 3

2.2 Abstract 3

2.3 Introduction 4

2.4 Manufacturing Platforms for Cell Transplantation 7

2.5 Transplantation 10

2.5.1 Enhancing survival 11

2.5.2 Enhancing integration 13

2.5.3 Enhancing function 16

2.6 Immune Protection 17

2.6.1 Local immune modulation 17

2.6.2 Antigen-specific immune modulation 22

2.7 Final Thoughts 25

2.8 Abbreviations 26

2.9 Acknowledgments 26

2.10 Additional Information 26

2.11 Data Availability 26

2.12 References 26

Chapter 3 Polymer Scaffolds Delineate Healthy from Diseased States at Sites Distal from the Pancreas in Two Models of Type 1 Diabetes 44

3.1 Authors 44

3.2 Abstract 44

3.3 Introduction 45

3.4 Results 47

3.4.1 Immune cell trafficking to the IN exhibits similar dynamics to the pancreas 47

3.4.2 IN implantation and surveillance does not perturb diabetes incidence in two models of disease 48

3.4.3 IN analysis separates diseased from healthy groups in NOD.scid/Adoptive transfer model of T1D 50

3.4.4 IN analysis successfully separates pre-symptomatic from symptomatic groups in the NOD model 51

3.4.5 Gene set enrichment analysis identified common pathways impacted by diabetes onset 53

3.5 Discussion 55

3.6 Methods 60

3.6.1 Scaffold fabrication 60

3.6.2 Glucose monitoring 60

3.6.3 Scaffold implantation 60

3.6.4 Adoptive transfer model 61

3.6.5 Scaffold explantation 62

3.6.6 RNA sequencing 62

3.6.7 cDNA synthesis and OpenArray 63

3.6.8 Computational analysis 63

3.6.9 Flow cytometry 64

3.7 Author contributions 65

3.8 Acknowledgements 65

3.9 Supplemental Information 66

3.10 References 67

Chapter 4 Polymer Scaffolds Enable Longitudinal Monitoring of Disease Progression in the NOD Model of Type 1 Diabetes 77

4.1 Authors 77

4.2 Abstract 77

4.3 Introduction 78

4.4 Results 79

4.4.1 IN enables longitudinal monitoring by repeatable biopsies 79

4.4.2 IN analysis separates all NOD mice from NOR controls regardless of disease progression 81

4.4.3 NOD progressors and non-progressors are separable as early as 6 weeks of age 82

4.4.4 IN analysis identifies pre-symptomatic disease 7 weeks before symptom onset 85

4.4.5 Progression signature genes correspond to cell types found in the pancreas 88

4.5 Discussion 89

4.6 Methods 94

4.6.1 IN fabrication 94

4.6.2 Glucose monitoring 94

4.6.3 IN implantation 94

4.6.4 IN explantation 95

4.6.5 RNA sequencing 95

4.6.6 Computational analysis 96

4.7 Acknowledgements 96

4.8 References 97

Chapter 5 Metabolic Network Reconstruction of SC-Islets Enables Simulation of Metabolic Treatments *In Silico* 103

5.1 Authors 103

5.2 Abstract 103

5.3 Introduction 104

5.4 Results 105

5.4.1 Transcriptomic data identifies metabolic flux differences between mature and sc-islets when implemented in a metabolic reconstruction 105

5.4.2 Model sensitivity to differentiation efficiency is dependent on objective function selection 106

5.4.3 PPAR agonist treatment simulation recapitulates sc-islet improvements found via in vitro testing 108

5.4.4 Knock-in simulation of downregulated genes identifies target for improving stage 6 cells 110

5.4.5 In vitro testing of elements of the NMNAT3 pathway suggest this target may improve metabolism 111

5.5 Discussion 113

5.6 Methods 117

5.6.1 hPSC culture 117

5.6.2 RNA sequencing 117

5.6.3 Metabolic reconstruction 117

5.7 Acknowledgements 118

5.8 Supplemental information 118

5.9 References 119

Chapter 6 Engineering a Translatable, Retrievable Islet Transplant Site with Microporous Scaffolds to Treat Type 1 Diabetes 124

6.1 Authors 124

6.2 Abstract 124

6.3 Introduction 125

6.4 Results 127

6.4.1 Human islets and NHP islets on scaffolds effectively lower blood glucose in diabetic mice 127

6.4.2 Acellular, irradiated scaffolds elicit minimal immune response in NHPs after 30 days 127

6.4.3 1:30 PLG:NaCl scaffolds support islet survival in NHPs, but do not immediately support restoration of euglycemia or insulin independence 128

6.4.4 Characterization of 1.25:30 PLG:NaCl scaffolds, and successful implementation in mice, suggests adequate compensation for effects of γ irradiation 131

6.4.5 1.25:30 PLG:NaCl scaffolds do not improve transplant outcomes in a NHP model 132

6.4.6 Adjustment of the PLG:NaCl ratio compensates for irradiation without compromising islet survival and function 133

6.5 Discussion 134

6.6 Conclusion 137

6.7 Methods 138

6.7.1 Scaffold fabrication and sterilization 138

6.7.2 Islet isolation, shipment, and culture 140

6.7.3 NSG mouse studies 140

6.7.4 Implantation of acellular, irradiated scaffolds in NHPs to assess immunoreactivity 142

6.7.5 Allogeneic islet transplantation in diabetic NHPs 142

6.7.6 Comparison of non-sterilized and γ irradiated scaffolds with μCT 146

6.7.7 Compressive testing of irradiated and non-irradiated scaffolds 147

6.7.8 Statistical analysis 147

6.8 Acknowledgements 148
6.9 Supplemental information 148
6.10 References 148
Chapter 7 Conclusion and Future Directions 152
7.1 Summary of findings and significance 152
7.2 Future directions 154
7.2.1 Gene signatures to inform immunotherapy administration 154
7.2.2 Non-progressor signature as targets for T1D prevention 155
7.2.3 Early differentiation interventions in metabolic network models 155
7.2.4 Modeling of metabolic stress conditions 156
7.2.5 Metabolic network analysis in other disease models 156

List of Tables

Table 6.1: Summary of scaffold conditions included in this study. Variable parameters are listed in each column. The range for PLG weight includes the upper 5% error, since having too little PLG is detrimental to scaffold integrity; the range for NaCl weight includes the lower 5% error. 139

Table 6.2: Summary of insulin regimens used for each NHP transplant. *See Table 6.3. 144

Table 6.3: Sliding scales used for post-transplant insulin administration for Animals 1, 2, and 4..... 144

List of Figures

Figure 2.1: Survival and function of islets or β-cell clusters on microporous scaffolds posttransplantation. Following seeding, islets or hPSC-derived β-cells settle into the pores of the microporous scaffold. Three of the major challenges to survival and function include vascularization, inflammation, and adaptive immune responses. Scaffold modifications can be used to enhance vascularization or to attenuate the impact of inflammation or adaptive immune responses, with the arrows indicating that scaffold modifications can increase vascularization, transition a proinflammatory to an anti-inflammatory environment, or induce Tregs that can attenuate Teff responses at the graft. Vascularization: Release of growth factors such as VEGF or platelet-derived growth factor and/or co-transplant of supportive cells can enhance vascularization within the scaffold (13-15). Inflammation: Release of anti-inflammatory cytokines such as CXCL, IL-4, and IL-10 can be used to transition from a proinflammatory to an anti-inflammatory state (16, 17). Adaptive immune response: Modifying the scaffold with FasL108 or CCL22105 microparticles have been shown to induce regulatory T-cells upon release, as has systemic treatment with ECDI treated splenocytes (18). (Original diagram content developed by authors JL King and LD Shea with illustration by Jennifer Harley). 6

Figure 2.2: Porous scaffolds used for Islet/β-cell transplantation. Biocompatible materials used to fabricate microporous scaffolds (A-D) (A) Poly (lactide-co-glycolide) (PLG) with 250-425 μm pores—scale bar 500 μm. Adapted from Gibly RF, Zhang X, Graham ML, et al. Extrahepatic islet transplantation with microporous polymer scaffolds in syngeneic mouse and allogeneic porcine models. Biomaterials. 2011;32(36):9677–9684. doi:10.1016/j.biomaterials.2011.08.084 with permission from Elsevier. (B) Polydimethylsiloxane (PDMS)—scale bar 500 μm. Adapted from Jiang K, Weaver JD, Li Y, Chen X, Liang J, Stabler CL. Local release of dexamethasone from macroporous scaffolds accelerates islet transplant engraftment by promotion of anti-inflammatory M2 macrophages. Biomaterials. 2017;114:71–81. doi:10.1016/j.biomaterials.2016.11.004 with permission from Elsevier. (C) Silk fibroin 200-400 μm pores—scale bar 50 μm. Adapted from Mao D, Zhu M, Zhang X, et al. A macroporous heparin-releasing silk fibroin scaffold improves islet transplantation outcome by promoting islet revascularization and survival. Acta Biomater. 2017;59:210–220. doi:10.1016/j.actbio.2017.06.039 with permission from Elsevier. (D) Polyethylene glycol (PEG) hydrogel—scale bar 1 mm. Adapted from Rios PD, Skoumal M, Liu J, et al. Evaluation of encapsulating and microporous nondegradable hydrogel scaffold designs on islet engraftment in rodent models of diabetes. Biotechnol Bioeng. 2018;115(9):2356–2364. doi:10.1002/bit.26741 with permission from John Wiley and Sons. (E) PLG scaffold used to culture pancreatic progenitors into insulin producing β-cells: top, extracellular matrix deposition within pores of the scaffold by hPSC derived β-cells; bottom, effect of pore size on insulin gene expression. Adapted from Youngblood RL, Sampson JP, Lebioda KR, Shea LD. Microporous scaffolds support assembly and differentiation of

pancreatic progenitors into β-cell clusters. Acta Biomater. 2019;96:111–122. doi:10.1016/j.actbio.2019.06.032 with permission from Elsevier. 7

Figure 2.3: Strategies for enhancing survival post transplantation. (A) Fibrin–heparin and VEGF-loaded collagen scaffolds containing oxygen generating microparticles (MPs) enhanced islet revascularization and improved restoration of euglycemia. Adapted from Montazeri L, Hojjati-Emami S, Bonakdar S, et al. Improvement of islet engrafts by enhanced angiogenesis and microparticle-mediated oxygenation. Biomaterials. 2016;89:157–165. doi:10.1016/j.biomaterials.2016.02.043 with permission from Elsevier. (B) Layered microporous PLG scaffolds loaded with the trophic factor exendin-4 enhance restoration of euglycemia compared to blank scaffolds. Adapted from Hlavaty KA, Gibly RF, Zhang X, et al. Enhancing Human Islet Transplantation by Localized Release of Trophic Factors From PLG Scaffolds. Am J Transpl. 2014;14(7):1523–1532. doi:10.1111/ajt.12742 with permission from John Wiley and Sons. 13

Figure 2.4: Immunomodulation strategies. CCL22 released microparticles in VCA model and Fas-L attached microgels in T1D model. (A) Characterization and 40-day release profile of recruitment-MP. Treatment with Recruitment-MP (50 mg) prolongs allograft survival indefinitely. Hindlimb allograft survival curve showing indefinite survival (>200 days) in 6 of 8 rats treated with Recruitment-MP (50 mg). Adapted from Fisher JD, Zhang W, Balmert SC, et al. In Situ Recruitment of Regulatory T Cells Promotes Donor-Specific Tolerance in Vascularized Composite Allotransplantation. Vol 6.; 2020. http://advances.sciencemag.org/. with permission from Creative Commons Attribution-Non Commercial license. (B) Flow-focusing microfluidics were used to generate biotinylated microgels from biotin-functionalized PEG-4MAL macromers. Islet graft survival: SA-FasL-presenting or control microgels and unmodified BALB/c islets were co-transplanted under the kidney capsule of chemically diabetic C57BL/6 recipients. Adapted from Headen DM, Woodward KB, Coronel MM, et al. Local immunomodulation with Fas ligand-engineered biomaterials achieves allogeneic islet graft acceptance. Nat Mater. 2018;17(8):732–739. doi:10.1038/s41563-018-0099-0 originally published in Nature Materials, with permission from author Dr. Lonnie D. Shea. 20

Figure 2.5: Immunomodulation strategies. ECDI-treated donor lymphoid cell infusion and ECDI-attached PLG nanoparticles in T1D model. (A) Glycemic control posttransplant: 4 ECDI-DLI experimental group and 2 control group diabetic nonhuman primates each promptly achieved normoglycemia post-allogeneic islet transplant. Adapted from Lei J, Kim JI, Shi S, et al. Pilot Study Evaluating Regulatory T Cell-Promoting Immunosuppression and Nonimmunogenic Donor Antigen Delivery in a Nonhuman Primate Islet Allotransplantation Model. Am J Transplant. 2015;15(10):2739–2749. doi:10.1111/ajt.13329 with permission from John Wiley and Sons. (B) Scanning transmission electron microscopy image and size of PLG particles prior to lysate coupling with ECDI. A short course of low dose rapamycin with PLG-dAg demonstrated significantly greater islet allograft survival (n = 11) compared with mice treated with rapamycin alone (n = 9) **P < .01. Adapted with permission from Bryant J, Hlavaty KA, Zhang X, et al. Nanoparticle delivery of donor antigens for transplant tolerance in allogeneic islet transplantation. Biomaterials. 2014;35(31):8887–8894. doi:10.1016/j.biomaterials.2014.06.044 with permission from Elsevier. 24

Figure 3.1: Immune cell population dynamics captured at the IN and pancreas. (a) INs and the pancreas were explanted from NOD mice at 7-, 11-, and 15-week timepoints. (b) Glucose monitoring showed no incidence of diabetes at the 7-, and 11-week timepoints, and two diabetic mice at the 15-week timepoint. There were significant decreases in the (c) CD11b+ and (d) F4/80+ populations at the scaffold, but not the pancreas between initial and later timepoints. There were no significant changes in the CD3 + CD4+ (e) or CD3 + CD8+ (f) populations at the scaffold or pancreas. There were no significant differences between diabetic and nondiabetic mice for any cell populations at the scaffold at the 15-week timepoint. n = 5 mice for 7- and 11-week timepoints, n = 7 mice for the 15-week timepoint. At the 15-week timepoint, n = 5 nondiabetic, and n = 2 diabetic mice. Significance determined by mixed effects analysis in c–f, and multiple unpaired t-tests in g. IN, immunological niche..... 48

Figure 3.2: The IN does not affect disease progression in two models of T1D. (a) In the adoptive transfer model, mice received subcutaneous IN implants 2 weeks before adoptive transfer of diabetogenic T cells, or OVA reactive controls. INs were explanted on the day of T cell transfer, Day 0, and on Day 10. (b) None of the OVA controls became diabetic, and there was no difference in time to glucose elevation between mice that received BDC2.5 T cells and IN implants and mice that received BDC2.5 T cells only. (c) No mice that received BDC2.5 T cells remained euglycemic following 12 days post transfer in either the IN recipient or non-recipient group. (d) In the NOD mouse model, mice were implanted with INs at 4 weeks old, had an initial explant at 6 weeks old, and then were monitored for the blood glucose increase that resulted in their final explant timepoint. (e) The NOD mice developed hyperglycemia at differing rates, shown here by the glucose tracking data for each individual mouse, leading to different time points for the final explant. (f) There was no significant difference in the incidence of hyperglycemia between mice that received IN transplants and those that did not. IN, immunological niche. 50

Figure 3.3: IN analysis separates diseased from healthy groups in an adoptive transfer model of T1D. (a) PCA plots of the gene expression analysis of the sequencing data from the IN separates all initial timepoints from both diabetic Day 10 and control Day 10, (b) and separates all nondiabetic samples from the diabetic samples. (c) Heatmap of the six gene signature shows clustering of the genes resulting in group separation. (d) Plot of Random Forest prediction score versus SVD shows separation of the diabetic Day 10 BDC2.5 recipients from all Day 0 timepoints and Day 10 OVA recipients. n = 9 for Day 0, n = 4 for OVA Day 10, and n = 5 for BDC Day 10. IN, immunological niche; SVD, singular value decomposition. 51

Figure 3.4: IN analysis separates presymptomatic from symptomatic groups in the NOD mouse model of T1D. (a) PCA plot of the gene expression analysis of INs separates diabetic from healthy NOD mice. (b) Heatmap of the eight gene signature and clustering that results in separation between groups. (c) Plot of Random Forest prediction score versus SVD shows separation between diabetic and healthy groups. (d) Random Forest score for diabetic and healthy groups from both the NOD and adoptive transfer models show elevated scoring in the diabetic group across both models. n = 5 for diabetic and healthy NOD groups. IN, immunological niche; SVD, singular value decomposition. 53

Figure 3.5: Gene set enrichment analysis identifies differentially expressed pathways between diabetic and nondiabetic groups. (a) Bar plots show the pathways enriched in diabetic samples

in the adoptive transfer and (b) NOD models. (c, d) Gene-concept network plots show the connections of genes to biological processes. (e) A bar chart illustrates the proportion of overlapping pathways between the two models compared to the total number of enriched pathways. 54

Figure 3.6: IN analysis produces signature with non-sequencing gene analysis. (A-B) An additional cohort of NOD mice was tracked from the time of IN implantation to the time of glucose elevation. (C) PCA plot of the gene expression analysis of OpenArray data from the IN separates diabetic from healthy timepoints. (D) Heatmap of the six gene signature shows expression levels of genes contributing to the separation. (E) Plot of Random Forest prediction score versus SVD shows poor separation between diabetic and healthy groups based on scoring. (F) ROC curve shows an AUC = 0.96 and a false positive rate of 0.4..... 66

Figure 3.7: Flow gating for immune cell identification. (A) Flow data was first gated via forward scatter and side scatter to remove non-cellular debris, with all events outside of the selected area representing cells. (B) Cells were then gated by forward scatter area and height to remove any doublets. (C) Live single cells were identified as those negative for Zombie-NIR stain, and (D) CD45.1+ cells were identified with a PE antibody from the live cell population. All subsequent gating was done from the CD45.1+ population, with (E) CD11b+ gated with a Spark Blue 550 antibody, (F) F4/80+ gated with an APC antibody, and (G) CD3+ gated with a PE-Dazzle 594 antibody. The (H) CD8+ and (I) CD4+ populations were gated from the CD3+ population by Brilliant Violet 785 and Brilliant Violet 421 antibodies respectively. 67

Figure 4.1: Weekly IN explants enables longitudinal monitoring of NOD and NOR mice. (A) NOD and NOR mice were implanted with INs at 4 weeks old and underwent scaffold biopsy and replacement until the time of hyperglycemia onset (progressors) or 30 week of age (non-progressors and NOR). Scaffolds were selected for sequencing based on proximity to hyperglycemia or age for progressors and non-progressors/NOR respectively. (B) NOD and NOR mice are background matched at the MHC H2g7 locus. (C) No NOR mice became diabetic, and approximately 50% of NOD mice developed symptomatic disease during the study. (D) Both NOR and NOD non-progressor mice maintained stable glucose levels throughout the duration of the study. (E) Initial filtering of bulk sequencing data from all groups identified 4,593 of the 23,096 sequenced genes above our expression and variance filters for all samples..... 80

Figure 4.2: IN analysis separates all NOD mice from NOR controls regardless of disease progression. (A) All NOD mice (n=97) are separable from NOR controls (n=23) across timepoints using a 101 gene signature. (B) Group seperation has a ROC performance above 0.9 for 50 iterations of training/test data partitioning for fitting the elastic net model. (C) PCA of the samples using the 101 gene signature shows complete separation of the two groups. (D) Samples from NOR mice across six timepoints identify 39 genes that vary with age. (E) PCA of the NOR time signature shows separation of the diabetic and 1 week before onset timepoints from all earlier timepoints on PCA1, and separation of the earlier three timepoints on PC2. (F) GSVA of the NOR time course signature identified 13 genes from the curated mouse chemical and genetic gene sets that are related to the time course signature..... 82

Figure 4.3: NOD progressors and non-progressors are separable as early as 6 weeks of age (A) Elastic net regression performed on week six samples from NOD progressors (n=10) and NOD non-progressors (n=11) identified a 13 gene signature. (B) PCA of the 13 gene signature results in group separation, with no overlap of the two groups. (C) IPGTT of a separate group of progressors and non-progressors (n=4 per group) showed no significant difference in glucose tolerance at 8 weeks of age. (D) Five iterations of train and test partitioning validation performed with ROC>0.8 for alpha=0.55, showing predictive power not shown by the IPGTT functional test. 83

Figure 4.4: Six week signature can be applied to all time points in non-progressors, and relates to changes at the pancreas.(A) Elastic net regression performed on week six samples from NOD progressors (n=10) and NOD non-progressors from all time points (n=39) identified an eight gene signature. (B) The eight gene signature performed with ROC>0.8 across 50 iterations of train and test partitioning validation. (C) PCA of the eight gene signature results in group separation with two false positives, and no overlap of the two groups' confidence intervals. (D) Six of the eight signature genes are present in a single cell RNA sequencing data set performed on NOD islets at three timepoints: 4, 8, and 15 weeks of age. (E) A dot plot showing the average expression and percentage of cells expressing the signature genes identifies upregulation of Sox11 in islet endothelial cells at week 4, of Dlk1in lymphoid cells at week 8, and of F2rl1 in plasma at week 15. 85

Figure 4.5: A 13 gene signature separates NOD progressors 7 weeks before onset from all later time points. (A) PCA of an elastic net regression run on all NOD progressor time points (n=8 for -7 weeks, n=10 all other groups) normalized to week 6 shows separation between -7 and -3 through onset, with -5 spanning the middle. (B) Elastic net regression of -7 versus -5 resulted in a 13 gene signature, and (C) PCA shows complete separation of the two groups according to the signature. (D) All time points were scored using random forest and singular value decomposition according to the 13 gene signature, showing separation of -7 and week 6 from the later time points. (E) The random forest scores on a per mouse basis show significant difference between -7 and -5, ($p<0.0001$) and no significant difference between -5 and later times. (F) SVD per mouse shows a significant difference between 6 weeks and all later time points ($p<0.0001$), and no significant difference between -7 and later time points. (G) Train and test partition validation of -7 versus all later time points performed with ROC>0.85 for 50 iterations. 87

Figure 4.6: NOD progressor signature genes are found in the pancreatic islets. (A) A publicly accessible data set for single cell sequencing of the pancreatic islets of NOD at three time points was annotated to identify cell clusters during the time course of disease progression. (B) Dot plot analysis of the annotated data show that 11 of the 13 genes in the -7 versus -5 signature are expressed in immune, endothelial, or mesenchymal cells within pancreatic islets. (C) Quantification of the number of cells expressing each signature gene over time shows higher cell counts for signature expressing cells at weeks 4 and 8 compared to week 15 for 5 genes: Chp1, Rbfa, Mgat2, Ccdc85b, and Erdr1. (D) The number of cells expressing signature genes by cell type show the greatest number of endothelial cells for all cells expressing signature genes, with appreciable leukocyte populations present for 7 genes: Chp1, Rbfa, Zc3h12a, Mgat2, Amd1, Ccdc85b, and Erdr1. 89

Figure 5.1: Transcriptomic data identifies metabolic flux differences between mature and sc-islets when implemented in a metabolic reconstruction. (A) RNA sequencing (RNAseq) samples were generated from each stage of a six stage differentiation protocol for the differentiation of hPSCs into sc-islets. (B) The sequencing data were analyzed for differential gene expression, and these results were used to generate stage specific constraints in a human metabolic network reconstruction. The reconstruction was used to perform flux balance analysis of stage 6, or sc-islets, versus human islet controls. (D) Of the 3744 reactions in the reconstruction, 20 were identified with a flux difference between stage 6 and human islets >0.01. 8 of the 20 reactions are related to NAD/NADH or NADP/NADPH metabolism, which are needed as electron donors for mitochondrial respiration. 106

Figure 5.2: Model sensitivity to differentiation efficiency is dependent on objective function selection. (A) PCA of gene expression data for stage 6 and human islet samples shows separate sub-populations within the stage 6 group. (B) A representative example of flow cytometry from one of the differentiations in the group closer to human islets in the PCA show good differentiation efficiency. (C) A representative flow cytometry result for a differentiation further from human islets in PCA, with poor differentiation efficiency. (D) PCA of the flux results for the metabolic reconstruction with ATP transport set as the objective function has minimal separation between good and poor differentiations. (E) PCA of flux results for the same model with calcium ion transport set as the objective has greater separation between the good and poor differentiations. (F) Euclidean distances calculated for good and poor stage 6 groups to human islets show the smallest Euclidean distance for good differentiations, using calcium transport as the objective function. 108

Figure 5.3: Simulation of PPAR agonist treatment recapitulates beta cell improvements found via in vitro testing. (A) Transcription factor analysis of the RNAseq data identified PPARα and PPARγ as having high perturbation in stage 6 compared to human islets. (B) WY14643 is a PPARα agonist, with some gamma effects. 42 downstream genes for PPARα in humans have been identified in the literature: 39 upregulated, and 3 downregulated. (C) Comparing the PPARα downstream genes to the genes in the metabolic reconstruction, 19 are present: 17 upregulated, 2 downregulated. (D) WY14643 treatment of stage 6 cells was simulated in the metabolic reconstruction by adding the PPARα downstream genes to the arrays of weighted reactions for stage 6 cells and adding a 20% increase or decrease to their reaction weights according to their regulation. PCA of the treatment simulation shows an increase in the similarity of the treated group to human islets compared to untreated. (E) The improvement in stage 6 cells following WY treatment is also demonstrated in vitro, with glucose stimulated insulin secretion being significantly increased in the treated group compared to untreated. (Panel E adapted from Lietzke, Bealer, Crumley, King et al. doi: https://doi.org/10.1101/2024.07.26.605318) 110

Figure 5.4: Knock-in simulation of downregulated genes identifies target for improving stage 6 cell. (A) A knock-in simulation was run by removing the downregulated reaction weight for each of the 443 genes downregulated between stage 6 cells and human islets. This screen identified NMNAT3 as the gene with the greatest flux similarity to human islets following knock-in. (B) NMNAT3 encodes an enzyme that regulates the production of nicotinamide adenine dinucleotide (NAD^+) from nicotinamide mononucleotide. (C) An additional simulation of supplementing stage 6 cells with NAD^+ shows no difference between treated and untreated

groups, indicating that the knock-in improvement is not based solely on increased production of NAD^+. 111

Figure 5.5: In vitro testing of elements of the NMNAT3 pathway suggest this target may improve metabolism. (A) FK866 is an inhibitor of NAMPT, which is needed to produce NAD^+ from nicotinic acid. It is possible that this inhibition has an indirect upregulation of NMNAT3 activity as a compensatory effect to produce NAD^+ via alternative pathways. (B) Stage 6 cells were treated with 50nM FK866, 10mM NMN, or a combination of the two between days three and ten of stage 6 differentiation. At day 7, cells were taken out of planar culture and reaggregated as clusters until the time of assessment. (C-D) ATP and ADP concentrations were measured at low (2mM) and high (20mM) glucose concentrations. (C) ATP concentration was higher for control and singly treated samples, but these groups also had the highest ADP concentration (D) indicating poor efficiency in ADP to ATP conversion. (E) ATP to ADP ratios show trends of higher performance in the groups that received multiple treatments (n=1). 113

Figure 5.6: Flow cytometry results for sc-islet samples taken on the day of reaggregation and stained for NKX6.1 (Alexa 405) and C-peptide (Alexa 647). Analysis was performed for treatment groups: (A) control, (B) 10mM NMN, (C) 50nM FK866, and (D) 10mM NMN and 50nM FK866. 118

Figure 6.1: Comparison of glycemic control between mice transplanted with 2,000 IEQ human islets (n = 4) and nonhuman primate islets (n = 2) on non-irradiated scaffolds fabricated with a 1:30 w/w PLG:NaCl ratio. 127

Figure 6.2: Immunoreactivity study of acellular, irradiated PLG scaffolds, fabricated with a 1:30 PLG:NaCl ratio, in cynomolgus monkeys. (A) Visualization of the scaffold being placed in the omentum. (B) Entire excised omentum, with the location of the PLG scaffold magnified. (C) Necropsy images. (i) Gross view of the omentum with no fibrotic tissue visible. (ii) Gross view of the omentum overlaying the colon. (iii) Gross view of the liver, gallbladder, and surrounding viscera. (D) Sections of the PLG scaffold and omentum were stained for α-SMA (fibroblasts), CD11b (macrophages), and CD8 (cytotoxic T cells). Hematoxylin and eosin staining was also performed to examine the tissues for signs of inflammation. All scale bars = 200 μm. 128

Figure 6.3: Allogeneic islet transplantation on irradiated scaffolds, fabricated with a 1:30 PLG:NaCl ratio, in the omentum of NHPs. (A) (i) Manual seeding of islets on the scaffold. (ii-iii) Scaffold after seeding with islets. (iv) Insertion of a cell-laden scaffold in the omentum. (B) Immunohistochemical staining of an explanted scaffold from Animal 2, retrieved 41 days after transplantation. Insulin (green) and DAPI (blue) are colocalized throughout the image. Scale bar = 100 μm. (C-E) Timewise blood glucose and total daily exogenous insulin in diabetic NHP recipients. (F-H) IVDTTs were conducted before and after induction of diabetes with STZ, then again at serial timepoints after transplantation. (I-K) Serum C-peptide levels were measured before and after induction of diabetes, then again after transplantation until termination of the study. 130

Figure 6.4: Characterization of γ-irradiated scaffolds versus non-sterilized scaffolds, fabricated with a 1.25:30 PLG:NaCl ratio. (A) Representative μCT images of (i) a γ-irradiated scaffold and (ii) a non-irradiated scaffold, visualized using the ImageJ2 3D Viewer. (B) Compressive testing of irradiated and non-irradiated PLG scaffolds. (i) Photograph of testing setup. (ii) The slope of the force-displacement curve was measured over a defined displacement interval (beginning at 0.1 mm) for each specimen, with statistical differences determined using a two-tailed t test with Welch's correction. (C) Porosity of γ-irradiated and non-irradiated scaffolds (*n* = 3 scaffolds per condition, each measured in triplicate). (D) Mean trabecular thickness (i.e. thickness of interior PLG branches) in γ-irradiated and non-irradiated scaffolds (*n* = 3 scaffolds per condition, each measured in triplicate). 132

Figure 6.5: Pilot study of 1.25:30 PLG:NaCl scaffold for use in allogeneic islet transplantation in a NHP model. (A) Timewise blood glucose and total daily exogenous insulin. (B) IVDTTs. (C) Serum C-peptide. 133

Figure 6.6: Further adjustment of PLG:NaCl ratio for xenogeneic islet transplants on irradiated scaffolds in NSG mice. (A-C) Timewise fasting blood glucose levels for individual mice, which received 2,000 IEQ of human islets on scaffolds fabricated with a (A) 1.05:30, (B) 1.15:30, or (C) 1.25:30 w/w PLG:NaCl ratio (n = 4 per condition). Once a mouse had two consecutive blood glucose readings ≥350 mg/dL, the mouse was eliminated from the study. (D) Reflecting this criterion, all mice are displayed in a Kaplan-Meier survival curve showing maintenance of fasting blood glucose below 350 mg/dL. 134

Figure 6.7: Serum C-peptide measurements taken during IVDTTs for Animal 1..... 148

Abstract

Type 1 diabetes (T1D) is an autoimmune disease with a prevalence of over 8 million people globally. Following autoimmune destruction of their pancreatic islets, T1D patients rely on exogenous insulin therapy to regulate their blood glucose levels. This lifelong therapy is associated with high burden of disease, and long-term risks for complications. As a result, the T1D research field has pursued cell replacement therapies as a treatment for patients with active disease, and preventive immunotherapies for recent onset patients who maintain a functional islet mass. This dissertation investigates the use of microporous polymer scaffolds as tools to address existing challenges in the development of cell replacement therapy and disease monitoring. We identify deficiencies in current cell replacement approaches and develop methods to improve cell quality and delivery. We also develop a monitoring platform for T1D progression that has the potential to inform immunotherapy treatment timing to sustain the greatest functional islet mass.

In order to address the challenge of disease monitoring in a glucose agnostic manner, we implemented PCL scaffolds as immunological niches (IN) at a subcutaneous site. We first established that sequencing analysis of the IN distinguishes healthy from diabetic conditions in two murine models of T1D. We next investigated if the IN could distinguish risk and progression status in the NOD mouse model of T1D. We found that elastic net regression analysis of RNA sequencing data from the IN identifies gene signatures that separate at-risk from non-risk groups, progressors from non-progressors, and time to disease onset for progressors. These gene signatures

identify disease progression at a time prior to measurable glucose dysregulation, outperforming the current clinical standard of a glucose tolerance test.

We next investigated existing challenges to cell replacement therapy related to cell quality and cell delivery. Low availability of donor islets has led to development of pluripotent stem cell derived islets (sc-islets) as a potentially limitless source. However, sc-islets lack the metabolic maturity of donor islets, and the protocols to generate these cells take on the order of 30 days, making *in vitro* testing of a large number of treatments time and resource intensive. To investigate the effects of drug and metabolite treatments on sc-islet maturity without the need for lengthy cultures, we developed a metabolic network reconstruction specific to sc-islets. Transcriptomic data from mature human islets and sc-islets were used to tailor the model to our existing differentiation output, and we then used the model to screen a validated drug treatment and individual gene knock-ins for 443 genes. *In vitro* testing indicates that our model is capable of identifying targets to enhance metabolism in sc-islets *in silico.* To address delivery challenges, we investigated the role of polymer ratio on efficacy of scaffolds as an islet transplantation platform. Taken together, the dual approach of monitoring and therapeutic cell enhancement demonstrates the multifaceted needs of the T1D community. Enhanced monitoring has the potential to improve preventive treatment as incidence continues to rise, and improving cell therapies addresses the long-term needs of the existing T1D population.

Chapter 1 Introduction

Over 8 million people globally live with Type 1 Diabetes (T1D) with incidence on the rise. Despite advancements in glucose management with the invention of insulin pumps and continuous glucose monitors, burden of care and complication risk remain high. Promising treatments for both prevention and cell replacement have been developed, but improvements are needed to improve efficacy and maintenance of long-term euglycemia. Microporous polymer scaffolds offer an implantable, retrievable platform capable of capturing circulating immune cells for monitoring, and of delivering therapeutic cells. The work presented herein leverages the scaffold's capabilities to put forth new strategies to further disease monitoring and treatment in T1D.

Chapter 2 introduces existing approaches, and the challenges associated with cell replacement therapy. This chapter introduces the capabilities of polymeric scaffolds as a platform for islet or sc-islet transplantation.

Chapter 3 establishes the scaffold as an immunological niche (IN), capable of delineating healthy from diseased states in two models of T1D. We establish that IN implantation and monitoring does not effect disease incidence in two murine models, and that immune cell populations present at the pancreas of NOD mice also traffic to the IN.

Chapter 4 builds on our work with the IN in the NOD mouse model. We identify gene signatures that identify which mice will progress to disease as early as 6 weeks of age, which is before the clinical standard glucose tolerance test detects differences between progressors and non-progressors. We also generate a gene signature from IN analysis that separates early progressors

from late progressors, demonstrating the signature's potential as an indicator for preventive treatment.

Chapter 5 addresses the challenge of a high quality cell source for cell replacement therapy. We generate a metabolic network reconstruction to model the maturity discrepancy between sc-islets and mature human islets. We validate our model by comparing simulation results to *in vitro* results, both of which show improved metabolic function in the treatment group. We also propose a new drug target for enhancement of sc-islet maturation. A pilot validation of this target suggests that sc-islets treated based on our modeling results demonstrate improved ATP metabolism.

Chapter 6 investigates translatability of the scaffold as an islet transplant platform. We show that scaffolds support islet survival, but not restoration of euglycemia in non-human primate models. We show that altering the polymer to salt ratio in scaffold manufacturing results in variable efficacy for islet transplants in mice, indicating that minimal changes in scaffold production can have significant impact on transplant outcomes.

Chapter 7 provides conclusions and potential future directions for this dissertation. Future directions and implications are discussed for both the research and clinical applications of this work.

Chapter 2 Integration of Islet/Beta-Cell Transplants with Host Tissue Using Biomaterial Platforms

2.1 Authors

Daniel W. Clough*, Jessica L. King*, Feiran Li*, Lonnie D Shea

*These authors contributed equally to this work.

2.2 Abstract

Cell-based therapies are emerging for type I diabetes mellitus (T1D), an autoimmune disease characterized by the destruction of insulin-producing pancreatic β-cells, as a means to provide long-term restoration of glycemic control. Biomaterial scaffolds provide an opportunity to enhance the manufacturing and transplantation of islets or stem cell–derived β-cells. In contrast to encapsulation strategies that prevent host contact with the graft, recent approaches aim to integrate the transplant with the host to facilitate glucose sensing and insulin distribution, while also needing to modulate the immune response. Scaffolds can provide a supportive niche for cells either during the manufacturing process or following transplantation at extrahepatic sites. Scaffolds are being functionalized to deliver oxygen, angiogenic, anti-inflammatory, or trophic factors, and may facilitate cotransplantation of cells that can enhance engraftment or modulate immune responses. This local engineering of the transplant environment can complement systemic approaches for maximizing β-cell function or modulating immune responses leading to rejection. This review discusses the various scaffold platforms and design parameters that have been identified for the manufacture of human pluripotent stem cell–derived β-cells, and the transplantation of islets/β-cells to maintain normal blood glucose levels.

2.3 Introduction

Type I diabetes (T1D), which affects an estimated 1.6 million Americans, is caused by the autoimmune destruction of the pancreatic β-cells within the islets of Langerhans. Individuals with T1D must currently rely on lifelong exogenous insulin therapy. Advanced insulin pumps and continuous glucose monitoring and feedback systems have given individuals with T1D tighter control of their blood glucose levels in recent years (1, 2). Despite the use of this technology and advanced algorithms, blood glucose levels are not maintained within the normal range as effectively as native islets, which puts individuals at risk for vascular complications and dangerous hypoglycemic events (1-3). The Edmonton Protocol, first published in 2000, has been utilized clinically to transplant islets via hepatic vein infusion in conjunction with immunosuppressive therapy (4). Individuals receiving islet transplantation have shown lower levels of glycated hemoglobin, more time spent in the healthy glycemic range, and a reduced risk for hypoglycemic events compared with recipients of continuous subcutaneous insulin infusion or multiple daily insulin injections (5). The Edmonton Protocol has shown the enormous promise for long-term, tightly controlled glucose levels without exogenous insulin; however, several drawbacks prevent wide adoption of this strategy (6). Hepatic vein infusion exposes cells directly to the blood without protection, resulting in an instant blood–mediated inflammatory reaction (IBMIR). The required systemic immunosuppression brings harsh side effects, putting patients at risk for infection, organ damage, and developing cancer. The harsh environment and need for lifelong immunosuppression provide a strong motivation to develop extrahepatic delivery strategies.

The limited supply of acceptable islets from cadaver donors requires alternative cell sources to be investigated and developed for T1D cell replacement therapy. Alternative cell sources that have shown promise include xenogeneic sources and human pluripotent stem cell

(hPSC) sources, which include embryonic stem cells (hESCs) and adult induced pluripotent stem cells (iPSCs). While xenogeneic sources, such as porcine islets, have shown positive results in preclinical nonhuman primate studies, the xenogeneic immune response is considered an additional barrier to an already challenging immune response (7). Numerous studies have demonstrated the ability to generate pancreatic progenitors, cells committed to the pancreatic lineage, from pluripotent cells (8-11). These hPSC-derived pancreatic progenitors provide a means of overcoming the shortage of allogeneic donor tissue for this therapy (12).

Biomaterial scaffolds are being developed as a platform for delivering islets or hPSC-derived β-cells to extrahepatic sites. Extrahepatic sites are desired to avoid IBMIR, which introduces new challenges. Immediately following transplantation, transplanted cells face multiple challenges: they must rely on diffusion for oxygen, nutrients, and waste exchange during the period prior to revascularization, and they must overcome or avoid the inflammatory response and host autoimmune and allogeneic response (Fig. 2.1) (13-18). Biomaterials have been widely used for delivering islets, largely in an encapsulation approach that creates a physical barrier between therapeutic cells and the host immune system (19). Innovation with encapsulation technologies, such as novel materials to limit fibrosis (20), or thinner coatings (21), continues to reduce the transplant volume. Nevertheless, this approach restricts access to vascular ingrowth that is present within native islets and contributes to their function. Nonencapsulating scaffolds, in contrast to encapsulating hydrogels, allow for integration of transplanted cells with host tissue, which can support long-term survival and function (16, 22-24). These scaffolds have included microporous or fibrous scaffolds that allow for cell infiltration following cell transplantation, as well as degradable hydrogel systems that initially encapsulate cells, with subsequent degradation allowing for host tissue infiltration and

integration. Scaffolds can provide support for cell adhesion and signals through functionalization of the material with peptides or proteins, or localized delivery of trophic factors. Collectively, scaffolds provide the opportunity to engineer the local microenvironment at the site of transplantation to support the integration, survival, and long-term function of transplanted cells.

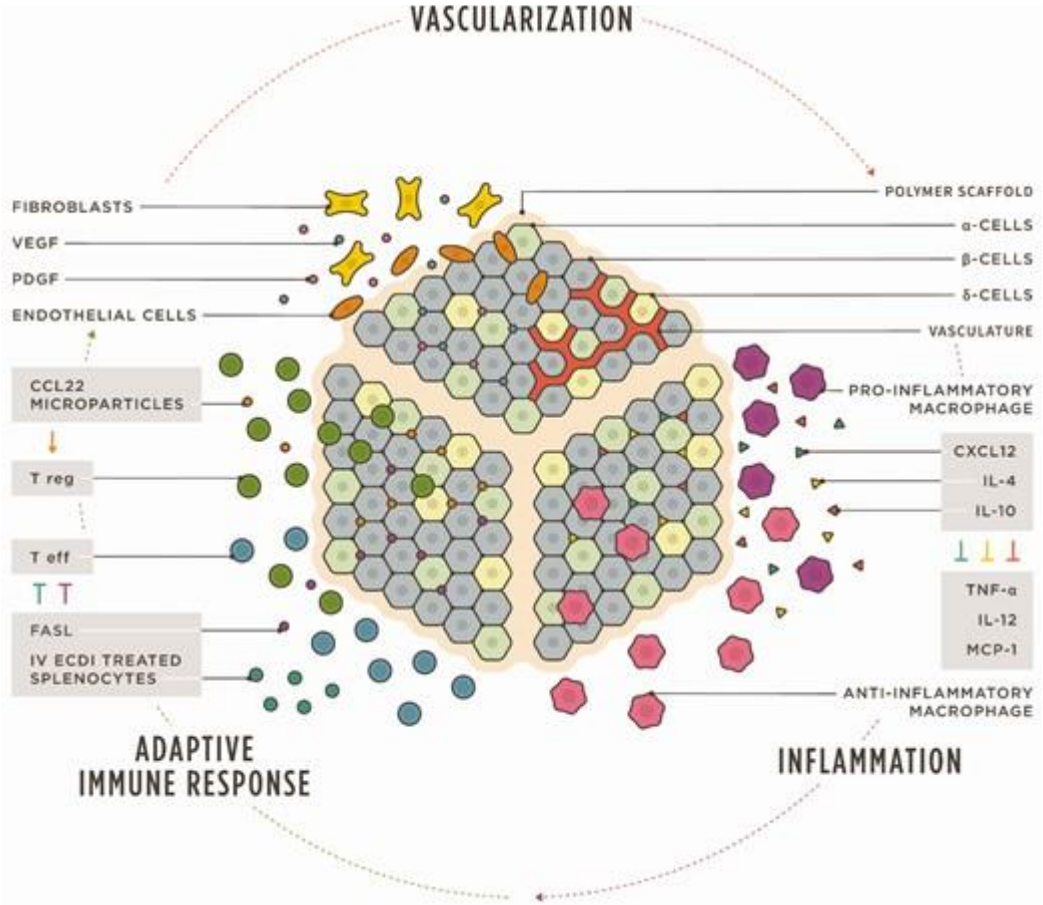


Figure 2.1: Survival and function of islets or β-cell clusters on microporous scaffolds posttransplantation. Following seeding, islets or hPSC-derived β-cells settle into the pores of the microporous scaffold. Three of the major challenges to survival and function include vascularization, inflammation, and adaptive immune responses. Scaffold modifications can be used to enhance vascularization or to attenuate the impact of inflammation or adaptive immune responses, with the arrows indicating that scaffold modifications can increase vascularization, transition a proinflammatory to an anti-inflammatory environment, or induce Tregs that can attenuate Teff responses at the graft. Vascularization: Release of growth factors such as VEGF or platelet-derived growth factor and/or co-transplant of supportive cells can enhance vascularization within the scaffold (13-15). Inflammation: Release of anti-inflammatory cytokines such as CXCL, IL-4, and IL-10 can be used to transition from a proinflammatory to an anti-inflammatory state (16, 17). Adaptive immune response: Modifying the scaffold with FasL108 or CCL22105 microparticles have been shown to induce regulatory T-cells upon release, as has systemic treatment with ECDI treated splenocytes (18). (Original diagram content developed by authors JL King and LD Shea with illustration by Jennifer Harley).

Herein, we provide an overview of scaffold platforms that are being employed for manufacturing hPSC-derived β-cell products and can deliver islets or β-cells to extrahepatic locations for integration with the host (Fig. 2.2A-D) (25-29). We review strategies towards enhancing the maturation and function of therapeutic β-cells, supporting survival of transplanted insulin-producing cells amid revascularization and inflammation, and the application of immune engineering methods to allow transplanted cells to avoid autoimmune or allogeneic host immune responses.

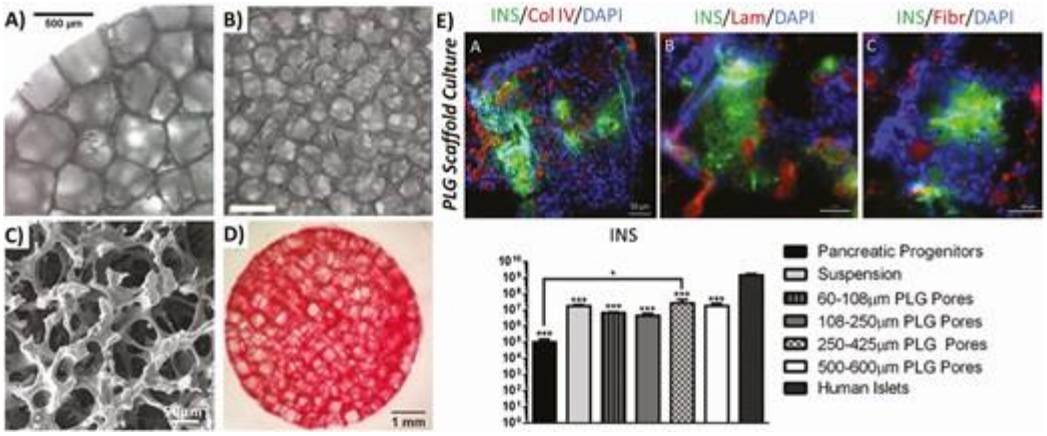


Figure 2.2: Porous scaffolds used for Islet/β-cell transplantation. Biocompatible materials used to fabricate microporous scaffolds (A-D) (A) Poly (lactide-co-glycolide) (PLG) with 250-425 μm pores—scale bar 500 μm. Adapted from Gibly RF, Zhang X, Graham ML, et al. Extrahepatic islet transplantation with microporous polymer scaffolds in syngeneic mouse and allogeneic porcine models. Biomaterials. 2011;32(36):9677–9684. doi:10.1016/j.biomaterials.2011.08.084 with permission from Elsevier. (B) Polydimethylsiloxane (PDMS)—scale bar 500 μm. Adapted from Jiang K, Weaver JD, Li Y, Chen X, Liang J, Stabler CL. Local release of dexamethasone from macroporous scaffolds accelerates islet transplant engraftment by promotion of anti-inflammatory M2 macrophages. Biomaterials. 2017;114:71–81. doi:10.1016/j.biomaterials.2016.11.004 with permission from Elsevier. (C) Silk fibroin 200-400 μm pores—scale bar 50 μm. Adapted from Mao D, Zhu M, Zhang X, et al. A macroporous heparin-releasing silk fibroin scaffold improves islet transplantation outcome by promoting islet revascularization and survival. Acta Biomater. 2017;59:210–220. doi:10.1016/j.actbio.2017.06.039 with permission from Elsevier. (D) Polyethylene glycol (PEG) hydrogel—scale bar 1 mm. Adapted from Rios PD, Skoumal M, Liu J, et al. Evaluation of encapsulating and microporous nondegradable hydrogel scaffold designs on islet engraftment in rodent models of diabetes. Biotechnol Bioeng. 2018;115(9):2356–2364. doi:10.1002/bit.26741 with permission from John Wiley and Sons. (E) PLG scaffold used to culture pancreatic progenitors into insulin producing β-cells: top, extracellular matrix deposition within pores of the scaffold by hPSC derived β-cells; bottom, effect of pore size on insulin gene expression. Adapted from Youngblood RL, Sampson JP, Lebioda KR, Shea LD. Microporous scaffolds support assembly and differentiation of pancreatic progenitors into β-cell clusters. Acta Biomater. 2019;96:111–122. doi:10.1016/j.actbio.2019.06.032 with permission from Elsevier.

2.4 Manufacturing Platforms for Cell Transplantation

While hPSC-derived pancreatic progenitors have shown promise as allogeneic donor tissue, further development of manufacturing methods is required prior to successful clinical application. Large-scale production of hPSC-derived insulin-producing cells requires strict

control of aggregate formation and differentiation factors for weeks of culture. The traditional culture system for cell-based therapies involves bioreactors for large-scale manufacturing, in which the cells are provided reagents at distinct stages and the cells self-assemble into clusters. Upon the completion of culture, these clusters are collected for direct infusion or embedded within materials for transplantation (10, 20). Biomaterial platforms provide a tool that can assist with assembly of cells into structures of tunable size, which is controlled by the material properties rather than the shear rate of the culture media (30). Additionally, as cells are cultured within the platform, the factors they secrete are deposited within a niche that may support their long-term function. Finally, upon completion of culture, the material platform can be directly transplanted with minimal cell manipulation and without disruption of the cellular niches.

Degradable hydrogels have been widely used for 3D differentiation of hPSCs (31-33). Matrigel-based materials have successfully produced islet organoids, as well as increased functional insulin secretion compared with 2D culture (34). Recent work has shown that functional β-cells can be produced from 2D culture under specific conditions. A recent protocol reproducibly generated cells with comparable or better functionality than suspension cultures (9). The condition optimized for this protocol was the addition of a 24-hour treatment with latrunculin A, which is a factor that depolymerizes the actin cytoskeleton and increases endocrine induction (9). While promising, Matrigel is sourced from murine tumors and generally not considered a translatable platform due to its batch to batch variability, undefined composition, and potential to transfer pathogens and facilitate tumor formation and growth (35-37). Collagen scaffolds and fibrin gels are two naturally occurring hydrogels that have been shown to support 3D hPSC differentiation into β-cells (32). A number of hydrogels have been employed for organoid culture with the ability to promote the formation of 3D structures that

contain multiple cell types found in islets (33, 34, 38). These materials provide mechanical support for the formation of structures, and are modified with biological cues such as growth factors, cell adhesion ligands, immunomodulatory drugs, or enzyme degradation sites (39, 40). Proteomic and ribonucleic acid sequencing analysis was used to probe regulatory pathways during pancreatic differentiation of hPSCs, and the results suggested 3D confinement of the cells promoted integrin signaling and β-cell differentiation (31). These hydrogels can generate cells with a greater expression for β-cell genes and enhanced glucose-responsive function compared with 2D culture (31, 34).

Microporous scaffolds are also being developed as a platform for manufacturing hPSC-derived β-cells (29). Microporous scaffolds have commonly been used in regenerative medicine to allow seeded cells to form into tissues for subsequent transplantation. Specific to islets, the size of transplanted islets impacts insulin secretion and viability, and the pore size can regulate the size at which islet organoids form (41). After settling into pores, hPSCs form cell–cell interactions and mature into β-cells with transcription marker expression and glucose-stimulated insulin secretion comparable with or higher in scaffold cultured cells than in suspension culture (29). Additionally, hPSCs differentiated in microporous scaffolds were shown to form an extracellular matrix through deposition of collagen IV, laminin, and fibronectin (Fig. 2.2E). Extracellular matrix proteins could also be deposited onto the material surface in order to provide cues that promote the differentiation to islet organoids. Multiple biomaterials have been investigated for their potential to support islet organoid formation, such as polyethylene glycol or the poly (lactide-co-glycolide) (PLG), both of which have shown promise for islet transplantation in diabetic mouse models (22, 42-44). Importantly, the scaffolds that initially function as a support for organoid maturation can then be directly transplanted. Transplanting β-

cells differentiated on a microporous scaffold avoids disruption of the existing cell–cell and cell–matrix interaction that may occur during the handling of suspension cultured cells for transplantation.

2.5 Transplantation

Pancreatic islets and β-cells are highly metabolically active with oxygen and glucose requirements that are greater than many other cell types, and the extrahepatic transplantation site must support these metabolic demands for a relatively large number of cells (≈500 000 islet equivalents (IEQ) per human transplant recipient) (45). In preclinical models, the kidney capsule is widely used, though this site is challenging to surgically access, cannot readily be altered as with the liver, and has the potential comorbidity of nephropathy, which would likely reduce healthy vasculature (46). The intraperitoneal and omental pouch have been widely used in preclinical and for clinical transplantation due to its large capacity for transplanting cells, which can also be delivered on scaffolds or with biologics that create a supportive environment. The subcutaneous space has an advantage of easy surgical access and could have sufficient space for large numbers of cells, though this site is less vascularized than other sites (47). The reduced vasculature in the subcutaneous tissue can lead to cell necrosis at the center of unmodified scaffolds as early as 24 hours after implantation (13). The intramuscular site offers a rich vascularization (48, 49), yet choosing an appropriate method of delivery at an intramuscular site is key to avoiding a detrimental fibrotic response (49). The native home of islets, the pancreas, has been considered as a transplant site, but it is widely considered less clinically promising due to the site requiring an invasive procedure (46). Collectively, a major challenge for clinical translation is providing an environment at the transplantation site that is able to support the

metabolic needs of a large number of metabolically active cells, with hPSC-derived β-cells also requiring an environment that supports their maturation.

2.5.1 Enhancing survival

The initial challenge following transplantation is survival of the transplanted cells, and the properties of the transplantation site are critical. Oxygen is considered a limiting factor following transplantation, and a robust vasculature in close proximity to the graft can supply oxygen by diffusion. Scaffolds allow for oxygen and nutrient diffusion through the pores, yet passive diffusion is often insufficient to support the entire cell population for significant times. Alternatively, prevascularizing of the transplant site to enhance the local vascularity can enhance survival following the addition of islets. The temporary placement of a biomaterial to promote a proangiogenic inflammatory response successfully prevascularized a subcutaneous transplantation site and supported restoration of euglycemia following syngeneic islet transplantation (50). Fingolimod (FTY720), which targets sphingosine-1-phosphate (S1P) receptors on endothelial cells and smooth muscle cells to increase the density of surrounding microvascular networks, was loaded in scaffolds to prime an extrahepatic transplant site, and increased the formation of microvessels in diabetic mice, which supported islet function posttransplantation (51). Scaffolds loaded with vascular endothelial growth factor (VEGF) and fibrinogen have effectively prevascularized the site prior to islet transplantation (52-54). However, the efficacy of VEGF to induce vascularization is site dependent (55). A polyethylene glycol (PEG) hydrogel loaded with VEGF enhanced vascularization and reduced blood glucose when implanted in the epididymal fat pad, yet had no significant effect when implanted in the subcutaneous space or small bowel mesentery (55). While the epididymal fat pad, analogous to the omentum in humans, is considered a clinically translatable site, other methods to promote

vascularization may be needed at alternative sites in order to support the needs of the cell graft. At a subcutaneous site, poly(D,L,-lactide-co-ε-caprolactone) scaffolds were allowed to prevascularize for 4 weeks prior to islet delivery. All mice in the diabetic cohort receiving 1200 islets into prevascularized poly(D,L,-lactide-co-ε-caprolactone) scaffolds achieved normoglycemia, while none of the mice in the cohort receiving the same islet dose into an unmodified subcutaneous pocket achieved normoglycemia (53). The Sernova Corporation has developed a device for islet transplantation called the Cell Pouch™, which is currently in a clinical trial, and is based on allowing 6 weeks for prevascularization in the subcutaneous space prior to islets being transplanted within cylindrical immune-isolating chambers (56). However, the islet loading levels and the diameter of cylinders within the Cell Pouch™ may contribute to hypoxia induced cell death, and future devices must limit the thickness of avascular tissue requiring oxygen diffusion (57). A complementary strategy to prevascularization involves drug delivery to inhibit apoptosis. Diabetic mice receiving islet transplants codelivered with V5, a BCL2-associated X protein–inhibiting peptide, had grafts with significantly enhanced function and a larger number of surviving islets (58). Collectively, prevascularizing the transplantation or blocking apoptosis are emerging strategies aimed at enhancing graft survival at early time points.

Oxygen has been directly delivered at the transplantation site to enhance survival prior to vascularization of the islets or islet organoids. Beta O2 has developed an implantable device called βAir, which has a refillable oxygen chamber designed to provide oxygen to encapsulated islets. This system has successfully restored euglycemia in diabetic rats and minipigs (59, 60). However, significant functionality was not yet achieved in a phase I clinical trial (61). Alternatively, oxygen generating compounds can be embedded within materials that can immediately provide oxygen to the transplanted cells for days to weeks, which spans the critical

time prior to integration with the host vasculature (Fig. 2.3A) (43, 62-64). Incorporation of hydrogen peroxide or calcium peroxide into scaffolds has been developed to locally provide oxygen release following transplantation and has been shown to improve graft function (62-64). Once the oxygen generating compound is depleted, hypoxia will return unless sufficient integration with the host vasculature has occurred. Increasing compound loading onto scaffolds may increase the length of oxygen delivery, yet the loading and release must be balanced to provide the necessary oxygen without the excessive production of harmful reactive oxygen species (64).

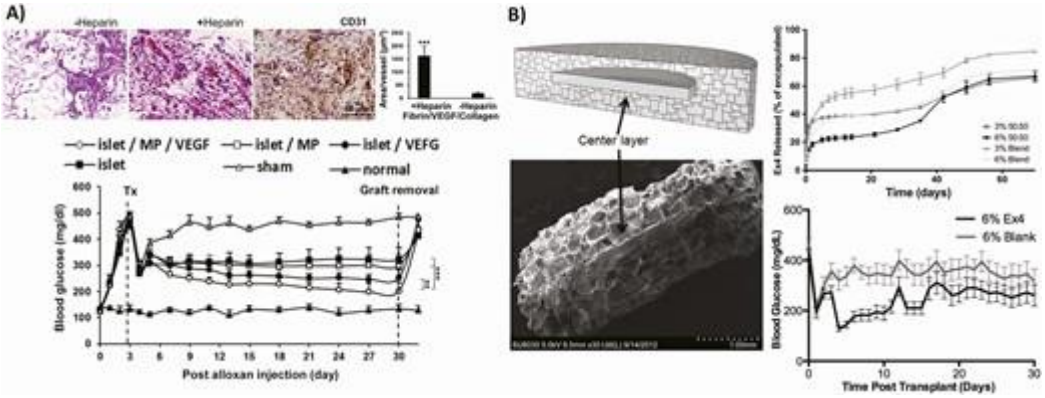


Figure 2.3: Strategies for enhancing survival post transplantation. (A) Fibrin–heparin and VEGF-loaded collagen scaffolds containing oxygen generating microparticles (MPs) enhanced islet revascularization and improved restoration of euglycemia. Adapted from Montazeri L, Hojjati-Emami S, Bonakdar S, et al. Improvement of islet engrafts by enhanced angiogenesis and microparticle-mediated oxygenation. Biomaterials. 2016;89:157–165. doi:10.1016/j.biomaterials.2016.02.043 with permission from Elsevier. (B) Layered microporous PLG scaffolds loaded with the trophic factor exendin-4 enhance restoration of euglycemia compared to blank scaffolds. Adapted from Hlavaty KA, Gibly RF, Zhang X, et al. Enhancing Human Islet Transplantation by Localized Release of Trophic Factors From PLG Scaffolds. Am J Transpl. 2014;14(7):1523–1532. doi:10.1111/ajt.12742 with permission from John Wiley and Sons.

2.5.2 Enhancing integration

Long-term function of the transplanted cells is enabled by integration of the cells with the host vasculature, which can provide the necessary nutrients and allow for the sensing of blood glucose and the distribution of secreted insulin. Long-term islet function is maintained in part through a capillary network among the islets, indicating the need to integrate the cells with the vascular network posttransplantation (65). One of the major barriers to successful integration is

the foreign body response. Viacyte's cell replacement product VC-01 is an encapsulating device used to subcutaneously deliver hPSC-derived pancreatic progenitors. The recent clinical trial of VC-01 showed surviving cells out to 24 months, yet the function and integration of the device were limited by the foreign body response (66). The choice of biocompatible materials and the use of degradable platforms can influence the fibrotic response (67, 68). Microporous scaffolds, and degradable hydrogels support engraftment and revascularization (42, 69, 70). Microporous scaffolds typically have a large surface area to volume ratio, so that the distribution of cells near the surface minimizes the distance to host vasculature and the competition for nutrients. Additionally, the pores of the scaffold are generally sufficiently large to support vessel ingrowth; whereas the degradable hydrogels must undergo local degradation to create space for vessel ingrowth. Collectively, these examples illustrate that multiple strategies are being developed to enhance vascularization and engraftment, including the release of angiogenic factors and cell cotransplantation.

Angiogenic growth factors have been incorporated into scaffolds with the goal of enhancing the rate of vascularization and graft survival and function. The formation of robust vasculature networks depends on many aspects of the microenvironment, and the specific factors needed may differ depending on the properties of the site and the transplantation platform (71). Growth factors such as VEGF, platelet-derived growth factor, and acidic fibroblast growth factor have all been shown to increase vascularization of transplanted scaffolds and decrease time to euglycemia (13-15). The identity of the angiogenic factors, as well as its loading and release rate, can impact both vascularization and function. A collagen scaffold utilizing fibrin-conjugated heparin affinity based release of VEGF showed increased formation of new microvessels compared with control scaffolds containing only fibrin and VEGF (Fig. 2.3A) (62). Local release

of these angiogenic factors increases the rate of vascularization, and importantly used factors that are endogenous to islets and pose minimal risk to the transplanted cells. As mentioned above, FTY720 was able to enhance prevascularization of scaffolds; however, the delivery of cells concurrently with FTY720 decreased islet function and failed to restore euglycemia (72, 73). Furthermore, not all growth factors result in long-term improvement of function. Acidic fibroblast growth factor, in particular, resulted in worse long-term function compared with control groups (15). The scaffold itself may also be modified to induce the expression of angiogenic factors by the transplanted or infiltrating cells. Heparin modified scaffolds upregulated VEGF expression and decreased time to restore euglycemia in diabetic mice when compared with control scaffolds (27). This release or induction of angiogenic factors can be combined with oxygen generating compound, with the coupling of these 2 approaches enhancing function following depletion of the oxygen generators (62). Combination strategies increase complexity of scaffold design, and require careful consideration of possible negative interaction. However, note that incorporation of multiple elements is likely to increase the regulatory burden.

Cotransplantation of support cells with β-cells can enhance integration with the host, and may provide cues that are beneficial to β-cells (74-76). Cotransplant of islets or hPSC-derived β-cells have been conducted with a variety of cell types, including endothelial cells (ECs), parathyroid glands, and fibroblasts (77-80). The mechanism of enhanced engraftment occurs through stimulation of growth factor release (parathyroid glands and ECs stimulate VEGF), and by providing the cells needed to generate new vasculature (ECs) (78, 79). Providing multiple cell types has the potential to recapitulate native pancreatic tissue, which may lead to enhanced function and engraftment. ECs have enhanced the maturation of hPSC-derived pancreatic progenitor cells in vitro (38, 80). An important consideration when designing an EC/β-cell

cotransplantation strategy is that ECs experience increased cell death and dysregulation in elevated glucose environments (81). In order to support engraftment of hPSC-derived β-cells in vivo, ECs must be able to survive the posttransplant environment. Furthermore, the cotransplantation approach may differ for islets, which are already functional for restoring euglycemia, relative to hPSC-derived β-cells that may require further in vivo maturation.

2.5.3 Enhancing function

Local delivery of trophic factors to transplanted β-cells can stimulate receptors and signaling pathways known to regulate survival, proliferation, differentiation, and insulin secretion. The glucagon-like peptide-1 agonist exendin-4 stimulates glucose-dependent insulin secretion in β-cells, promotes β-cell proliferation, and protects against apoptosis (82, 83). In vitro culture of cells in a supporting hydrogel and receiving Exendin-4 had higher insulin secretion and less apoptosis than controls (84). The local and sustained release of exendin-4 allowed for up to a 25% decrease in the number of human islets in order to enhance glycemic control (Fig. 2.3B) (43). Scaffolds similarly releasing exendin-4 were used to support hPSC-derived pancreatic progenitors, and enhance maturation and c-peptide secretion (85). Alternatively, nerve growth factor (NGF) has promoted glucose responsive insulin secretion in β-cells through activation of calcium channels (86). Islets were transplanted into diabetic mice on a gelatin sponge, known as Gelitaspon, with or without NGF (87). Mice receiving islets transplanted on Gelitaspon soaked in 100 ng/mL NGF had significantly lower blood glucose and an improved response to intraperitoneal glucose tolerance test compared with the control group. A number of other trophic factors (Prolactin (88), Growth hormone (GH), also known as somatotropin (16, 43, 82, 83, 89), Hepatocyte growth factor (90), insulin-like growth factor-1 (91,92), Betacellulin, and Activin-A (93)) have been identified with potential to influence β-cell responses

posttransplantation, yet these factors have not been investigated with scaffold based transplantation.

2.6 Immune Protection

The process of immune recognition and immune destruction of transplanted cells for an allogeneic transplantation occurs in a 4-step manner described as follows: (1) inflammation; (2) activation of allogeneic or self-dendritic cells (DCs) and migration to draining lymph nodes; (3) T cell activation by DCs, resulting in expansion of antidonor T cells; and (4) migration of T cells to the graft where they mediate cytotoxicity (16, 94). The development of the Edmonton Protocol dramatically improved clinical outcomes in islet transplantation by using sirolimus, low-dose tacrolimus, and induction anti-interleukin-2 receptor antibody. While improvements have been made in the immunosuppression protocol, these patients require lifelong immunosuppression, which can be problematic for a disease with a juvenile onset (95). The side effects brought by the permanent use of such systemically administered agents include increased vulnerability to infection, cytotoxicity or even diabetogenicity to the transplanted islets/cells. This section describes emerging research counteracting immune recognition and immune destruction, either locally at the site of transplant and/or systemically, that could enhance engraftment of the allogeneic cell transplant.

2.6.1 Local immune modulation

The local modulation of immune responses is motivated by at least 2 observations: (1) that the inflammatory response contributes to islet loss following hepatic infusion (96), and (2) immunoprivileged sites, such as those in the thymus, brain, and testis (46), can limit immune responses without the need for systemic immune suppression. The inflammatory response following cell transplantation reduces transplanted cell survival, often substantially, and is

mediated initially by innate immune cells, whereas adaptive immune cells mediate cell killing in many autoimmune and allogeneic cell transplantations (16). The function of innate and adaptive immune cells can be modulated at immunoprivileged sites in the body, such as the anterior chamber of the eye and the testis. The immunoprivileged properties for both the ocular and testes microenvironments result from a combination of structural features and immunoregulatory and immunosuppressive molecules (97). In the testes, the Sertoli cells provide a physical blood barrier to isolate germ cells from the immune system along with a host of immunoregulatory compounds that suppress proinflammatory responses from the immune cells to maintain the immunoprotected environment (98). The eye and testes are generally not considered translationally relevant due to the large number of islets that would need to be delivered into these small organs. Nevertheless, the basic principles associated with these immunoprivileged microenvironments have served to inspire approaches to protect allogeneic cell transplants at extrahepatic sites.

The local release of cytokines from scaffolds has been employed to modulate the inflammatory reaction and enhance both cell survival and function. These drugs and cytokines stimulate the recruitment of suppressive immune cells or polarize immune cells toward an anti-inflammatory phenotype. Examples of immune regulatory molecules that have been investigated for protection of islets and β-cells include transforming growth factor-β (TGF-β), interleukin (IL)-10, IL-4, C-C motif chemokine ligand 2 (CCL2 [MCP-1]), C-X-C motif chemokine ligand 12 (CXCL12 [SDF1]), indoleamine 2,3-dioxygenase 1 (IDO1), leukotriene B4 (LTB4), IL-33, and prostaglandin E2 (PGE2) (16, 19). An important consideration is the impact these factors have at the specific site of transplantation. While IL-33 exerted graft-protective effects in both murine skin transplant and cardiac transplant models (99-101), IL-33's ability to protect islets

has shown mixed results. IL-33 delivery with islet transplantation into the peritoneal fat IL-33 upregulated graft-protective T cells and prolonged graft survival; however, at this site, IL-33 also led to an increased expression of proinflammatory cytokines responsible for potential host protective immunity (44). TGF-β1 delivered from porous scaffolds downregulated tumor necrosis factor-α, IL-12, and MCP-1 population by at least 40% compared with control scaffolds (102). The transplanted allogenic islets on the TGF-β1 releasing scaffolds had an enhanced engraftment and functioned significantly longer than those transplanted on empty scaffold controls.

Chemokine delivery influences the function of numerous cell types within the environment. CXCL12 delivery protected transplanted islets and stem cell–derived β-cells, through either protection or enhanced function for allogeneic and xenogeneic sources (103). CXCL12 directs monocyte differentiation towards a macrophage phenotype with immunosuppressive functions (17). Additionally, dendritic cells derived following CXCL12 modulation induce activity from antigen-specific regulatory T cells (17, 104). CXCL12 can directly signal to β-cells for survival and regeneration (105), and increased the homing of autologous MSCs and HSCs that can substantially reduce the infiltration of inflammatory cells, and improve blood vessel formation (106, 107).

Chemokines invoked by tumor cells that protect tumors from immune destruction have also been employed for local immunomodulation. CCL22 is released by tumor cells to recruit regulatory T cells (Tregs) to the site through a chemokine receptor (CCR4) expressed on Tregs. Tregs possess potential capabilities of mitigating autoimmunity in T1D and inducing local and systemic tolerogenic effects. This tolerogenic effect is achieved by suppressing T-cell and DC maturation and activation by secreting immunosuppressive factors, such as IL-10 and TGF-β1

(108, 109). Donor-specific tolerance to fully mismatched islet allografts has been achieved by locally recruiting Tregs in CCL22-expressing allografts (Fig. 2.4A) (110-112). Allogeneic islets transduced to express CCL22 conferred prolonged protection and preservation of transplanted murine β-cells from rejection and maintained normoglycemia in 75% of recipients over 80 days, with elevated number of Tregs in the islet grafts and an absence of antidonor antibodies or lymphocyte proliferation after exposure to donor splenocytes. In a different transplant model, CCL22-releasing microparticles delivered locally at a graft prolonged complete MHC mismatched allograft survival over 200 days (111). Effector T cells were significantly reduced in skin and draining lymph nodes of treated transplant recipients, with a resulting tissue architecture similar to muscle and skin biopsies from normal tissue.

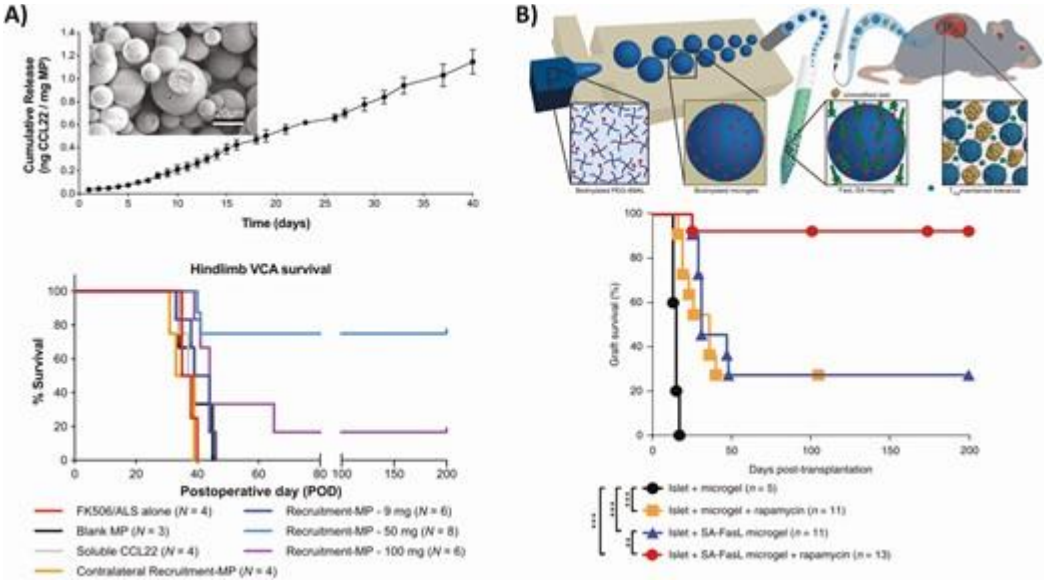


Figure 2.4: Immunomodulation strategies. CCL22 released microparticles in VCA model and Fas-L attached microgels in T1D model. (A) Characterization and 40-day release profile of recruitment-MP. Treatment with Recruitment-MP (50 mg) prolongs allograft survival indefinitely. Hindlimb allograft survival curve showing indefinite survival (>200 days) in 6 of 8 rats treated with Recruitment-MP (50 mg). Adapted from Fisher JD, Zhang W, Balmert SC, et al. In Situ Recruitment of Regulatory T Cells Promotes Donor-Specific Tolerance in Vascularized Composite Allotransplantation. Vol 6.; 2020. http://advances.sciencemag.org/. with permission from Creative Commons Attribution-Non Commercial license. (B) Flow-focusing microfluidics were used to generate biotinylated microgels from biotin-functionalized PEG-4MAL macromers. Islet graft survival: SA-FasL-presenting or control microgels and unmodified BALB/c islets were co-transplanted under the kidney capsule of chemically diabetic C57BL/6 recipients. Adapted from Headen DM, Woodward KB, Coronel MM, et al. Local immunomodulation with Fas ligand-engineered biomaterials achieves allogeneic islet graft acceptance. Nat Mater.

2018;17(8):732–739. doi:10.1038/s41563-018-0099-0 originally published in Nature Materials, with permission from author Dr. Lonnie D. Shea.

Natural immunoprivileged sites often employ constitutive expression of FasL to control the entry of lymphoid cells expressing Fas. A synthetic FasL was developed by Yolcu et al., which consisted of an engineered streptavidin-FasL (SA-FasL) that could be attached to biotinylated pancreatic islet grafts. This FasL modification of islets in combination with a transient course of rapamycin treatment (0.2 mg/kg daily for 15 days) resulted in indefinite survival and function of allogeneic cells in the absence of chronic immunosuppression (113). In another study, graft recipients were also systemically immunomodulated by intraperitoneal injection of donor SA-FasL- engineered splenocytes on days 1, 3, and 5 after the transplantation of the S-FasL-attached islets. This regimen resulted in the survival of all allogeneic islet grafts for the 250-day observation period since SA-FasL protein preferentially induced apoptosis in autoreactive T-effector cells while sparing CD4+CD25+FoxP3+ T-regulatory cells (114). This result has recently been translated to biomaterials used for islet transplantation, with the materials being biotinylated and functionalized with FasL rather than the islets. PEG hydrogel beads modified with FasL that were cotransplanted with islets, or FasL-modified porous PLG scaffolds supported allogeneic islet transplantation and function for over 200 days (Fig. 2.4B) (112, 115). Decreased numbers of both CD4+ and CD8+ T-effector cells and increased number of T-regulatory cells were observed in the tissues of mice receiving SA-FasL-engineered microgels. These islets were transplanted into either the kidney capsule or the epididymal fat pad with transient administration of rapamycin. These islets had sustained survival and normalized blood glucose levels in chemically diabetic graft recipients. Long-term graft recipients generated a normal immune response to donor alloantigens, implicating localized tolerance to the graft.

An alternative to delivery or presenting factors within the environment is to directly transplant cells to modulate the immune response. Biomaterial scaffolds can serve to support the colocalization of the cell types. Perhaps the most widely studied cell type for cotransplantation involves mesenchymal stem cells (MSCs) (116, 117). MSCs, derived from the infrapatellar fat pad, have been cotransplanted with islets in order to capitalize on the immunomodulatory (118) and proangiogenic (119) properties of MSCs. MSC treatment significantly enhanced islet engraftment and function, resulting in stabilized blood glucose levels, reduced exogenous insulin requirement, and increased numbers of regulatory T cells in peripheral blood (120). An alternative to recruiting Tregs is the direct transplantation of Tregs with islets. Tregs cotransplanted with islets on a microporous PLG scaffold provided long-term graft protection from an autoimmune response (121). The seeded Tregs were replaced by recipient-derived Tregs over time, suggesting that host-derived Tregs induce tolerance to islet grafts on the PLG scaffold. Normoglycemia was restored, and cotransplanted Tregs extended graft survival indefinitely in several instances. Interestingly, in this study, local codelivery of Tregs with an initial islet transplant also led to protection against autoimmune destruction of a second islet transplant (without Tregs), indicating systemic tolerance to islet antigens.

2.6.2 Antigen-specific immune modulation

Antigen-specific immune modulation strategies represent a significant opportunity for all cell and solid organ transplantation, which currently employ systemic immunosuppression to prevent rejection of the graft yet is associated with increased risk of infection and neoplasia for the patient. Modulation of systemic immune responses may be an alternative or complementary strategy to local immune modulation. These systemic therapies may be administered prior to cell transplantation, and/or as needed following transplantation. These strategies aim to either (1)

delete autoreactive or alloreactive T cells, (2) induce anergy in the naïve cells, and/or (3) induce the formation of regulatory T cells that can modulate the graft reactive T cells. Immunosuppressive drugs, such as those used in the Edmonton Protocol, function by suppressing the function of one or more cell types in an antigen-independent manner. Localized delivery of these immunosuppressive factors can reduce the required dose and avoid some of the systemic side effects of the compounds (122). This localized delivery strategy can prolong graft survival; however, the graft contains a finite quantity of drug and seems unlikely to support indefinite graft survival and function. Numerous strategies are being investigated, such as pharmaceuticals, nanoparticles, or engineered cells, to limit allograft rejection and have been reviewed elsewhere (123-125), and we describe a few representative examples applied to islet transplantation.

Antigen-specific immune modulation offers the opportunity to prevent rejection of the graft while leaving the remainder of the immune system intact. One approach toward this goal has been the use of donor splenocytes, which have donor antigen and upon treatment with 1-ethyl-3-(3-dimethylaminopropyl)carbodiimide (ECDI) and subsequent intravenous infusion has had success in inducing tolerance in a variety of autoimmune and allotransplant models (18, 126-128). Treated splenocytes, which induce apoptosis in the donor splenocytes, are infused with one dose prior to transplantation and 1 dose posttransplantation. Infusions of ECDI-treated donor splenic antigen-presenting cells result in indefinite survival of allogeneic islet grafts in the absence of immunosuppression (Fig. 2.5A) (18, 129, 130). The site of islet transplantation does influence the effectiveness of tolerance induction, with the kidney capsule and epididymal fat pad having high levels of success, and with 1 report indicating lower levels of tolerance induction in the liver (128). Recently, this approach of ECDI-treated splenocytes has been translated to studies in nonhuman primates using ECDI-treated apoptotic donor leukocytes. The

regimen promoted stable islet allograft tolerance (>356 days) in monkeys by suppressing effector cell expansion and expanding regulatory networks (131).

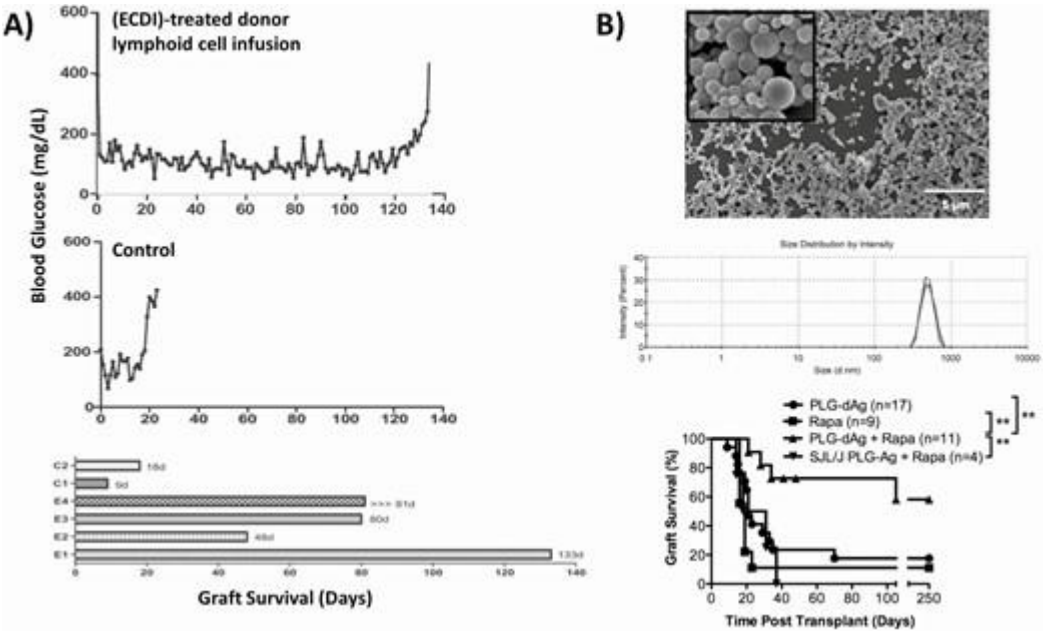


Figure 2.5: Immunomodulation strategies. ECDI-treated donor lymphoid cell infusion and ECDI-attached PLG nanoparticles in T1D model. (A) Glycemic control posttransplant: 4 ECDI-DLI experimental group and 2 control group diabetic nonhuman primates each promptly achieved normoglycemia post-allogeneic islet transplant. Adapted from Lei J, Kim JI, Shi S, et al. Pilot Study Evaluating Regulatory T Cell-Promoting Immunosuppression and Nonimmunogenic Donor Antigen Delivery in a Nonhuman Primate Islet Allotransplantation Model. Am J Transplant. 2015;15(10):2739–2749. doi:10.1111/ajt.13329 with permission from John Wiley and Sons. (B) Scanning transmission electron microscopy image and size of PLG particles prior to lysate coupling with ECDI. A short course of low dose rapamycin with PLG-dAg demonstrated significantly greater islet allograft survival (n = 11) compared with mice treated with rapamycin alone (n = 9) **P < .01. Adapted with permission from Bryant J, Hlavaty KA, Zhang X, et al. Nanoparticle delivery of donor antigens for transplant tolerance in allogeneic islet transplantation. Biomaterials. 2014;35(31):8887–8894. doi:10.1016/j.biomaterials.2014.06.044 with permission from Elsevier.

The capability of ECDI-coupled splenocytes to treat autoimmune disease and prevent transplant rejection has been extended to synthetic nanoparticles, which have the potential for greater consistency in GMP manufacturing that would facilitate translation. In autoimmune models of diabetes, antigen-loaded nanoparticles have been able to prevent islet destruction with nanoparticles administered prior to and after disease initiation (132). Additionally, this approach has been extended to allogeneic cell transplantation by coupling of cell lysates to the nanoparticles and subsequent infusion prior to and after allogeneic cell transplantation (114). The

particles in combination with a 3-day course of low-dose rapamycin were able to induce long-term graft function in the absence of sustained immunosuppression (Fig. 2.5B) (130). The particles were effective at limiting T-cell activation induced by indirect antigen presentation; however, the particles were not able to influence T-cell activation by direct antigen presentation (133). This inability to affect T-cell responses resulting from direct antigen presentation likely reflects that antigen coupling to particles or cells does not appear to modulate activation induced by major antigen mismatch (133).

2.7 Final Thoughts

Substantial advances have been made in recent years for the differentiation of hPSC to β-cells. These advances have substantially raised the prospect of a cell-based therapy for T1D and highlight the critical need for cell manufacturing and delivery systems that can provide adequate numbers of cells that can efficiently engraft and function for long times without the need for sustained immunosuppression. Advances in CRISPR technology may also allow for the engineering of cells that have improved capacity for insulin secretion, or the ability to evade the immune system (134). These opportunities in cellular engineering will benefit from technologies that can provide control over the cellular microenvironment, both during cell manufacturing and following transplantation. These biomaterial platforms provide the tools to sequester key signaling factors, facilitate the organization of cells into structures, support cell–cell and cell–matrix interactions, recruit or deliver accessory cells to aid maturation or function, limit inflammatory responses, and evade the adaptive immune responses. Establishing a supportive environment at the time of manufacture or transplantation can create a stable niche that can support cell function for extended periods of time. Collectively, the capabilities of hPSC-derived

β-cells have advanced, and engineering the microenvironment can help to translate these capabilities.

2.8 Abbreviations

DC, dendritic cell; EC, endothelial cell; ECDI, 1-ethyl-3-(3-dimethylaminopropyl)carbodiimide; ESC, embryonic stem cell; hPSC, human pluripotent stem cell; IBMIR, instant blood-mediated inflammatory reaction; IL, interleukin; iPSC, induced pluripotent stem cell; MSC, mesenchymal stem cell; NGF, nerve growth factor; PEG, polyethylene glycol; PLG, poly (lactide-co-glycolide); PTH, parathyroid gland; T1D, type I diabetes mellitus; TGF, transforming growth factor; Treg, regulatory T cell; VEGF, vascular endothelial growth factor.

2.9 Acknowledgments

Financial Support: Funding for this work was provided by NIH R01 EB009910, R21AI147677, and the Juvenile Diabetes Research Foundation (JDRF).

2.10 Additional Information

Disclosure Summary: L.D.S. consults for and has financial interests in Cour Pharmaceuticals.

2.11 Data Availability

Data sharing is not applicable to this article as no datasets were generated or analyzed during the current study.

This work was published as doi: 10.1210/endocr/bqaa156.

2.12 References

1. Oliver N, Gimenez M, Calhoun P, et al. Continuous glucose monitoring in people with type 1 diabetes on multiple-dose injection therapy: the relationship between glycemic control and hypoglycemia. Diabetes Care. 2020;43(1):53-58.

2. Tamborlane WV, Beck RW, Bode BW, et al. Continuous glucose monitoring and intensive treatment of type 1 diabetes. N Engl J Med. 2008;359(14):1464–1476.
3. Dassau E, Zisser H, Harvey RA, et al. Clinical evaluation of a personalized artificial pancreas. Diabetes Care. 2013;36(4):801-809.
4. McCall M, Shapiro AM. Update on islet transplantation. Cold Spring Harb Perspect Med. 2012;2(7):a007823.
5. Holmes-Walker DJ, Gunton JE, Hawthorne W, et al. Islet transplantation provides superior glycemic control with less hypoglycemia compared with continuous subcutaneous insulin infusion or multiple daily insulin injections. Transplantation. 2017;101(6):1268-1275.
6. Langer RM. Islet transplantation: lessons learned since the Edmonton breakthrough. Transplant Proc. 2010;42(5):1421–1424.
7. Hering BJ, Walawalkar N. Pig-to-nonhuman primate islet xenotransplantation. Transpl Immunol. 2009;21(2):81-86.
8. Pagliuca FW, Millman JR, Gürtler M, et al. Generation of functional human pancreatic β cells in vitro. Cell. 2014;159(2):428-439.
9. Hogrebe NJ, Augsornworawat P, Maxwell KG, Velazco-Cruz L, Millman JR. Targeting the cytoskeleton to direct pancreatic differentiation of human pluripotent stem cells. Nat Biotechnol. 2020;38(4):460-470.
10. Velazco-Cruz L, Song J, Maxwell KG, et al. Acquisition of dynamic function in human stem cell-derived β cells. Stem Cell Reports. 2019;12(2):351-365.
11. Rezania A, Bruin JE, Arora P, et al. Reversal of diabetes with insulin-producing cells derived in vitro from human pluripotent stem cells. Nat Biotechnol. 2014;32(11):1121-1133.

12. Helman A, Melton DA. A stem cell approach to cure type 1 diabetes. [Published online ahead of print, March 2, 2020]. Cold Spring Harb Perspect Biol. 2020:a035741. doi:10.1101/cshperspect.a035741
13. Gebe JA, Preisinger A, Gooden MD, D'Amico LA, Vernon RB. Local, controlled release in vivo of vascular endothelial growth factor within a subcutaneous scaffolded islet implant reduces early islet necrosis and improves performance of the graft. Cell Transplant. 2018;27(3):531-541.
14. Brady AC, Martino MM, Pedraza E, et al. Proangiogenic hydrogels within macroporous scaffolds enhance islet engraftment in an extrahepatic site. Tissue Eng Part A. 2013;19(23-24):2544-2552.
15. Smink AM, Li S, Swart DH, et al. Stimulation of vascularization of a subcutaneous scaffold applicable for pancreatic islet-transplantation enhances immediate post-transplant islet graft function but not long-term normoglycemia. J Biomed Mater Res A. 2017;105(9):2533-2542.
16. Gibly RF, Graham JG, Luo X, Lowe WL Jr, Hering BJ, Shea LD. Advancing islet transplantation: from engraftment to the immune response. Diabetologia. 2011;54(10):2494-2505.17. Sánchez-Martín L, Estecha A, Samaniego R, Sánchez-Ramón S, Vega MÁ, Sánchez-Mateos P. The chemokine CXCL12 regulates monocyte-macrophage differentiation and RUNX3 expression. Blood. 2011;117(1):88-97.

Google ScholarCrossref Find in my library PubMedWorldCat

18. Luo X, Pothoven KL, McCarthy D, et al. ECDI-fixed allogeneic splenocytes induce donor-specific tolerance for long-term survival of islet transplants via two distinct mechanisms. Proc Natl Acad Sci U S A. 2008;105(38):14527-14532.

19. Desai T, Shea LD. Advances in islet encapsulation technologies. Nat Rev Drug Discov. 2017;16(5):367.
20. Vegas AJ, Veiseh O, Gürtler M, et al. Long-term glycemic control using polymer-encapsulated human stem cell-derived beta cells in immune-competent mice. Nat Med. 2016;22(3):306–311.
21. Stock AA, Manzoli V, De Toni T, et al. Conformal coating of stem cell-derived islets for β cell replacement in type 1 diabetes. Stem Cell Reports. 2020;14(1):91-104.
22. Blomeier H, Zhang X, Rives C, et al. Polymer scaffolds as synthetic microenvironments for extrahepatic islet transplantation. Transplantation. 2006;82(4):452-459.
23. Berman DM, O'Neil JJ, Coffey LC, et al. Long-term survival of nonhuman primate islets implanted in an omental pouch on a biodegradable scaffold. Am J Transplant. 2009;9(1):91-104.
24. Salvay DM, Rives CB, Zhang X, et al. Extracellular matrix protein-coated scaffolds promote the reversal of diabetes after extrahepatic islet transplantation. Transplantation. 2008;85(10):1456-1464.
25. Gibly RF, Zhang X, Graham ML, et al. Extrahepatic islet transplantation with microporous polymer scaffolds in syngeneic mouse and allogeneic porcine models. Biomaterials. 2011;32(36):9677–9684.
26. Jiang K, Weaver JD, Li Y, Chen X, Liang J, Stabler CL. Local release of dexamethasone from macroporous scaffolds accelerates islet transplant engraftment by promotion of anti-inflammatory M2 macrophages. Biomaterials. 2017;114:71-81.

27. Mao D, Zhu M, Zhang X, et al. A macroporous heparin-releasing silk fibroin scaffold improves islet transplantation outcome by promoting islet revascularisation and survival. Acta Biomater. 2017;59:210-220.
28. Rios PD, Skoumal M, Liu J, et al. Evaluation of encapsulating and microporous nondegradable hydrogel scaffold designs on islet engraftment in rodent models of diabetes. Biotechnol Bioeng. 2018;115(9):2356-2364.
29. Youngblood RL, Sampson JP, Lebioda KR, Shea LD. Microporous scaffolds support assembly and differentiation of pancreatic progenitors into β-cell clusters. Acta Biomater. 2019;96:111-122.
30. Lee B, Borys BS, Kallos MS, Rodrigues CA V, Silva TP, Cabral JMS. Challenges and solutions for commercial scale manufacturing of allogeneic pluripotent stem cell products. Bioengineering. 2020;7(2):31.
31. Legøy TA, Vethe H, Abadpour S, et al. Encapsulation boosts islet-cell signature in differentiating human induced pluripotent stem cells via integrin signalling. Sci Rep. 2020;10(1):414.
32. Niknamasl A, Ostad SN, Soleimani M, et al. A new approach for pancreatic tissue engineering: human endometrial stem cells encapsulated in fibrin gel can differentiate to pancreatic islet beta-cell. Cell Biol Int. 2014;38(10):1174-1182.
33. Augsornworawat P, Velazco-Cruz L, Song J, Millman JR. A hydrogel platform for in vitro three dimensional assembly of human stem cell-derived islet cells and endothelial cells. Acta Biomater. 2019;97:272-280.
34. Wang W, Jin S, Ye K. Development of islet organoids from H9 human embryonic stem cells in biomimetic 3D scaffolds. Stem Cells Dev. 2017;26(6):394-404.

35. Hughes CS, Postovit LM, Lajoie GA. Matrigel: a complex protein mixture required for optimal growth of cell culture. Proteomics. 2010;10(9):1886-1890.
36. Rezakhani S, Gjorevski N, Lutolf MP. Low-defect Thiol-Michael addition hydrogels as Matrigel substitutes for epithelial organoid derivation. Adv Funct Mater. 2020:2000761. doi:10.1002/adfm.202000761
37. Bao L, Matsumura Y, Baban D, Sun Y, Tarin D. Effects of inoculation site and Matrigel on growth and metastasis of human breast cancer cells. Br J Cancer. 1994;70(2):228-232.
38. Candiello J, Grandhi TSP, Goh SK, et al. 3D heterogeneous islet organoid generation from human embryonic stem cells using a novel engineered hydrogel platform. Biomaterials. 2018;177:27-39.
39. Borg DJ, Bonifacio E. The use of biomaterials in islet transplantation. Curr Diab Rep. 2011;11(5):434-444.
40. Xu L, Guo Y, Huang Y, Xu Y, Lu Y, Wang Z. Hydrogel materials for the application of islet transplantation. J Biomater Appl. 2019;33(9):1252-1264.
41. Lehmann R, Zuellig RA, Kugelmeier P, et al. Superiority of small islets in human islet transplantation. Diabetes. 2007;56(3):594-603.
42. Gibly RF, Zhang X, Lowe WL Jr, Shea LD. Porous scaffolds support extrahepatic human islet transplantation, engraftment, and function in mice. Cell Transplant. 2013;22(5):811-819.
43. Hlavaty KA, Gibly RF, Zhang X, et al. Enhancing human islet transplantation by localized release of trophic factors from PLG scaffolds. Am J Transplant. 2014;14(7):1523-1532.

44. Liu JMH, Zhang X, Joe S, Luo X, Shea LD. Evaluation of biomaterial scaffold delivery of IL-33 as a localized immunomodulatory agent to support cell transplantation in adipose tissue. J Immunol Regen Med. 2018;1:1-12.
45. Carlsson PO, Nordin A, Palm F. pH is decreased in transplanted rat pancreatic islets. Am J Physiol Endocrinol Metab. 2003;284(3):E499-E504.
46. Merani S, Toso C, Emamaullee J, Shapiro AM. Optimal implantation site for pancreatic islet transplantation. Br J Surg. 2008;95(12):1449-1461.
47. van der Windt DJ, Echeverri GJ, Ijzermans JN, Cooper DK. The choice of anatomical site for islet transplantation. Cell Transplant. 2008;17(9):1005-1014.
48. Vériter S, Gianello P, Dufrane D. Bioengineered sites for islet cell transplantation. Curr Diab Rep. 2013;13(5):745-755.
49. Svensson J, Lau J, Sandberg M, Carlsson PO. High vascular density and oxygenation of pancreatic islets transplanted in clusters into striated muscle. Cell Transplant. 2011;20(5):783-788.
50. Pepper AR, Gala-Lopez B, Pawlick R, Merani S, Kin T, Shapiro AM. A prevascularized subcutaneous device-less site for islet and cellular transplantation. Nat Biotechnol. 2015;33(5):518-523.
51. Bowers DT, Chhabra P, Langman L, Botchwey EA, Brayman KL. FTY720-loaded poly(DL-lactide-co-glycolide) electrospun scaffold significantly increases microvessel density over 7 days in streptozotocin-induced diabetic C57b16/J mice: preliminary results. Transplant Proc. 2011;43(9):3285-3287.

52. Kasoju N, Pátíková A, Wawrzynska E, et al. Bioengineering a pre-vascularized pouch for subsequent islet transplantation using VEGF-loaded polylactide capsules. Biomater Sci. 2020;8(2):631-647.
53. Smink AM, Li S, Hertsig DT, et al. The efficacy of a prevascularized, retrievable Poly(D,L,-lactide-co-ε-caprolactone) subcutaneous scaffold as transplantation site for pancreatic islets. Transplantation. 2017;101(4):e112-e119.
54. Smink AM, Hertsig DT, Schwab L, et al. A retrievable, efficacious polymeric scaffold for subcutaneous transplantation of rat pancreatic islets. Ann Surg. 2017;266(1):149-157.
55. Weaver JD, Headen DM, Aquart J, et al. Vasculogenic hydrogel enhances islet survival, engraftment, and function in leading extrahepatic sites. Sci Adv. 2017;3(6):e1700184.
56. US National Library of Medicine. ClinicalTrails.gov. A safety, tolerability and efficacy study of Sernova's Cell Pouch for clinical islet transplantation. https://clinicaltrials.gov/ct2/show/study/NCT03513939. https://clinicaltrials.gov/ct2/show/NCT01652911.
57. Colton CK WG. Commentary – A hard lesson about transplanting islets into prevascularized devices – CellR4. CellR4. 2017. https://www.cellr4.org/article/2251. Accessed August 8, 2020.
58. Rivas-Carrillo JD, Soto-Gutierrez A, Navarro-Alvarez N, et al. Cell-permeable pentapeptide V5 inhibits apoptosis and enhances insulin secretion, allowing experimental single-donor islet transplantation in mice. Diabetes. 2007;56(5):1259-1267.
59. Barkai U, Weir GC, Colton CK, et al. Enhanced oxygen supply improves islet viability in a new bioartificial pancreas. Cell Transplant. 2013;22(8):1463-1476.

60. Neufeld T, Ludwig B, Barkai U, et al. The efficacy of an immunoisolating membrane system for islet xenotransplantation in minipigs. PLoS One. 2013;8(8):e70150.
61. Carlsson PO, Espes D, Sedigh A, et al. Transplantation of macroencapsulated human islets within the bioartificial pancreas βAir to patients with type 1 diabetes mellitus. Am J Transplant. 2018;18(7):1735-1744.
62. Montazeri L, Hojjati-Emami S, Bonakdar S, et al. Improvement of islet engrafts by enhanced angiogenesis and microparticle-mediated oxygenation. Biomaterials. 2016;89:157-165.
63. Coronel MM, Liang JP, Li Y, Stabler CL. Oxygen generating biomaterial improves the function and efficacy of beta cells within a macroencapsulation device. Biomaterials. 2019;210:1-11.
64. Razavi M, Primavera R, Kevadiya BD, Wang J, Buchwald P, Thakor AS. A collagen based cryogel bioscaffold that generates oxygen for islet transplantation. Adv Funct Mater. 2020:1902463. doi:10.1002/adfm.201902463
65. Ballian N, Brunicardi FC. Islet vasculature as a regulator of endocrine pancreas function. 2007;31:705–714.
66. Henry RR, Pettus J, Wilensky J, et al. Initial clinical evaluation of VC-01TM combination product—a stem cell–derived islet replacement for Type 1 Diabetes (T1D). Diabetes. 2018;67(Suppl 1):138-OR.
67. Vegas AJ, Veiseh O, Doloff JC, et al. Combinatorial hydrogel library enables identification of materials that mitigate the foreign body response in primates. Nat Biotechnol. 2016;34(3):345–352.

68. Veiseh O, Doloff JC, Ma M, et al. Size- and shape-dependent foreign body immune response to materials implanted in rodents and non-human primates. Nat Mater. 2015;14(6):643-651.
69. Buitinga M, Assen F, Hanegraaf M, et al. Micro-fabricated scaffolds lead to efficient remission of diabetes in mice. Biomaterials. 2017;135:10-22.
70. Dufour JM, Rajotte RV, Zimmerman M, et al. Development of an ectopic site for islet transplantation, using biodegradable scaffolds. Tissue Eng. 2005;11(9-10):1323-1331.
71. Yancopoulos GD, Davis S, Gale NW, Rudge JS, Wiegand SJ, Holash J. Vascular-specific growth factors and blood vessel formation. Nature. 2000;407(6801):242-248.
72. Bowers DT, Olingy CE, Chhabra P, et al. An engineered macroencapsulation membrane releasing FTY720 to precondition pancreatic islet transplantation. J Biomed Mater Res B Appl Biomater. 2018:1–26.
73. Frei AW, Li Y, Jiang K, Buchwald P, Stabler CL. Local delivery of fingolimod from three-dimensional scaffolds impacts islet graft efficacy and microenvironment in a murine diabetic model. J Tissue Eng Regen Med. 2018;12(2):393-404.
74. Lebreton F, Lavallard V, Bellofatto K, et al. Insulin-producing organoids engineered from islet and amniotic epithelial cells to treat diabetes. Nat Commun. 2019;10(1):4491.
75. Song W, Chiu A, Wang LH, et al. Engineering transferrable microvascular meshes for subcutaneous islet transplantation. Nat Commun. 2019;10(1):4602.
76. Forbes S, Bond AR, Thirlwell KL, et al. Human umbilical cord perivascular cells improve human pancreatic islet transplant function by increasing vascularization. Sci Transl Med. 2020;12(526):5907.

77. Li Y, Fan P, Ding XM, et al. Polyglycolic acid fibrous scaffold improving endothelial cell coating and vascularization of islet. Chin Med J (Engl). 2017;130(7):832–839.
78. Faleo G, Ward C, Parent A, et al. Co-transplant of parathyroid gland and stem cell-derived insulin-producing cells enhances graft survival through release of pro-angiogenic and pro-survival factors. Transplantation. 2018;102:S350.
79. Kaufman-Francis K, Koffler J, Weinberg N, Dor Y, Levenberg S. Engineered vascular beds provide key signals to pancreatic hormone-producing cells. PLoS One. 2012;7(7):e40741.
80. Weizman A, Michael I, Wiesel-Motiuk N, Rezania A, Levenberg S. The effect of endothelial cells on hESC-derived pancreatic progenitors in a 3D environment. Biomater Sci. 2014;2(11):1706-1714.
Google ScholarCrossref Find in my library PubMedWorldCat
81. Wang X, Ackermann M, Neufurth M, et al. Restoration of impaired metabolic energy balance (ATP pool) and tube formation potential of endothelial cells under “high glucose,” diabetic conditions by the bioinorganic polymer polyphosphate. Polymers (Basel). 2017;9(11).
82. Li L, El-Kholy W, Rhodes CJ, Brubaker PL. Glucagon-like peptide-1 protects beta cells from cytokine-induced apoptosis and necrosis: role of protein kinase B. Diabetologia. 2005;48(7):1339-1349.
83. Göke R, Fehmann HC, Linn T, et al. Exendin-4 is a high potency agonist and truncated exendin-(9-39)-amide an antagonist at the glucagon-like peptide 1-(7-36)-amide receptor of insulin-secreting beta-cells. J Biol Chem. 1993;268(26):19650-19655.

84. Duncanson S, Sambanis A. Dual factor delivery of CXCL12 and Exendin-4 for improved survival and function of encapsulated beta cells under hypoxic conditions. Biotechnol Bioeng. 2013;110(8):2292-2300.
85. Kasputis T, Clough D, Noto F, Rychel K, Dye B, Shea LD. Microporous polymer scaffolds for the transplantation of embryonic stem cell derived pancreatic progenitors to a clinically translatable site for the treatment of type I diabetes. ACS Biomater Sci Eng. 2018;4(5):1770-1778.
86. Rosenbaum T, Sánchez-Soto MC, Hiriart M. Nerve growth factor increases insulin secretion and barium current in pancreatic beta-cells. Diabetes. 2001;50(8):1755-1762.
87. Hussey AJ, Winardi M, Wilson J, et al. Pancreatic islet transplantation using vascularised chambers containing nerve growth factor ameliorates hyperglycaemia in diabetic mice. Cells Tissues Organs. 2010;191(5):382-393.
88. Johansson M, Olerud J, Jansson L, Carlsson PO. Prolactin treatment improves engraftment and function of transplanted pancreatic islets. Endocrinology. 2009;150(4):1646-1653.
89. Huang Y, Chang Y. Regulation of pancreatic islet beta-cell mass by growth factor and hormone signaling. In: Progress in Molecular Biology and Translational Science. Vol 121. Elsevier BV; 2014:321–349.
90. Garcia-Ocaña A, Takane KK, Syed MA, Philbrick WM, Vasavada RC, Stewart AF. Hepatocyte growth factor overexpression in the islet of transgenic mice increases beta cell proliferation, enhances islet mass, and induces mild hypoglycemia. J Biol Chem. 2000;275(2):1226-1232.

91. Liu W, Chin-Chance C, Lee EJ, Lowe WL Jr. Activation of phosphatidylinositol 3-kinase contributes to insulin-like growth factor I-mediated inhibition of pancreatic beta-cell death. Endocrinology. 2002;143(10):3802-3812.
92. Giannoukakis N, Mi Z, Rudert WA, Gambotto A, Trucco M, Robbins P. Prevention of beta cell dysfunction and apoptosis activation in human islets by adenoviral gene transfer of the insulin-like growth factor I. Gene Ther. 2000;7(23):2015-2022.
93. Li L, Yi Z, Seno M, Kojima I. Activin A and betacellulin: effect on regeneration of pancreatic beta-cells in neonatal streptozotocin-treated rats. Diabetes. 2004;53(3):608-615.
94. Mellor AL, Munn DH. Creating immune privilege: active local suppression that benefits friends, but protects foes. Nat Rev Immunol. 2008;8(1):74-80.
95. Nanji SA, Shapiro AM. Islet transplantation in patients with diabetes mellitus: choice of immunosuppression. Biodrugs. 2004;18(5):315-328.
96. Tomei AA. engineering confined and prevascularized sites for islet transplantation. Transplantation. 2018;102(11): 1793-1794.
97. Taylor AW. Ocular immune privilege. Eye (Lond). 2009;23:1885–1889.
98. Ar'Rajab A, Dawidson IJ, Harris RB, Sentementes JT. Immune privilege of the testis for islet xenotransplantation (rat to mouse). Cell Transplant. 1994;3(6):493-498.
99. Gajardo T, Morales RA, Campos-Mora M, Campos-Acuña J, Pino-Lagos K. Exogenous interleukin-33 targets myeloid-derived suppressor cells and generates periphery-induced Foxp3^{+} regulatory T cells in skin-transplanted mice. Immunology. 2015;146(1):81-88.

100. Turnquist HR, Zhao Z, Rosborough BR, et al. IL-33 expands suppressive CD11b+ Gr-1(int) and regulatory T cells, including ST2L+ Foxp3+ cells, and mediates regulatory T cell-dependent promotion of cardiac allograft survival. J Immunol. 2011;187(9):4598-4610.
101. Yin H, Li XY, Jin XB, et al. IL-33 prolongs murine cardiac allograft survival through induction of TH2-type immune deviation. Transplantation. 2010;89(10):1189-1197.
102. Liu JMH, Zhang J, Zhang X, et al. Transforming growth factor-beta 1 delivery from microporous scaffolds decreases inflammation post-implant and enhances function of transplanted islets. Biomaterials. 2016;80:11-19.
103. Chen T, Yuan J, Duncanson S, et al. Alginate encapsulant incorporating CXCL12 supports long-term allo- and xenoislet transplantation without systemic immune suppression. Am J Transplant. 2015;15(3):618–627.
104. Karin N. The multiple faces of CXCL12 (SDF-1alpha) in the regulation of immunity during health and disease. J Leukoc Biol. 2010;88(3):463-473.
105. Alagpulinsa DA, Cao JJL, Sobell D, Poznansky MC. Harnessing CXCL12 signaling to protect and preserve functional β-cell mass and for cell replacement in type 1 diabetes. Pharmacol Ther. 2019;193:63-74.
106. Alagpulinsa DA, Cao JJL, Driscoll RK, et al. Alginate-microencapsulation of human stem cell-derived β cells with CXCL12 prolongs their survival and function in immunocompetent mice without systemic immunosuppression. Am J Transplant. 2019;19(7):1930-1940.
107. Thevenot PT, Nair AM, Shen J, Lotfi P, Ko CY, Tang L. The effect of incorporation of SDF-1alpha into PLGA scaffolds on stem cell recruitment and the inflammatory response. Biomaterials. 2010;31(14):3997-4008.

108. Shevach EM. Mechanisms of foxp3+ T regulatory cell-mediated suppression. Immunity. 2009;30(5):636-645.
109. Nakamura K, Kitani A, Strober W. Cell contact-dependent immunosuppression by CD4(+)CD25(+) regulatory T cells is mediated by cell surface-bound transforming growth factor beta. J Exp Med. 2001;194(5):629-644.
110. Montane J, Obach M, Alvarez S, et al. CCL22 prevents rejection of mouse islet allografts and induces donor-specific tolerance. Cell Transplant. 2015;24(10):2143-2154.
111. Fisher JD, Zhang W, Balmert SC, et al. In situ recruitment of regulatory T cells promotes donor-specific tolerance in vascularized composite allotransplantation. Sci Adv. 2020;6(11):eaax8429.
112. Headen DM, Woodward KB, Coronel MM, et al. Local immunomodulation Fas ligand-engineered biomaterials achieves allogeneic islet graft acceptance. Nat Mater. 2018;17(8):732-739.
113. Yolcu ES, Zhao H, Bandura-Morgan L, et al. Pancreatic islets engineered with SA-FasL protein establish robust localized tolerance by inducing regulatory T cells in mice. J Immunol. 2011;187(11):5901-5909.
114. Yolcu ES, Zhao H, Shirwan H. Immunomodulation with SA-FasL protein as an effective means of preventing islet allograft rejection in chemically diabetic NOD mice. Transplantation Proc. 2013;45:1889–1891.
115. Skoumal M, Woodward KB, Zhao H, et al. Localized immune tolerance from FasL-functionalized PLG scaffolds. Biomaterials. 2019;192:271-281.

116. Gamble A, Pawlick R, Pepper AR, et al. Improved islet recovery and efficacy through co-culture and co-transplantation of islets with human adipose-derived mesenchymal stem cells. PLoS One. 2018;13(11):e0206449.

117. Domínguez-Bendala J, Lanzoni G, Inverardi L, Ricordi C. Concise review: mesenchymal stem cells for diabetes. Stem Cells Transl Med. 2012;1(1):59-63.

118. Abdi R, Fiorina P, Adra CN, Atkinson M, Sayegh MH. Immunomodulation by mesenchymal stem cells: a potential therapeutic strategy for type 1 diabetes. Diabetes. 2008;57(7):1759-1767.

119. Wu Y, Chen L, Scott PG, Tredget EE. Mesenchymal stem cells enhance wound healing through differentiation and angiogenesis. Stem Cells. 2007;25(10):2648-2659.

120. Berman DM, Willman MA, Han D, et al. Mesenchymal stem cells enhance allogeneic islet engraftment in nonhuman primates. Diabetes. 2010;59(10):2558-2568.

121. Graham JG, Zhang X, Goodman A, et al. PLG scaffold delivered antigen-specific regulatory T cells induce systemic tolerance in autoimmune diabetes. Tissue Eng Part A. 2013;19(11-12):1465-1475.

122. Gajanayake T, Olariu R, Leclère FM, et al. A single localized dose of enzyme-responsive hydrogel improves long-term survival of a vascularized composite allograft. Sci Transl Med. 2014;6(249):249ra110.

123. Pearson RM, Casey LM, Hughes KR, Miller SD, Shea LD. In vivo reprogramming of immune cells: technologies for induction of antigen-specific tolerance. Adv Drug Deliv Rev. 2017;114:240-255.

124. Leventhal JR, Ildstad ST. Tolerance induction in HLA disparate living donor kidney transplantation by facilitating cell-enriched donor stem cell Infusion: the importance of durable chimerism. Hum Immunol. 2018;79(5):272-276.

125. Raffin C, Vo LT, Bluestone JA. Treg cell-based therapies: challenges and perspectives. Nat Rev Immunol. 2020;20(3):158-172.

126. Getts DR, McCarthy DP, Miller SD. Exploiting apoptosis for therapeutic tolerance induction. J Immunol. 2013;191(11):5341-5346.

127. Serra P, Santamaria P. Antigen-specific therapeutic approaches for autoimmunity. Nat Biotechnol. 2019;37(3):238-251.

128. Kheradmand T, Wang S, Bryant J, et al. Ethylenecarbodiimide-fixed donor splenocyte infusions differentially target direct and indirect pathways of allorecognition for induction of transplant tolerance. J Immunol. 2012;189(2):804-812.

129. Lei J, Kim JI, Shi S, et al. Pilot study evaluating regulatory T cell-promoting immunosuppression and nonimmunogenic donor antigen delivery in a nonhuman primate islet allotransplantation model. Am J Transplant. 2015;15(10):2739-2749.

130. Bryant J, Hlavaty KA, Zhang X, et al. Nanoparticle delivery of donor antigens for transplant tolerance in allogeneic islet transplantation. Biomaterials. 2014;35(31):8887-8894.

131. Singh A, Ramachandran S, Graham ML, et al. Long-term tolerance of islet allografts in nonhuman primates induced by apoptotic donor leukocytes. Nat Commun. 2019;10(1):3495.

132. Hunter Z, McCarthy DP, Yap WT, et al. A biodegradable nanoparticle platform for the induction of antigen-specific immune tolerance for treatment of autoimmune disease. ACS Nano. 2014;8(3):2148-2160.

133. Shah S, Daneshmandi S, Hughes KR, et al. Optimizing PLG nanoparticle-peptide delivery platforms for transplantation tolerance using an allogeneic skin transplant model. Biomaterials. 2019;210:70-82.

134. Lanza R, Russell DW, Nagy A. Engineering universal cells that evade immune detection. Nat Rev Immunol. 2019;19(12):723-733.

Chapter 3 Polymer Scaffolds Delineate Healthy from Diseased States at Sites Distal from the Pancreas in Two Models of Type 1 Diabetes

3.1 Authors

Jessica L. King, Russell R. Urie, Aaron H. Morris, Laila Rad, Elizabeth Bealer, Tadas Kasputis, and Lonnie D. Shea

3.2 Abstract

Type 1 Diabetes (T1D) prevention is currently limited by the lack of diagnostic tools able to identify disease prior to autoimmune destruction of the pancreatic β cells. Autoantibody tests are used to predict risk and, in combination with glucose dysregulation indicative of β-cell loss, to determine administration of immunotherapies. Our objective was to remotely identify immune changes associated with the disease, and we have employed a subcutaneously implanted microporous poly(e-caprolactone) (PCL) scaffold to function as an immunological niche (IN) in two models of T1D. Biopsy and analysis of the IN enables disease monitoring using transcriptomic changes at a distal site from autoimmune destruction of the pancreas, thereby gaining cellular level information about disease without the need for a biopsy of the native organ. Using this approach, we identified gene signatures that stratify healthy and diseased mice in both an adoptive transfer model and a spontaneous onset model of T1D. The gene signatures identified herein demonstrate the ability of the IN to identify immune activation associated with diabetes across models.

3.3 Introduction

Type 1 diabetes (T1D) is an autoimmune disease that affects an estimated 8.4 million people globally (Gregory et al., 2022). The diagnosis of T1D frequently occurs following the irreversible autoimmune destruction of the pancreatic β cells, which leads to patients with T1D requiring lifelong exogenous insulin therapy to maintain normal blood glucose levels. Insulin therapy is associated with a high burden of care due to the need for constant monitoring of blood glucose levels (Balcázar-Hernández et al., 2023; Commissariat et al., 2020). Even with diligent monitoring, glucose levels often leave the normal range, leaving people at risk for long-term complications (Tamborlane et al., 2008). While the development of insulin pumps and continuous blood glucose monitors have improved the management of this disease for those with access to them, the lifelong need for exogenous insulin administration remains.

New immunotherapies are emerging to preserve native islet function and prevent autoimmune destruction of β cells, and detection strategies that identify the earliest stages of disease could guide administration of these therapies. Antibody treatments, such as the FDA approved teplizumab that delays disease onset, and other emerging therapies (Bluestone et al., 2021; Herold et al., 2019; Sims et al., 2021) offer the opportunity to preserve islet mass and function in individuals with recent disease onset. Currently, the administration of teplizumab is indicated for patients diagnosed with stage 2 T1D, when patients test positive for two autoantibodies and demonstrate glucose dysregulation, the latter of which is indicative of β cell loss (Keam, 2023). Thus, the therapy is not applied until some tissue loss has occurred. Furthermore, these therapeutics have associated risks, and their efficacy is dependent on the timing of administration (Ramos et al., 2023). As a result, these therapies require identifying the timing of disease onset to ensure they are administered at the correct time and to the correct patients. Blood tests have been the most investigated approach for determining disease onset,

which has led to the identification of autoantibodies that convey a risk status but are not a definitive indicator for time to disease onset (Jacobsen et al., 2020; Taplin & Barker, 2008; Ziegler et al., 2013). Consequently, advanced screening tools that identify disease through monitoring of immunological changes targeting β cells rather than waiting for symptom onset has the potential to provide immunotherapies that can preserve greater β cell mass.

In this report, we investigated the feasibility of employing a microporous scaffold as an immunological niche (IN) to identify changes in immune activity with the onset of Type 1 Diabetes. We employed poly(e-caprolactone) (PCL) scaffolds implanted at a subcutaneous site, with the scaffold becoming infiltrated with host tissue and vascularized, leading to the recruitment of immune cells due to the foreign body response (Lutzweiler et al., 2020). Changes within the microenvironment of the IN have been correlated with the changes observed in diseased tissues for models of cancer, multiple sclerosis, and transplant rejection (Bushnell et al., 2019; Morris et al., 2020; Oakes et al., 2020; Urie et al., 2024). Additionally, work in the multiple sclerosis and transplant models demonstrates that blood measurements alone are insufficient to delineate healthy and diseased groups (Morris et al., 2020; Urie et al., 2024). Thus, the IN may serve as a surrogate to the pancreas to identify immune responses, with the IN being more accessible for biopsy than the pancreas, and capable of capturing immune changes that are not apparent in the blood. We investigated the feasibility of the IN in two models of T1D, (1) the NOD/ShiLtJ (NOD) mouse and (2) NOD.Cg-Prkdcscid/J (NOD.scid) mice adoptively transferred with BDC2.5 reactive T cells. Gene expression analyses from the cells in the IN were used to create signatures that separate samples taken before and after disease. The two signatures demonstrate our ability to distinguish the diabetic diseased state from pre-

symptomatic conditions from a remote site. These signatures and the methods used to obtain them may provide a framework for enhanced disease monitoring.

3.4 Results

3.4.1 Immune cell trafficking to the IN exhibits similar dynamics to the pancreas

We initially investigated the immune cell types in the pancreas and the IN across disease. Flow cytometry of explanted pancreas tissue and INs was performed at 3 timepoints in NOD mice (Figure 3.1A). Blood glucose levels showed that no mice were diabetic at the 7- and 11-week time points, and 2 of 7 mice were diabetic at the 15-week time point (Figure 3.1B). Flow cytometry of scaffold and pancreas samples demonstrated the scaffolds' ability to track population changes over time for CD11b+ neutrophils (Figure 3.1C), F4/80+ macrophages (Figure 3.1D), CD3+CD4+ T cells (Figure 3.1E), and CD3+CD8+ T cells (Figure 3.1F). Notably, the innate immune cell populations, CD11b+ neutrophils and F4/80+ macrophages, comprised decreasing percentages of the population at the scaffold compared to the initial timepoint (Figure 3.1C-D), while the adaptive CD3+CD4+ and CD3+CD8+ T cells had no significant changes in the scaffold or pancreas over time (Figure 3.1E-1F). No significant differences in cell populations were observed when comparing the week 15 mice that were hyperglycemic to those that were not (Figure 3.1G). These results demonstrate that the scaffold captures immune cell populations that are also present in the pancreas, and that immune cell changes at the IN are not predictive of disease.

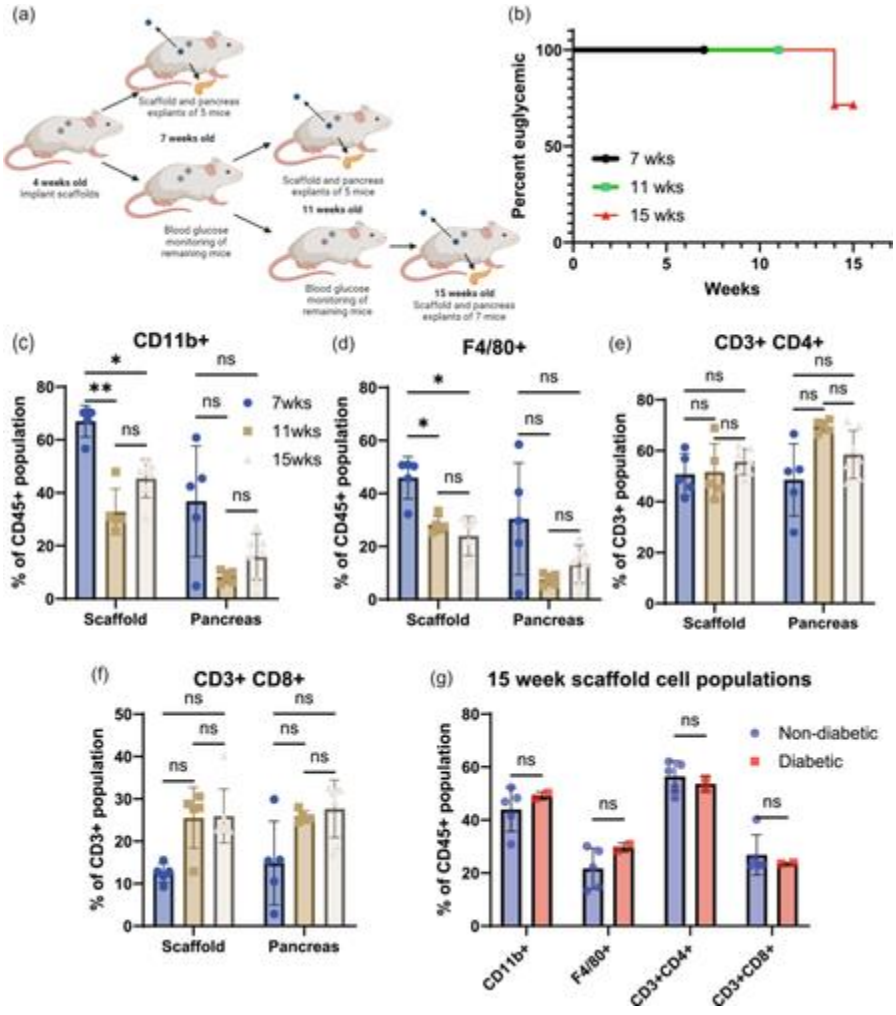


Figure 3.1: Immune cell population dynamics captured at the IN and pancreas. (a) INs and the pancreas were explanted from NOD mice at 7-, 11-, and 15-week timepoints. (b) Glucose monitoring showed no incidence of diabetes at the 7-, and 11-week timepoints, and two diabetic mice at the 15-week timepoint. There were significant decreases in the (c) CD11b+ and (d) F4/80+ populations at the scaffold, but not the pancreas between initial and later timepoints. There were no significant changes in the CD3 + CD4+ (e) or CD3 + CD8+ (f) populations at the scaffold or pancreas. There were no significant differences between diabetic and nondiabetic mice for any cell populations at the scaffold at the 15-week timepoint. n = 5 mice for 7- and 11-week timepoints, n = 7 mice for the 15-week timepoint. At the 15-week timepoint, n = 5 nondiabetic, and n = 2 diabetic mice. Significance determined by mixed effects analysis in c–f, and multiple unpaired t-tests in g. IN, immunological niche.

3.4.2 IN implantation and surveillance does not perturb diabetes incidence in two models of disease

Subsequently, we investigated whether the presence of the scaffold would impact disease onset in the two models: adoptive transfer of T cells in NOD.scid mice and NOD mice that spontaneously develop diabetes. INs were implanted in both NOD.scid (Figure 3.2A) and NOD

(Figure 3.2D) mice prior to symptomatic disease onset. In the adoptive transfer model, cells taken from NOD BDC2.5 transgenic mice and activated with BDC2.5 peptide were transferred at a dosage of 500,000 cells per mouse into 6-week NOD.scid mice. No significant difference in disease incidence or time to disease onset was observed between mice that received IN implants and the adoptive transfer, and those that received the adoptive transfer only (Figure 3.2B-C). In the adoptive transfer model, no incidence of diabetes was present in the OVA control (Figure 3.2B-C). Similarly, in the spontaneous diabetes NOD model, no significant difference in disease incidence was observed between mice that received scaffold implants and those that did not (Figure 3.2E-F).

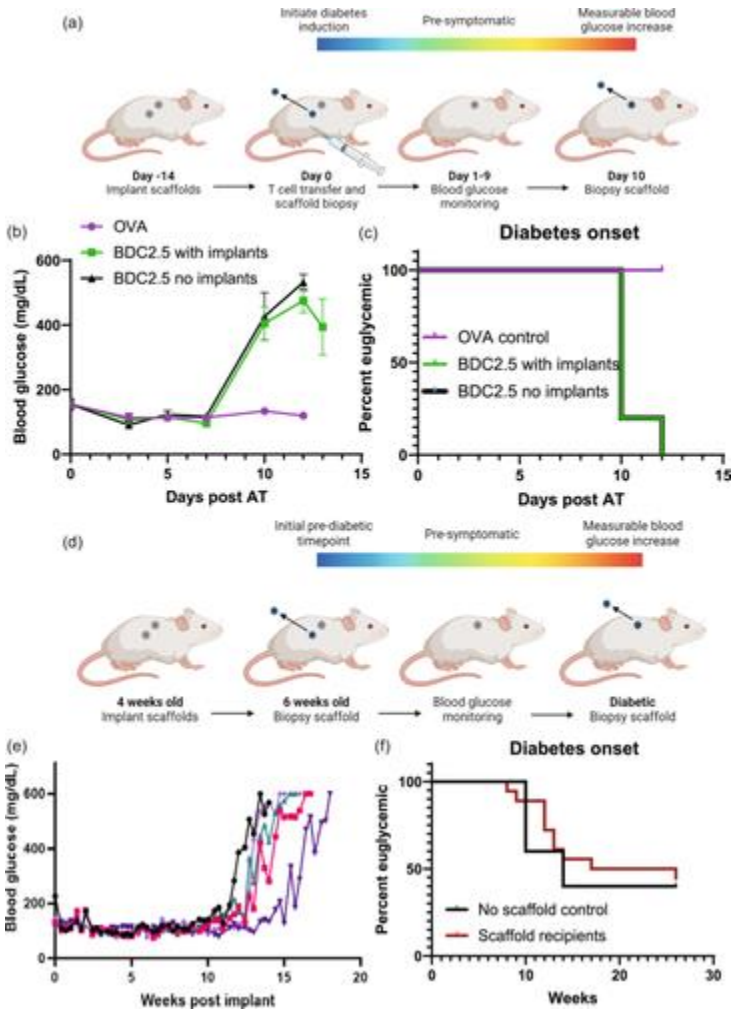


Figure 3.2: The IN does not affect disease progression in two models of T1D. (a) In the adoptive transfer model, mice received subcutaneous IN implants 2 weeks before adoptive transfer of diabetogenic T cells, or OVA reactive controls. INs were explanted on the day of T cell transfer, Day 0, and on Day 10. (b) None of the OVA controls became diabetic, and there was no difference in time to glucose elevation between mice that received BDC2.5 T cells and IN implants and mice that received BDC2.5 T cells only. (c) No mice that received BDC2.5 T cells remained euglycemic following 12 days post transfer in either the IN recipient or non-recipient group. (d) In the NOD mouse model, mice were implanted with INs at 4 weeks old, had an initial explant at 6 weeks old, and then were monitored for the blood glucose increase that resulted in their final explant timepoint. (e) The NOD mice developed hyperglycemia at differing rates, shown here by the glucose tracking data for each individual mouse, leading to different time points for the final explant. (f) There was no significant difference in the incidence of hyperglycemia between mice that received IN transplants and those that did not. IN, immunological niche.

3.4.3 IN analysis separates diseased from healthy groups in NOD.scid/Adoptive transfer model of T1D

Upon IN retrieval, we isolated RNA for sequencing and analyzed gene expression to develop a signature that correlates with disease. BDC2.5 reactive T cells induce diabetes when injected into immunodeficient mice(Prasad et al., 2018). Adoptively transferring BDC2.5 reactive T cells (diabetic) or OVA reactive T cells (control) into immunodeficient mice enabled a comparison of gene expression changes between mice that did and did not exhibit increased blood glucose levels respectively. Gene expression analysis separated NOD.scid mice that received an adoptive transfer of BDC2.5 T cells from mice that received an OVA control, as well as from initial healthy time points (Figure 3.3A). A signature consisting of six genes (Tgoln1, Scarb2, Ptdss2, Cyp51, Tmtc4, and Adrb1) was identified from the Elastic Net analysis that separated the healthy, including all day 0 mice and the day 10 OVA recipients, from mice that exhibit elevated blood glucose (Figure 3.3B-C). The six gene signature was then employed to develop a scoring system, using supervised and unsupervised techniques, that indicates a high disease score for the diabetic adoptive transfer recipients, and low scores for all initial timepoint and control animals (Figure 3.3D).

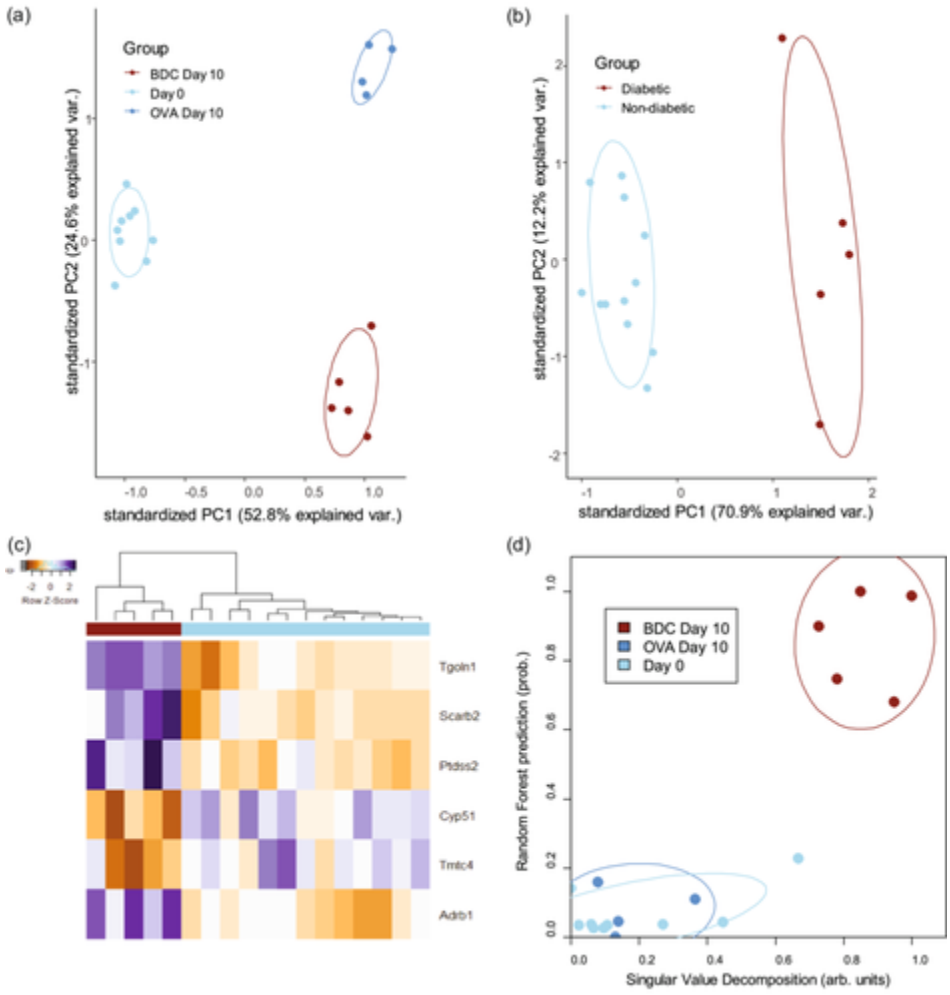


Figure 3.3: IN analysis separates diseased from healthy groups in an adoptive transfer model of T1D. (a) PCA plots of the gene expression analysis of the sequencing data from the IN separates all initial timepoints from both diabetic Day 10 and control Day 10, (b) and separates all nondiabetic samples from the diabetic samples. (c) Heatmap of the six gene signature shows clustering of the genes resulting in group separation. (d) Plot of Random Forest prediction score versus SVD shows separation of the diabetic Day 10 BDC2.5 recipients from all Day 0 timepoints and Day 10 OVA recipients. n = 9 for Day 0, n = 4 for OVA Day 10, and n = 5 for BDC Day 10. IN, immunological niche; SVD, singular value decomposition.

3.4.4 IN analysis successfully separates pre-symptomatic from symptomatic groups in the NOD model

We next investigated a gene signature from the IN in the NOD mouse model, which is well established as a model for spontaneous autoimmune diabetes (Anderson & Bluestone, 2005). Since insulitis can begin in NOD mice as early as 4 weeks of age, this model does not provide a truly healthy timepoint. To identify changes in the gene signature as the mice lost

functional β cell mass, we used 6 weeks of age as a non-diabetic state since no mice had developed symptomatic disease by this time (Figure 3.2F). Using this categorization, we separated the non-diabetic and diabetic NOD mice by computational analysis of the RNAseq data from the IN (Figure 3.4A). The two groups could be separated according to an eight gene signature: Dlk1, Chrna2, Klrb1a, Yy2, AA413626, Rsph6a, Trpc4, and 4930563J15Rik (Figure 3.4B). We also evaluated the signature using the disease scoring system, and demonstrated high scores for the diabetic timepoints, and low scores for the non-diabetic timepoint (Figure 3.4C). In comparing the signature scores between the adoptive transfer and NOD models, we observed that both signatures performed better using the supervised Random Forest technique than the unsupervised SVD approach (Figure 3.4D). In both cases, the combined scoring approach led to separation between all healthy and diseased timepoints (Figures 3.3D and 3.4C). The IN in the NOD model was also analyzed using the Open Array platform, which is a PCR based-system for measuring expression of inflammation related genes. This approach generated a six gene signature delineating diabetic and non-diabetic states (Figure 3.6C-D). This method supports the ability of a gene signature to identify disease; however, the signature from Open Array was less robust than the signature from sequencing and did not have clear separation upon scoring (Figure 3.6E).

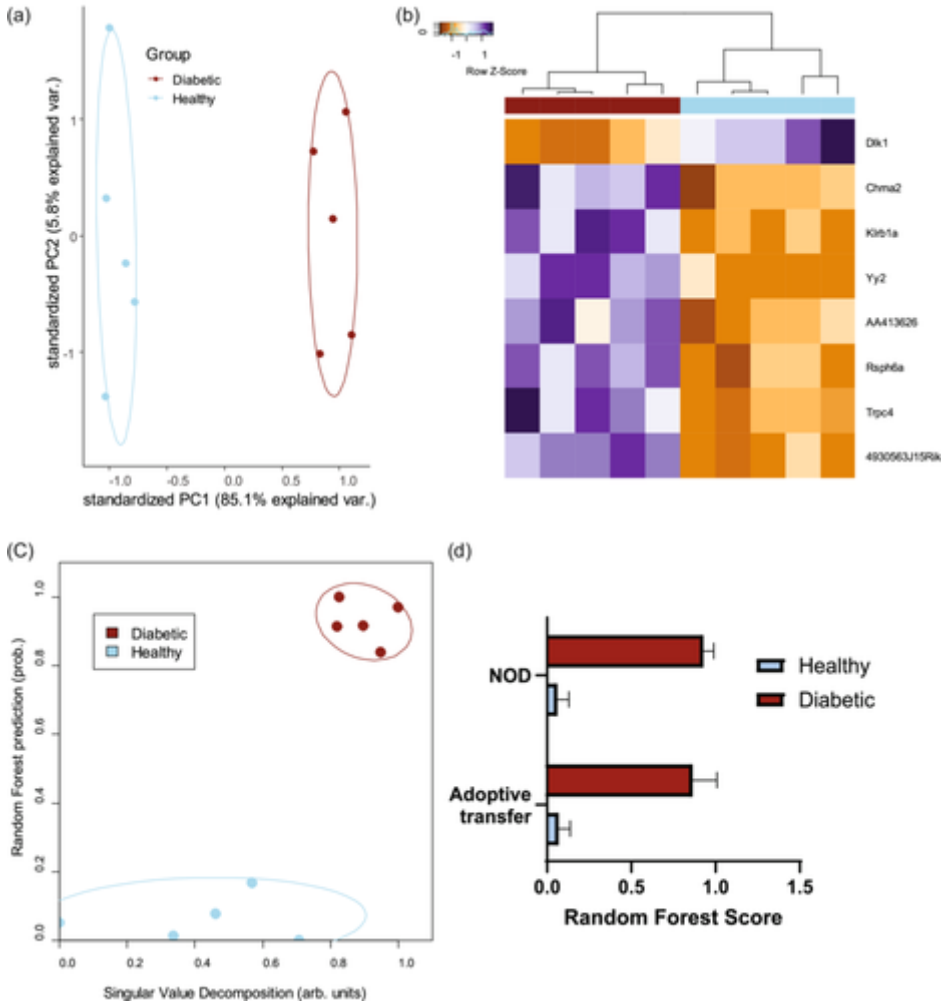


Figure 3.4: IN analysis separates presymptomatic from symptomatic groups in the NOD mouse model of T1D. (a) PCA plot of the gene expression analysis of INs separates diabetic from healthy NOD mice. (b) Heatmap of the eight gene signature and clustering that results in separation between groups. (c) Plot of Random Forest prediction score versus SVD shows separation between diabetic and healthy groups. (d) Random Forest score for diabetic and healthy groups from both the NOD and adoptive transfer models show elevated scoring in the diabetic group across both models. n = 5 for diabetic and healthy NOD groups. IN, immunological niche; SVD, singular value decomposition.

3.4.5 Gene set enrichment analysis identified common pathways impacted by diabetes onset

We investigated biological processes with known connections to the changing gene expression data identified by our computational analysis of the RNAseq data from the IN. Applying the clusterProfiler package(Wu et al., 2021) GSEA identified a total of 185 enriched pathways from the adoptive transfer model, and 2309 enriched pathways in the NOD model (Supplemental files 1-2). In the adoptive transfer model, GSEA identified several metabolic

processes connected to the changes in gene expression (Figure 3.5A). In the NOD model, the top biological processes that changed with disease were related to cell migration and organization (Figure 3.5B). For these upregulated pathways, the NOD model had a greater number of genes contributing to these gene sets in comparison to the adoptive transfer model (Figure 3.5C-D). Out of the enriched pathways identified by GSEA, 153 pathways overlapped between the two models (Figure 3.5E). Within the top 20 overlapping terms, multiple epithelial cell migration pathways were common across models (Supplemental files 3-4).

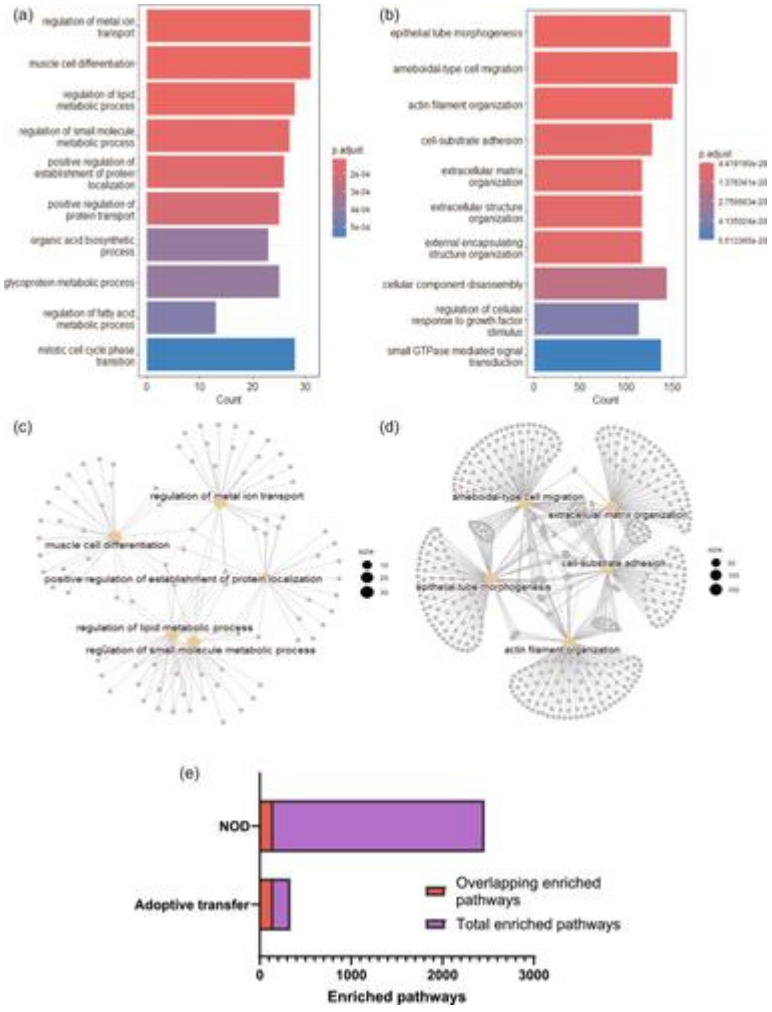


Figure 3.5: Gene set enrichment analysis identifies differentially expressed pathways between diabetic and nondiabetic groups. (a) Bar plots show the pathways enriched in diabetic samples in the adoptive transfer and (b) NOD models. (c, d) Gene-concept network plots show the connections of genes to biological processes. (e) A bar chart illustrates the proportion of overlapping pathways between the two models compared to the total number of enriched pathways.

3.5 Discussion

The development of teplizumab marks significant progress in improving therapies for individuals with T1D, which has created a need for diagnostics that will identify disease onset to allow for preventative care. Autoantibody screening has been able to stratify patient risk and has motivated a call for universal screening of autoantibodies, which could identify individuals who may benefit from further monitoring for disease. Nevertheless, antibody tests lack specificity in the timeline of disease onset, and risk status is variable depending on factors such as age, sex, and first-degree relatives with T1D (Jacobsen et al., 2020; Taplin & Barker, 2008). These tests provide a warning regarding disease yet do not definitively identify proximity to stage 3 disease, which motivated the studies herein to develop a technology to identify changing immune activity in T1D with symptomatic disease onset.

The immune cell populations in the pancreas were captured at the IN, yet the presence and numbers of these cells were insufficient to delineate a non-diabetic state from a diabetic state (Figure 3.1G). The only significant population changes at the scaffold were decreases in the innate immune cell populations between the 7- and 11-week timepoints (Figure 3.1C-D), which can likely be attributed to the transition from the dynamic acute phase to the relatively more stable chronic phase of the foreign body response following scaffold implantation. This foreign body response has previously been reported to be consistent across healthy and diseased groups in models of cancer and transplant rejection (Urie et al., 2024; Wang et al., 2023). Insulitis and diabetes onset is primarily driven by CD4+ and CD8+ T cells in the NOD mouse (Anderson & Bluestone, 2005; Miyazaki et al., 1985), and our results show the ability of the IN to capture these populations in a site distal to the pancreas (Figure 3.1E-F). While T cells are considered the drivers of disease onset in T1D, innate cells have been shown to be essential to diabetogenesis and T cell activation in murine models of T1D (H. S. Jun et al., 1999; Petrelli et al., 2022; Price

& Tarbell, 2015). Notably, it has been shown that targeting only innate cells, such as by depletion of tissue resident macrophages, can inhibit T1D progression (Carrero et al., 2017). Similarly, human samples taken from deceased donors with recent onset T1D exhibit macrophage infiltration as a component of insulitis, indicating their role in early disease (Willcox et al., 2009). Establishing the presence of both innate and adaptive immune cell populations at the IN over time demonstrates the IN's capability of monitoring the comprehensive immune response. While flow cytometry is useful in its ability to identify the cell populations that may be contributing to disease, the cell numbers and types alone are insufficient to distinguish diabetic mice from the pre-diabetic state as shown by the 15-week timepoint (Figure 3.1G). Changes in cell populations at the pancreas are not an effective marker of disease progression in humans either, as only approximately 30% of islets in recently diagnosed patients show evidence of insulitis (Pugliese, 2016; Willcox et al., 2009). Collectively, these results suggest that the scaffold may be a surrogate for the immunological changes in the pancreas, yet analyzing only cell types and numbers is inadequate to identify disease. Rather, the consistency in cell recruitment due to the foreign body response enables analysis of the variation in cell phenotypes which are changing systemically due to disease. Additionally, while blank polymeric scaffolds have been shown to demonstrate protective effects in models of type 2 diabetes (Hendley et al., 2019, 2020), these effects were not observed in our two models of T1D (Figure 3.2C, 3.2F).

Analysis of the IN by sequencing technology provided a comprehensive coverage of transcriptome changes that enabled the development of genetic signatures of disease. In the NOD model, the IN was analyzed using both RNAseq and OpenArray platforms (Figure 3.6). The OpenArray platform has been used in applications of the IN to EAE (Morris et al., 2020), and was applied herein to analyze 632 inflammatory disease related genes from the NOD samples.

Diabetes onset is characterized by inflammation of the islets due to immune cell infiltration, also known as insulitis, and thus the array could identify changes in inflammation between pre-symptomatic and diabetic states. Analysis of the OpenArray data produced a six gene signature that separated diseased and pre-symptomatic timepoints (Figure 3.6C). However, application of the disease scoring system to the OpenArray signature resulted in poor score separation between groups (Figure 3.6E). NOD mice develop insulitis as early as 4 weeks of age, and the inflammatory genes may be elevated long before symptom onset resulting in less dramatic differences between pre-symptomatic and diseased time points. In contrast, RNAseq analyzes the whole transcriptome, including inflammation and downstream processes that may be associated with activation of adaptive immune responses. Analysis of this RNAseq data demonstrated greater specificity in separating groups, with no false positives for symptomatic disease in the sequencing analysis compared to a false positive rate of 0.4 in the OpenArray analysis (Figure 3.6F). Expanding the possibilities for the signature improves the specificity of the analysis, which may result from capturing the impact of gene expression associated with processes outside of inflammation that are activated between the pre-symptomatic and diabetic states.

Gene expression analysis of the IN was able to stratify non-diabetic from diabetic states in both the NOD and adoptive transfer models. Our analysis of the adoptive transfer model produced a signature of six genes, Tgoln1, Scarb2, Ptdss2, Cyp51, Tmtc4, and Adrb1, which are all expressed in the pancreas (Fagerberg et al., 2014), indicating that changes in their transcriptional levels at the scaffold may indicate changes at the tissue of interest. In addition to their local expression at the pancreas, Tgoln1, Scarb2, Ptdss2, and Cyp51 have all been linked to lipid metabolism or biosynthesis (Heybrock et al., 2019; Sakaguchi et al., 2019; Sharma et al., 2013; R. Zhang et al., 2023). Studies have shown variation in lipid levels between healthy and

pre-diabetic subjects, with some lipid concentrations increasing before detection of autoantibodies (J. Zhang et al., 2022). Additionally, Tmtc4 and Adrb1 have been associated with Type 2 Diabetes (Galavi et al., 2018; Li et al., 2018). As the signature genes have not been directly linked to T1D onset or progression in the literature, they may represent new markers of disease onset.

Of the eight genes, Dlk1, Chrna2, Klrb1a, Yy2, AA413626, Rsph6a, Trpc4, and 4930563J15Rik, in the NOD model signature, four of these genes, Dlk1, Klrb1, Yy2, and Trpc4 are expressed in the pancreas (Fagerberg et al., 2014). Additionally, Trpc4 encodes one member of a family of calcium cation channels, and dysfunction in this group of proteins has been associated with several diabetic complications, such as atherosclerosis and diabetic neuropathy (Graham et al., 2012). Failure to activate Trpc4 in particular has been shown to impair β cell function (Srivastava et al., 2018). Chrna2 expression has been linked to fat regulation and the metabolism of obesity (H. Jun et al., 2018), and Dlk1 is essential to glucose metabolism (Abdallah et al., 2015). Klrb1a is a regulator of natural killer (NK) cells, which are an immune cell type involved in the autoimmune targeting of islets in T1D (Gardner & Fraker, 2021). AA413626, Rsph6a, and 4930563J15Rik do not have direct links to the pancreas or T1D at this time, but their utility in delineating healthy from disease groups in our signature indicate potential as new biomarkers that can be further studied for their potential as diagnostic tools or therapeutic targets.

For the adoptive transfer model, we compared the diseased state to a truly healthy state, as the NOD.scid mice would not develop disease without intervention. This comparison to healthy animals enabled filtering of more non-disease related genes in our analyses, as the manner of disease onset is not representative of the systemic level changes that contribute to

spontaneous disease. Additionally, the timeline of disease onset in this model is 10 days from the time of adoptive transfer to hyperglycemia, which is not representative of the timescale of disease onset in humans. In comparison, disease onset in the NOD mouse, which ranges from 10 to 30 weeks, more closely matches the dynamics of an immune response, such as insulitis, followed by a delay in progression to symptomatic disease. Comparing the gene expression between non-diabetic and diabetic states in both models identified common biological processes that are dysregulated during disease progression. In the adoptive transfer model, GSEA identified several metabolic processes connected to the changes in gene expression (Figure 3.5A). In the NOD model, the top biological processes changed with disease were related to cell migration and organization (Figure 3.5B). The pathway analysis was not constrained to immune pathways in order to take into consideration the systemic changes present with T1D onset that may have potential as a disease indicator prior to symptom onset. Of the 153 enriched terms shared between the two models, epithelium migration and regulation were common terms. Epithelial tissue is present throughout the body yet is notably present in the ductal cells of the pancreas. Ductal cells have a protective effect on the pancreas and can undergo regeneration following inflammatory injury (Reichert & Rustgi, 2011). Given these characteristics, epithelial pathways being enriched in both models of disease could indicate dysregulation of this pathway as a component of the mechanism underlying disease progression. Identification of non-immune pathways in connection with autoimmunity demonstrates the utility of our whole transcriptome analysis at, rather than focusing on specific immune cell populations.

In conclusion, these studies demonstrate the capability of the IN to serve as a surrogate tissue for monitoring immune processes during T1D progression in mice. The ability to monitor disease at a remote location may benefit therapeutic strategies in T1D. Tissue dysfunction, such

as that induced by immune cells, is commonly assessed clinically with biopsy. However, pancreatic biopsies in individuals at risk for T1D are not feasible, both due to their destructive nature, and that the risk of biopsy in healthy patients prior to their T1D diagnosis would be unacceptable. A subcutaneous IN therefore offers a minimally invasive alternative that can provide disease state information without manipulating the pancreas. Gene expression signatures from an IN may provide an opportunity to improve disease monitoring in at risk individuals, thereby allowing for preventative treatment.

3.6 Methods

3.6.1 Scaffold fabrication

PCL microporous scaffolds were prepared as previously described(Bushnell et al., 2019; Rao et al., 2016). In brief, PCL microspheres were mixed with 250-425 μm NaCl. The mixture was then pressed in a 5mm die at 1500 psi for 30 seconds, and the resulting disc was heated at 60 ˚C for 5 minutes on each side. The salt was leached from the scaffolds in deionized water, and then sterilized for animal studies with 70% ethanol followed by rinses with sterile PBS. Scaffolds were stored at -80 ˚C following sterilization and drying until the time of implantation.

3.6.2 Glucose monitoring

Blood glucose measurements were obtained from the tail-vein. Measurements were taken three times weekly, Monday, Wednesday, and Friday, for the duration of the studies. Glucose levels above 250 mg/dL on two consecutive days were considered diabetic.

3.6.3 Scaffold implantation

All animal work was conducted under approved protocols and regulations of the Institutional Animal Care and Use Committee of the University of Michigan. NOD/ShiltJ (strain

#001976) and NOD.Cg-Prkdcscid/J (strain #001303) mice were purchased from Jackson Laboratory at four weeks old. The four-week-old mice were anesthetized with 2% isoflurane and implanted with PCL scaffolds in the subcutaneous space. The mice received 5mg/kg carprofen analgesic at the time of surgery and 24 hours after surgery.

3.6.4 Adoptive transfer model

3.6.4.1 BDC2.5

A breeding pair of NOD BDC2.5 (Katz et al., 1993) (strain #004460) were purchased from Jackson Laboratory as T cell donor mice for the adoptive transfer model. Mice were bred and weaned according to the University of Michigan IACUC policies. Spleens were harvested from female NOD BDC2.5 mice at 6 weeks. Spleens were mashed through a cell strainer and spun down. The red blood cells were lysed with ACK for 5 minutes at room temperature, and the cells were resuspended in 25ml complete RPMI with Glutamax (10% FBS, 5 mM HEPES, 1 mM sodium pyruvate, NEAA and Pen/Strep). The cell suspension was filtered through another cell strainer, spun down, and counted. Cells were resuspended in complete media with 0.75 mg/ml BDC2.5 peptide (GenScript) per 7 million cell/ml. The cells were plated in T75 flasks at a density of greater than 2 million cells/cm2. Cells were then incubated for 72 hours at 37 ˚C, 5% CO2. Following incubation, cells were harvested from the plates, spun down, counted, and resuspended in PBS. The activated cells were then adoptively transferred via intraperitoneal injection at a dose of 500,000 cells per mouse into 6-week NOD.scid mice.

3.6.4.2 OVA controls

NOD donor mice were immunized with complete Freund's adjuvant (CFA) as previously reported(Miller et al., 2010). CFA consisted of an emulsion with a 1:1 mixture of incomplete Freund's adjuvant containing 4 mg/mL heat killed M. tuberculosis H37 Ra and phosphate-

buffered saline (PBS) with 2 mg/mL OVA323–339. 100 µL of CFA was subcutaneously injected across three sites in each mouse. Eleven days after immunization, spleens were harvested and processed in the same manner as the BDC2.5 donor mice. Cells were cultured as described above, with OVA peptide used for activation.

3.6.5 Scaffold explantation

Scaffolds were explanted from all mice at 6 weeks of age in both models. The explants were performed on the same day as cell injections in the adoptive transfer model. The same anesthetic and analgesics, 2% isoflurane and 5 mg/kg carprofen, were used in explantation as were administered at the time of scaffold implantation. A small incision was made directly above the scaffold, and the scaffold was removed from the subcutaneous space. In the adoptive transfer model, scaffolds were again explanted at 10 days post injection. For the NOD model, the diabetic timepoint was determined based on blood glucose levels on a mouse-by-mouse basis, and the scaffold was explanted following two consecutive blood glucose readings above 250 mg/dL. Explanted scaffolds were flash frozen in isopentane and stored at -80 ˚C until the time of RNA isolation.

3.6.6 RNA sequencing

Scaffolds were lysed in 800ul TRIzol reagent (Fisher Scientific, Cat. No. 15596026) and homogenized at 15000 RPM. The homogenized scaffold solution was centrifuged to pellet any remaining scaffold debris, and the supernatant was taken for RNA isolation. RNA isolation was performed using the Zymo Direct-zol RNA miniprep kit (Fisher Scientific, Cat. No. NC1047980), and the Zymo DNase 1 set with DNA digestion buffer (Fisher Scientific, Cat. No. NC0847937). Concentration of the isolated RNA was measured using a NanoDrop, and RNA was stored at -80 ˚C until being submitted for sequencing.

Sequencing was performed by the Advanced Genomics Core at the University of Michigan. For adoptive transfer samples, polyA library preparation was conducted using the QuantSeq platform, and sequencing was done on the Illumina NextSeq with 150 cycles. The NOD model samples' library preparation was completed using ribo depletion for a total RNA library preparation. Sequencing for the NOD samples was run on the Illumina NovaSeq S4 with 300 cycles.

3.6.7 cDNA synthesis and OpenArray

Prior to OpenArray analysis, samples were assessed with an RNA 6000 Nano Kit (Agilent Technologies), and samples with an RNA integrity (RIN) >8 were reverse transcribed and submitted for OpenArray. RT with RNA concentrations of 200 ng/μL was conducted with the SuperScript™ VILO™ cDNA Synthesis Kit. OpenArray panels (Applied Biosystems™ TaqMan™ OA Mouse Inflammation Panel, Cat. No. 4475393) were used by the UM Advanced Genomics Core on a fee-for-service basis using a QuantStudio 12k Flex RT-PCR system.

3.6.8 Computational analysis

Full code for computational analysis of RNA sequencing and OpenArray data can be found at https://github.com/shea-lab/IN_T1D_ATandNODmodels. Briefly, count data was read into R and categorized according to disease state and time. Count data was filtered to remove zero and very lowly expressed genes across samples, as well as a high-count filter. The data was then further filtered using a series of t-tests to isolate significantly expressed genes across conditions. Both the t-test filtered, and t-test unfiltered data were then passed through an elastic net regression to identify the genes most contributing to inter condition variance (the gene signature). Singular value decomposition (SVD) and random forest (RF) were then used to test the robustness of the signatures to other analysis, and the combination of SVD and RF

performance was used to determine the signature score. Gene set enrichment analysis was also performed on both data sets using the clusterProfiler package in R.

3.6.9 Flow cytometry

NOD mice were implanted with scaffolds at 4 weeks and monitored until their set explant time. Mice were sacrificed and the scaffolds and pancreas were explanted at 7-, 11-, and 15-week timepoints. A spleen was also taken for controls at each timepoint. Scaffolds were explanted into serum free RPMI, and pancreata and spleens were explanted into RPMI with 10%FBS (RPMI/FBS). Scaffolds were finely minced with a scalpel and digested with Liberase TL (Sigma Cat. No. 5401020001) for 20 minutes at 37 ˚C. Following digestion, scaffolds were passed through a 70 µm strainer and rinsed with RPMI/FBS. Pancreata were washed twice with PBS and digested with Collagenase P (1mg/ml) (Sigma Cat. No. 11213857001) for 15 minutes at 37 ˚C. Digestion was stopped with RPMI/FBS, and the pancreas samples were then washed twice more with RPMI/FBS before being passed through a 70 µm filter. Spleen samples were passed through a 70 µm filter, resuspended in PBS, decanted, and resuspended in ACK buffer for 5 minutes at room temperature. ACK lysis was stopped with 30 mL RPMI/FBS, and the suspension was refiltered through a 70 µm filter. All filtered samples were resuspended in PBS and counted.

Cells were stained with Zombie NIR (Biolegend Cat. No. 423106) for viability and blocked with CD16/32 (Biolegend Cat. No. 101302). Each sample was then stained with PE CD45.1, Spark Blue 550 CD11b, APC F4/80, PE/Dazzle 594 CD3, Brilliant Violet 421 CD4, and Brilliant Violet 785 CD8a (Biolegend Cat. Nos. 110707, 101290, 157306, 100246, 100443, 100750). Cells were fixed using the True-Nuclear Transcription Factor Buffer Set (Biolegend Cat. No. 424401) and analyzed on a Cytek Aurora spectral flow cytometer. Flow data was

analyzed with FlowJo v10.9.0, and positive populations were gated off of fluorescence minus one control and their proportion of live, CD45.1+ cells. CD4+ and CD8+ populations were additionally constrained to their proportion of the CD3+ population. The gating strategy is shown in Figure 3.7.

3.7 Author contributions

Studies were conceived by J.L.K, L.D.S., T.K., and A.H.M. J.L.K., L.R., and E.B., performed flow cytometry experiments. T.K. and A.H.M. conducted OpenArray studies. J.L.K. and A.H.M. performed adoptive transfer experiments. R.R.U. provided code for analysis. J.L.K. conducted NOD studies and sequencing analysis for all models. J.L.K. drafted the manuscript, and revised the manuscript in conjunction with L.D.S.

3.8 Acknowledgements

Support for this work was provided in part by NIH grants R01 DK121462 and R01 CA272940, and JDRF grant 2-SRA-2024-1480-S-B. This material is based upon work supported by the National Science Foundation Graduate Research Fellowship under Grant No. DGE-2241144, supporting J.L.K. A.H.M. was supported by NIH Pathway to Independence Award EB028840. Figures 3.1A, 3.2A, and 3.2D Created with Biorender.com.

This work was published as doi: 10.1002/bit.28824. Epub 2024 Jul 31.

3.9 Supplemental Information

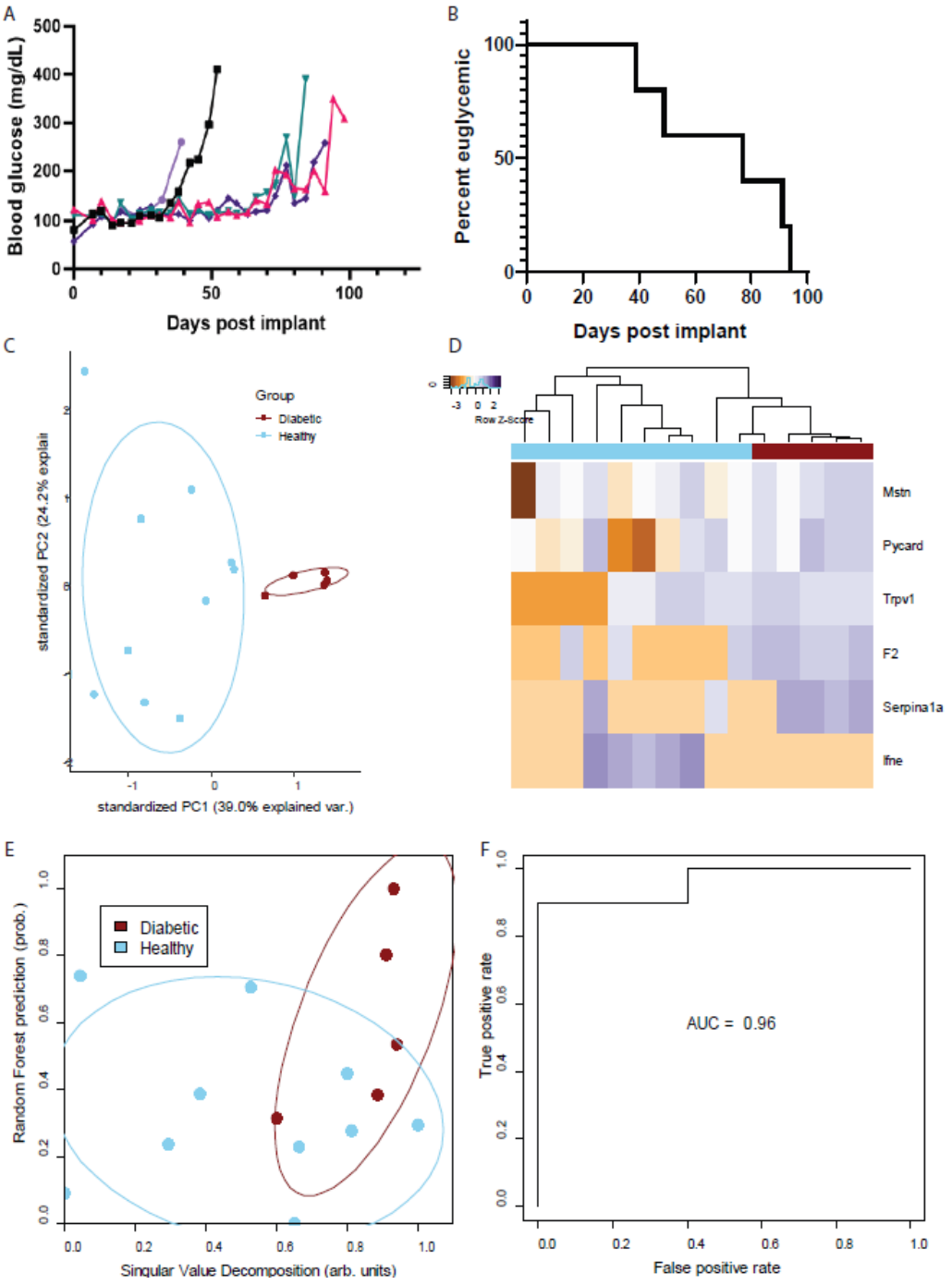


Figure 3.6: IN analysis produces signature with non-sequencing gene analysis. (A-B) An additional cohort of NOD mice was tracked from the time of IN implantation to the time of glucose elevation. (C) PCA plot of the gene expression analysis of OpenArray data from the IN separates diabetic from healthy timepoints. (D) Heatmap of the six gene signature shows expression levels of genes contributing to the separation. (E) Plot of Random Forest prediction score versus SVD shows poor separation between diabetic and healthy groups based on scoring. (F) ROC curve shows an AUC = 0.96 and a false positive rate of 0.4.

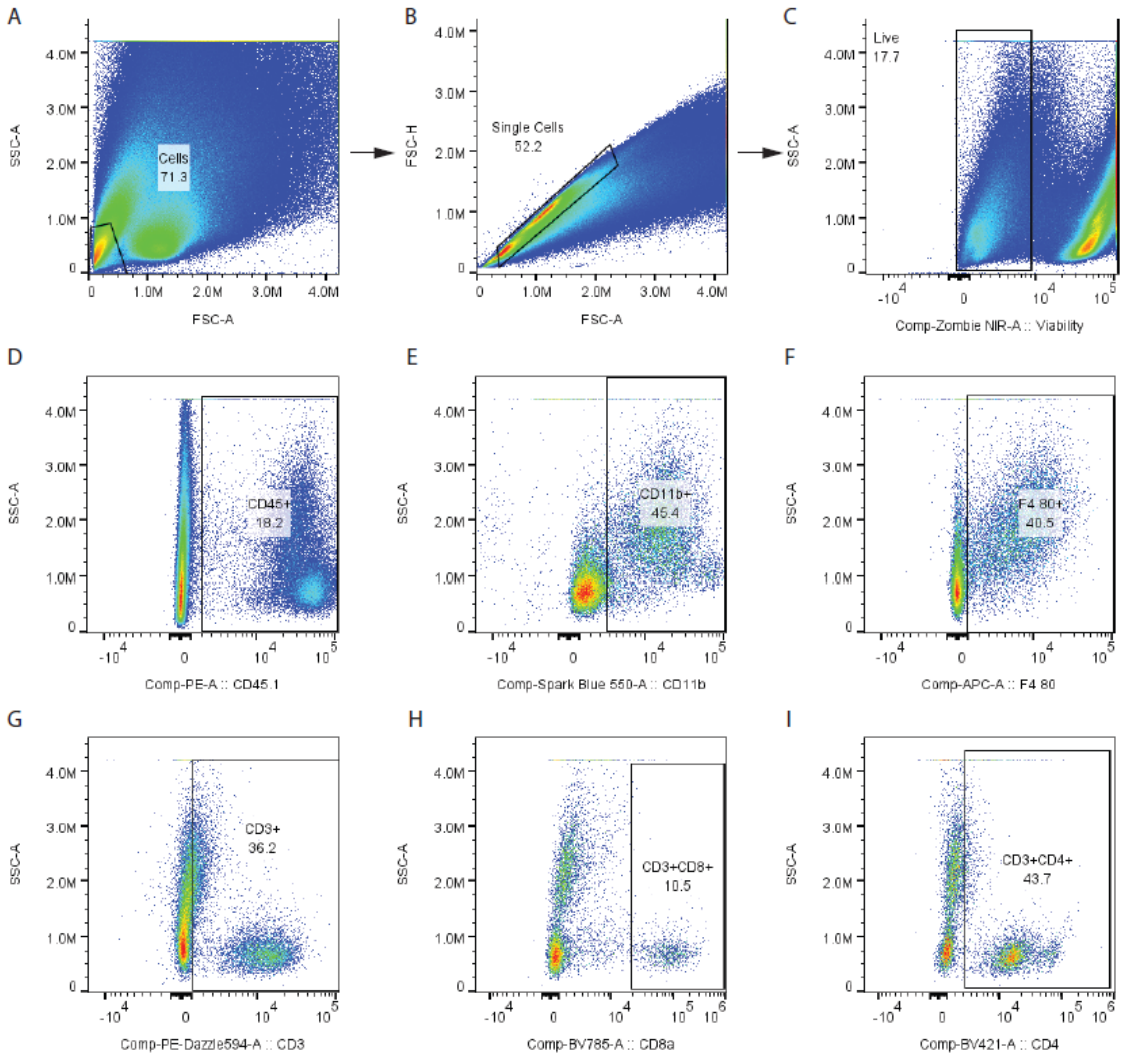


Figure 3.7: Flow gating for immune cell identification. (A) Flow data was first gated via forward scatter and side scatter to remove non-cellular debris, with all events outside of the selected area representing cells. (B) Cells were then gated by forward scatter area and height to remove any doublets. (C) Live single cells were identified as those negative for Zombie-NIR stain, and (D) CD45.1+ cells were identified with a PE antibody from the live cell population. All subsequent gating was done from the CD45.1+ population, with (E) CD11b+ gated with a Spark Blue 550 antibody, (F) F4/80+ gated with an APC antibody, and (G) CD3+ gated with a PE-Dazzle 594 antibody. The (H) CD8+ and (I) CD4+ populations were gated from the CD3+ population by Brilliant Violet 785 and Brilliant Violet 421 antibodies respectively.

3.10 References

Abdallah, B. M., Ditzel, N., Laborda, J., Karsenty, G., & Kassem, M. (2015). DLK1 regulates whole-body glucose metabolism: A negative feedback regulation of the osteocalcin-insulin loop. *Diabetes*, **64**(9), 3069–3080. https://doi.org/10.2337/db14-1642

Anderson, M. S., & Bluestone, J. A. (2005). The NOD mouse: A model of immune dysregulation. In *Annual Review of Immunology*, **23**, 447–485. https://doi.org/10.1146/annurev.immunol.23.021704.115643

Balcázar-Hernández, L., Huerta-Martínez, H., Garrido Magaña, E., Nishimura-Meguro, E., Jiménez Márquez, A., & Rivera-Hernández, A. (2023). Burden in primary informal caregivers of children and adolescents with type 1 diabetes: Is it associated with depression, family dysfunction, and glycemic control? *Frontiers in Endocrinology*, **13**, 1089160. https://doi.org/10.3389/fendo.2022.1089160

Bluestone, J. A., Buckner, J. H., & Herold, K. C. (2021). Immunotherapy: Building a bridge to a cure for type 1 diabetes. *Science*, **373**, 510–516. https://clinicaltrials.gov

Bushnell, G. G., Hardas, T. P., Hartfield, R. M., Zhang, Y., Oakes, R. S., Ronquist, S., Chen, H., Rajapakse, I., Wicha, M. S., Jeruss, J. S., & Shea, L. D. (2019). Biomaterial scaffolds recruit an aggressive population of metastatic tumor cells in vivo. *Cancer Research*, **79**(8), 2042–2053. https://doi.org/10.1158/0008-5472.CAN-18-2502

Carrero, J. A., McCarthy, D. P., Ferris, S. T., Wan, X., Hu, H., Zinselmeyer, B. H., Vomund, A. N., & Unanue, E. R. (2017). Resident macrophages of pancreatic islets have a seminal role in the initiation of autoimmune diabetes of NOD mice. *Proceedings of the National Academy of Sciences of the United States of America*, **114**(48), 10418. https://doi.org/10.1073/pnas.1713543114

Commissariat, P. V., Harrington, K. R., Whitehouse, A. L., Miller, K. M., Hilliard, M. E., Van Name, M., DeSalvo, D. J., Tamborlane, W. V., Anderson, B. J., DiMeglio, L. A., & Laffel, L. M. (2020). “I’m essentially his pancreas”: Parent perceptions of diabetes burden and

opportunities to reduce burden in the care of children <8 years old with type 1 diabetes. *Pediatric Diabetes*, **21**(2), 377–383. https://doi.org/10.1111/pedi.12956

Fagerberg, L., Hallstrom, B. M., Oksvold, P., Kampf, C., Djureinovic, D., Odeberg, J., Habuka, M., Tahmasebpoor, S., Danielsson, A., Edlund, K., Asplund, A., Sjostedt, E., Lundberg, E., Szigyarto, C. A. K., Skogs, M., Ottosson Takanen, J., Berling, H., Tegel, H., Mulder, J., … Uhlen, M. (2014). Analysis of the human tissue-specific expression by genome-wide integration of transcriptomics and antibody-based proteomics. *Molecular and Cellular Proteomics*, **13**(2), 397–406. https://doi.org/10.1074/mcp.M113.035600

Galavi, H., Noorzehi, N., Saravani, R., Sargazi, S., Mollashahee-Kohkan, F., & Shahraki, H. (2018). Genetic polymorphism in ADRB-1 is associated with type 2 diabetes susceptibility in Iranian population. *Gene Reports*, **12**, 171–174. https://doi.org/10.1016/j.genrep.2018.06.019

Gardner, G., & Fraker, C. A. (2021). Natural Killer Cells as Key Mediators in Type I Diabetes Immunopathology. In *Frontiers in Immunology* **12**, 722979. https://doi.org/10.3389/fimmu.2021.722979

Graham, S., Yuan, J. P., & Ma, R. (2012). Canonical transient receptor potential channels in diabetes. In *Experimental Biology and Medicine* **237**(2). https://doi.org/10.1258/ebm.2011.011208

Gregory, G. A., Robinson, T. I. G., Linklater, S. E., Wang, F., Colagiuri, S., de Beaufort, C., Donaghue, K. C., Magliano, D. J., Maniam, J., Orchard, T. J., Rai, P., & Ogle, G. D. (2022). Global incidence, prevalence, and mortality of type 1 diabetes in 2021 with projection to 2040: a modelling study. *The Lancet Diabetes and Endocrinology*, **10**(10), 741–760. https://doi.org/10.1016/S2213-8587(22)00218-2

Hendley, M. A., Isely, C., Murphy, K. P., Hall, H. E., Annamalai, P., & Gower, R. M. (2020). Scaffold Implant Into the Epididymal Adipose Tissue Protects Mice From High Fat Diet Induced Ectopic Lipid Accumulation and Hyperinsulinemia. *Frontiers in Bioengineering and Biotechnology*, **8**, 562. https://doi.org/10.3389/fbioe.2020.00562

Hendley, M. A., Murphy, K. P., Isely, C., Struckman, H. L., Annamalai, P., & Gower, R. M. (2019). The host response to poly(lactide-co-glycolide) scaffolds protects mice from diet induced obesity and glucose intolerance. *Biomaterials*, **217**, 119281. https://doi.org/10.1016/j.biomaterials.2019.119281

Herold, K. C., Bundy, B. N., Long, S. A., Bluestone, J. A., DiMeglio, L. A., Dufort, M. J., Gitelman, S. E., Gottlieb, P. A., Krischer, J. P., Linsley, P. S., Marks, J. B., Moore, W., Moran, A., Rodriguez, H., Russell, W. E., Schatz, D., Skyler, J. S., Tsalikian, E., Wherrett, D. K., … Greenbaum, C. J. (2019). An Anti-CD3 Antibody, Teplizumab, in Relatives at Risk for Type 1 Diabetes. *New England Journal of Medicine*, **381**(7), 603–613. https://doi.org/10.1056/nejmoa1902226

Heybrock, S., Kanerva, K., Meng, Y., Ing, C., Liang, A., Xiong, Z. J., Weng, X., Ah Kim, Y., Collins, R., Trimble, W., Pomès, R., Privé, G. G., Annaert, W., Schwake, M., Heeren, J., Lüllmann-Rauch, R., Grinstein, S., Ikonen, E., Saftig, P., & Neculai, D. (2019). Lysosomal integral membrane protein-2 (LIMP-2/SCARB2) is involved in lysosomal cholesterol export. *Nature Communications*, **10**(1), 3521. https://doi.org/10.1038/s41467-019-11425-0

Jacobsen, L. M., Bocchino, L., Evans-Molina, C., DiMeglio, L., Goland, R., Wilson, D. M., Atkinson, M. A., Aye, T., Russell, W. E., Wentworth, J. M., Boulware, D., Geyer, S., & Sosenko, J. M. (2020). The risk of progression to type 1 diabetes is highly variable in

individuals with multiple autoantibodies following screening. *Diabetologia*, **63**(3), 588–596. https://doi.org/10.1007/s00125-019-05047-w

Jun, H. S., Yoon, C. S., Zbytnuik, L., Van Rooijen, N., & Yoon, J. W. (1999). The role of macrophages in T cell-mediated autoimmune diabetes in nonobese diabetic mice. *Journal of Experimental Medicine*, **189**(2), 347–358. https://doi.org/10.1084/jem.189.2.347

Jun, H., Yu, H., Gong, J., Jiang, J., Qiao, X., Perkey, E., Kim, D. Il, Emont, M. P., Zestos, A. G., Cho, J. S., Liu, J., Kennedy, R. T., Maillard, I., Xu, X. Z. S., & Wu, J. (2018). An immune-beige adipocyte communication via nicotinic acetylcholine receptor signaling. *Nature Medicine*, **24**(6), 814–822. https://doi.org/10.1038/s41591-018-0032-8

Katz, J. D., Wang, B., Haskins, K., Benoist, C., & Mathis, D. (1993). Following a diabetogenic T cell from genesis through pathogenesis. *Cell*, **74**(6), 1089–1100. https://doi.org/10.1016/0092-8674(93)90730-E

Keam, S. J. (2023). Teplizumab: First Approval. *Drugs*, **83**(5), 439–445. https://doi.org/10.1007/s40265-023-01847-y

Li, J., Akil, O., Rouse, S. L., McLaughlin, C. W., Matthews, I. R., Lustig, L. R., Chan, D. K., & Sherr, E. H. (2018). Deletion of Tmtc4 activates the unfolded protein response and causes postnatal hearing loss. *Journal of Clinical Investigation*, **128**(11), 5150–5162. https://doi.org/10.1172/JCI97498

Lutzweiler, G., Halili, A. N., & Vrana, N. E. (2020). The overview of porous, bioactive scaffolds as instructive biomaterials for tissue regeneration and their clinical translation. In *Pharmaceutics.* **12**(7), 602, Issue 7). https://doi.org/10.3390/pharmaceutics12070602

Miller, S. D., Karpus, W. J., & Davidson, T. S. (2010). Experimental autoimmune encephalomyelitis in the mouse. In *Current Protocols in Immunology*, **88**, 1–18. https://doi.org/10.1002/0471142735.im1501s77

Miyazaki, A., Hanafusa, T., Yamada, K., Miyagawa, J., Fujino-Kurihara, H., & Nakajima, H. (1985). Predominance of T lymphocytes in pancreatic islets and spleen of pre-diabetic non-obese diabetic (NOD) mice: a longitudinal study. In *Clin. exp. Immunol*, **60**(3), 622–633.

Morris, A. H., Hughes, K. R., Oakes, R. S., Cai, M. M., Miller, S. D., Irani, D. N., & Shea, L. D. (2020). Engineered immunological niches to monitor disease activity and treatment efficacy in relapsing multiple sclerosis. *Nature Communications*, **11**(1), 3871. https://doi.org/10.1038/s41467-020-17629-z

Oakes, R. S., Bushnell, G. G., Orbach, S. M., Kandagatla, P., Zhang, Y., Morris, A. H., Hall, M. S., LaFaire, P., Decker, J. T., Hartfield, R. M., Brooks, M. D., Wicha, M. S., Jeruss, J. S., & Shea, L. D. (2020). Metastatic conditioning of myeloid cells at a subcutaneous synthetic niche reflects disease progression and predicts therapeutic outcomes. *Cancer Research*, **80**(3), 602–612. https://doi.org/10.1158/0008-5472.CAN-19-1932

Petrelli, A., Popp, S. K., Fukuda, R., Parish, C. R., Bosi, E., & Simeonovic, C. J. (2022). The Contribution of Neutrophils and NETs to the Development of Type 1 Diabetes. In *Frontiers in Immunology*, **13**, 930553. https://doi.org/10.3389/fimmu.2022.930553

Prasad, S., Neef, T., Xu, D., Podojil, J. R., Getts, D. R., Shea, L. D., & Miller, S. D. (2018). Tolerogenic Ag-PLG nanoparticles induce tregs to suppress activated diabetogenic CD4 and CD8 T cells. *Journal of Autoimmunity*, **89**, 112–124. https://doi.org/10.1016/j.jaut.2017.12.010

Price, J. D., & Tarbell, K. V. (2015). The role of dendritic cell subsets and innate immunity in the pathogenesis of type 1 diabetes and other autoimmune diseases. *Frontiers in Immunology*, **6**, 00288. https://doi.org/10.3389/fimmu.2015.00288

Pugliese, A. (2016). Insulitis in the pathogenesis of type 1 diabetes. In *Pediatric Diabetes*, **17**, 31–36. https://doi.org/10.1111/pedi.12388

Ramos, E. L., Dayan, C. M., Chatenoud, L., Sumnik, Z., Simmons, K. M., Szypowska, A., Gitelman, S. E., Knecht, L. A., Niemoeller, E., Tian, W., & Herold, K. C. (2023). Teplizumab and β-Cell Function in Newly Diagnosed Type 1 Diabetes. *New England Journal of Medicine*, **389**(23), 2151–2161. https://doi.org/10.1056/nejmoa2308743

Rao, S. S., Bushnell, G. G., Azarin, S. M., Spicer, G., Aguado, B. A., Stoehr, J. R., Jiang, E. J., Backman, V., Shea, L. D., & Jeruss, J. S. (2016). Enhanced survival with implantable scaffolds that capture metastatic breast cancer cells in vivo. *Cancer Research*, **76**(18), 5209–5218. https://doi.org/10.1158/0008-5472.CAN-15-2106

Reichert, M., & Rustgi, A. K. (2011). Pancreatic ductal cells in development, regeneration, and neoplasia. In *Journal of Clinical Investigation* **121**(12), 4572–4578. https://doi.org/10.1172/JCI57131

Sakaguchi, M., Cai, W., Wang, C. H., Cederquist, C. T., Damasio, M., Homan, E. P., Batista, T., Ramirez, A. K., Gupta, M. K., Steger, M., Wewer Albrechtsen, N. J., Singh, S. K., Araki, E., Mann, M., Enerbäck, S., & Kahn, C. R. (2019). FoxK1 and FoxK2 in insulin regulation of cellular and mitochondrial metabolism. *Nature Communications*, **10**(1), 1582. https://doi.org/10.1038/s41467-019-09418-0

Sharma, N. K., Langberg, K. A., Mondal, A. K., & Das, S. K. (2013). Phospholipid Biosynthesis Genes and Susceptibility to Obesity: Analysis of Expression and Polymorphisms. *PLoS ONE*, **8**(5), e65303. https://doi.org/10.1371/journal.pone.0065303

Sims, E. K., Bundy, B. N., Stier, K., Serti, E., Lim, N., Long, S. A., Geyer, S. M., Moran, A., Greenbaum, C. J., Evans-Molina, C., Herold, K. C., DiMeglio, L. A., Gitelman, S. E., Gottlieb, P. A., Marks, J. B., Moore, W., Rodriguez, H., Russell, W. E., Schatz, D., … Ziegler, A. G. (2021). Teplizumab improves and stabilizes beta cell function in antibody-positive high-risk individuals. *Science Translational Medicine*, **13**(583), eabc8980. https://doi.org/10.1126/scitranslmed.abc8980

Srivastava, S., Li, Z., Soomro, I., Sun, Y., Wang, J., Bao, L., Coetzee, W. A., Stanley, C. A., Li, C., & Skolnik, E. Y. (2018). Regulation of KATP channel trafficking in pancreatic β-cells by Protein histidine phosphorylation. *Diabetes*, **67**(5), 849–860. https://doi.org/10.2337/db17-1433

Tamborlane, W. V., Beck, R. W., Bode, B. W., Buckingham, B., Chase, H. P., Clemons, R., Fiallo-Scharer, R., Fox, L. A., Gilliam, L. K., Hirsch, I. B., Huang, E. S., Kollman, C., Kowalski, A. J., Laffel, L., Lawrence, J. M., Lee, J., Mauras, N., O'Grady, M., Ruedy, K. J., & Rodriguez, H. (2008). Continuous glucose monitoring and intensive treatment of type 1 diabetes. *New England Journal of Medicine*, **359**(14), 1464–1476. https://doi.org/10.1056/NEJMc082243

Taplin, C., & Barker, J. (2008). Autoantibodies in type 1 diabetes. *Autoimmunity*, **41**(1), 11–18. https://doi.org/10.1080/08916930701619169

Urie, R. R., Morris, A., Farris, D., Hughes, E., Xiao, C., Chen, J., Lombard, E., Feng, J., Li, J. Z., Goldstein, D. R., & Shea, L. D. (2024). Biomarkers from subcutaneous engineered tissues predict acute rejection of organ allografts. *Sci. Adv*, **10**, 6178. https://www.science.org

Wang, J., Ocadiz-Ruiz, R., Hall, M. S., Bushnell, G. G., Orbach, S. M., Decker, J. T., Raghani, R. M., Zhang, Y., Morris, A. H., Jeruss, J. S., & Shea, L. D. (2023). A synthetic metastatic niche reveals antitumor neutrophils drive breast cancer metastatic dormancy in the lungs. *Nature Communications*, **14**(1), 4790. https://doi.org/10.1038/s41467-023-40478-5

Willcox, A., Richardson, S. J., Bone, A. J., Foulis, A. K., & Morgan, N. G. (2009). Analysis of islet inflammation in human type 1 diabetes. *Clinical and Experimental Immunology*, **155**(2), 173–181. https://doi.org/10.1111/j.1365-2249.2008.03860.x

Wu, T., Hu, E., Xu, S., Chen, M., Guo, P., Dai, Z., Feng, T., Zhou, L., Tang, W., Zhan, L., Fu, X., Liu, S., Bo, X., & Yu, G. (2021). clusterProfiler 4.0: A universal enrichment tool for interpreting omics data. *Innovation*, **2**(3), 100141. https://doi.org/10.1016/j.xinn.2021.100141

Zhang, J., Xiao, Y., Hu, J., Liu, S., Zhou, Z., & Xie, L. (2022). Lipid metabolism in type 1 diabetes mellitus: Pathogenetic and therapeutic implications. In *Frontiers in Immunology*, **13**, 999108. https://doi.org/10.3389/fimmu.2022.999108

Zhang, R., Wang, Y., Wu, A., Wang, J., & Zhang, J. (2023). Strategies of targeting CYP51 for IFIs therapy: Emerging prospects, opportunities and challenges. In *European Journal of Medicinal Chemistry* **259**, 115658. https://doi.org/10.1016/j.ejmech.2023.115658

Ziegler, A. G., Rewers, M., Simell, O., Simell, T., Lempainen, J., Steck, A., Winkler, C., Ilonen, J., Veijola, R., Knip, M., Bonifacio, E., & Eisenbarth, G. S. (2013). Seroconversion to

Multiple Islet Autoantibodies and Risk of Progression to Diabetes in Children. *JAMA*, **309**(23), 2473–2479. https://jamanetwork.com/

Chapter 4 Polymer Scaffolds Enable Longitudinal Monitoring of Disease Progression in the NOD Model of Type 1 Diabetes

4.1 Authors

Jessica L. King, Elizabeth Bealer, Kelly Crumley, Jyotirmoy Roy, Russell R. Urie, Laila Rad, and Lonnie D. Shea

4.2 Abstract

With the advancement of immunotherapies for the prevention of autoimmune type 1 diabetes (T1D), new methods are needed to monitor for disease progression prior to symptom onset. Current diagnostic methods rely on autoantibody presence and dysglycemia, but this approach fails to identify the timeframe of islet destruction that precedes glucose dysregulation. In these studies, we implement a subcutaneous microporous scaffold as an immunological niche (IN), which reflects many of the immune changes observed in the pancreas. The IN enables longitudinal monitoring by capturing immune changes associated with the autoimmune destruction of β cells, without the need to biopsy the pancreas Analysis of RNA sequencing taken from IN samples successfully delineates at-risk from non-risk groups, as well as disease progressors from non-progressors as early as six weeks in the NOD mouse model of T1D. We also demonstrate separation within the progressors group, identifying disease progression five to seven weeks prior to disease onset. Early identification of progressors could inform treatment timing prior to symptom onset.

4.3 Introduction

Type 1 diabetes (T1D) is a chronic autoimmune disease that results in destruction of the pancreatic β cells, leading to hyperglycemia and the need for exogenous insulin therapy. Incidence of T1D is on the rise, with an estimated global population exceeding 13.5 million by 2040.[1] Current therapy requires daily administration of exogenous insulin, which comes with a heavy burden of care and does not alleviate the risk of long-term complications. Advancements in cell replacement therapies have enabled allogeneic pancreatic islet cell transplants from cadaveric donors and clinical trials of human pluripotent stem cell (hPSC) derived islet transplants.[2–4] However, in both of these cases transplants require immunosuppression to prevent graft rejection and are at risk of the same β cell targeting that destroyed the native cells.[5,6]

Recently, immunotherapies have been applied to attenuate the autoimmune response and prevent native β cell loss, which avoids the need for cell replacement therapy. Autoantibodies have been identified that indicate an autoimmune response to the native islets and denote a risk status for T1D progression.[7,8] Autoantibody screening has been advocated as a way to inform risk status and decrease the likelihood of life threatening events at the time of symptom onset,[9] however auto-antibodies do not convey time proximity to symptom onset, and that time is variable within the autoantibody positive population.[10] Lack of time specificity with autoantibody screening is additionally challenging as autoantibody positivity is used as an indicator in administration of immunotherapies that have variable efficacy based on timing of delivery.[11] One such treatment, the FDA approved Teplizumab, has shown efficacy in delaying disease progression in patients with recent onset T1D, defined as two or more autoantibody positive and dysglycemia indicated by a glucose tolerance test.[12–14] Dysglycemia is a result of β cell stress and destruction, so at the time of treatment there has already been a loss to the β cell mass. As such, a monitoring approach

that can identify proximity to disease without relying on dysglycemia could increase the preservation of β cell mass.

In these studies, we sought to identify transcriptomic changes that denote disease risk and status prior to functional loss. To that end, we implanted microporous poly(e-caprolactone) (PCL) scaffolds into the subcutaneous space of NOD/ShiltJ (NOD) and NOR/LtJ (NOR) mice to act as an immunological niche (IN). The IN has been previously shown to identify transcriptomic changes in models of T1D, cancer, multiple sclerosis, and transplant rejection.[15–17] In all of these models, the IN provides a retrievable surrogate to monitor disease in a native tissue that is either inaccessible, or too fragile for biopsy. In previous studies, we have shown that the IN captures gene expression changes capable of separating healthy from symptomatic disease time points in the NOD model of T1D.[15] Herein, we investigate the potential to delineate risk status (NOD vs NOR), eventual progression status (progressors and non-progressors), and progression timeframe via gene signatures derived from analysis of the IN. These signatures offer a method to monitor T1D progression in a manner that does not rely on dysglycemia and have the potential to inform treatment timing to maximize β cell preservation.

4.4 Results

4.4.1 IN enables longitudinal monitoring by repeatable biopsies

We initially investigated disease incidence with weekly IN biopsy in NOD and NOR mice, which could be employed to characterize transcriptomic changes in NOD and NOR mice over time. Both strains underwent implants at 4 weeks of age, with weekly explants beginning at 6 weeks of age, and terminating at the time of hyperglycemia or 30 weeks of age for NOD and NOR respectively (Figure 4.1A). NOR mice were used as a non-diabetic control in these studies as they are background matched to NOD at the diabetogenic $H2^{g7}$ locus, without progression to

hyperglycemia (Figure 4.1B).[18] During the course of the study none of the NOR controls developed hyperglycemia, compared to near 50% of the NOD mice (Figure 4.1C). While Jackson Laboratories reports incidence greater than 80% by 30 weeks, disease incidence is highly variable between colonies.[19] Of the NOD mice that did not progress to hyperglycemia, they had insignificant variation in blood glucose levels compared to NOR controls (Figure 4.1D). Samples from all three groups were taken for bulk RNA sequencing, with timepoints defined by proximity to disease in NOD progressors, and by age in NOD non-progressors and NOR controls (Figure 4.1A). Data from all samples underwent batch correction and initial filtering, and of the 23,096 genes sequenced, 4,593 met our thresholds for average count and variance across samples (Figure 4.1E). This filtered gene set was used for all subsequent analyses.

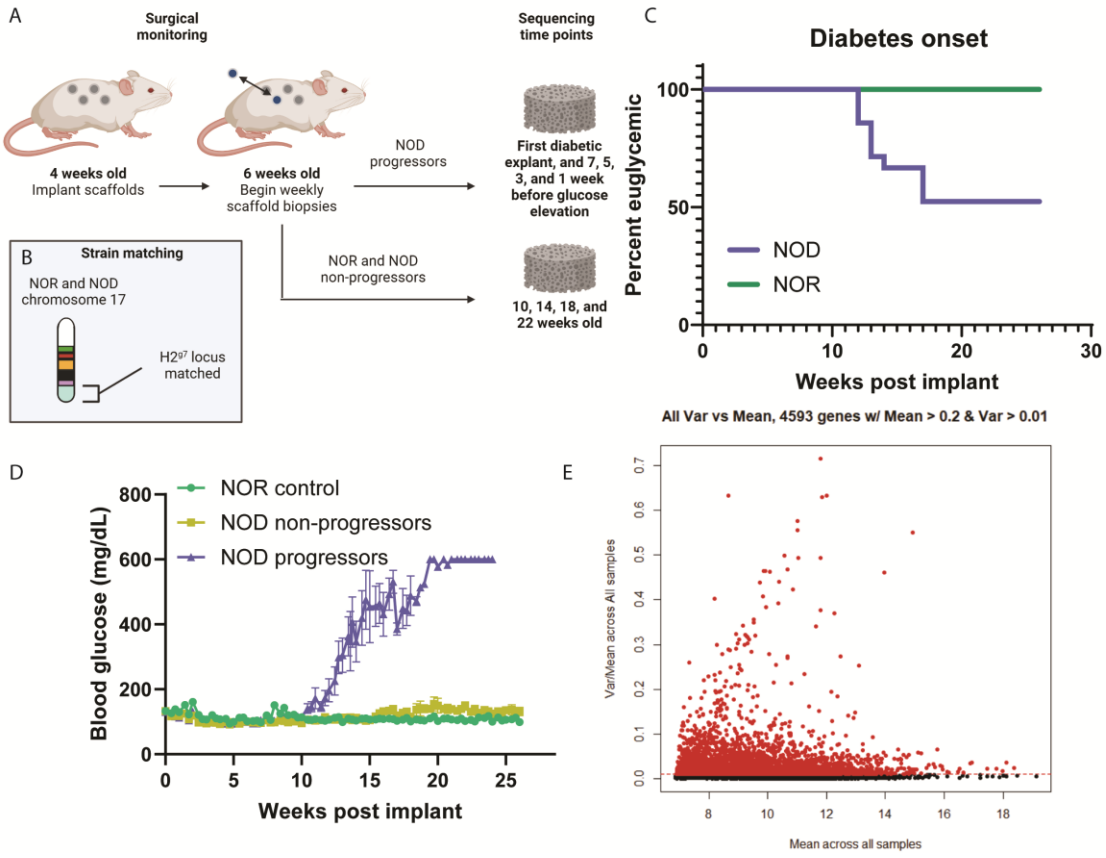


Figure 4.1: Weekly IN explants enables longitudinal monitoring of NOD and NOR mice. (A) NOD and NOR mice were implanted with INs at 4 weeks old and underwent scaffold biopsy and replacement until the time of hyperglycemia onset (progressors) or 30 week of age (non-progressors and NOR). Scaffolds were selected for

sequencing based on proximity to hyperglycemia or age for progressors and non-progressors/NOR respectively. (B) NOD and NOR mice are background matched at the MHC H2g7 locus. (C) No NOR mice became diabetic, and approximately 50% of NOD mice developed symptomatic disease during the study. (D) Both NOR and NOD non-progressor mice maintained stable glucose levels throughout the duration of the study. (E) Initial filtering of bulk sequencing data from all groups identified 4,593 of the 23,096 sequenced genes above our expression and variance filters for all samples.

4.4.2 IN analysis separates all NOD mice from NOR controls regardless of disease progression

We initially analyzed the data to determine if we can distinguish the healthy mice (NOR) from the mice that are at risk of developing diabetes (NOD). Following gene filtering, we analyzed this reduced gene set through an elastic net regression to identify the gene set that separates NOD mice from the NOR controls. We identified a 120 gene signature to distinguish NOD from NOR samples at all times (Figure 4.2A), which performed with a receiver operating characteristic curve score (ROC)>0.9 across 50 iterations of train and test partitioning (Figure 4.2B). Principal component analysis (PCA) was performed using this gene set, and we showed that it correctly separates all NOR and NOD samples (Figure 4.2C). In addition to separating the two groups, we also ran an elastic net regression on each time point for the NOR samples. We identified 39 genes (Figure 4.2D) that changes over time in the NOR mouse and separate early from late time points (Figure 4.2E). Analyzing the NOR group over time served as a control for aging and non-diabetes related changes on the background. We applied GSVA to these 39 genes to identify the cellular processes in which they are involved. Compared to the 3384 gene sets in the curated mouse chemical and genetic perturbations gene sets, this analysis identified 13 gene sets related to the time course signature, including gene sets associated with aging and cancer (Figure 4.2F).[20–23] The 39 genes from the NOR time course analysis were filtered out for all subsequent analyses, as their changes do not relate to T1D disease progression.

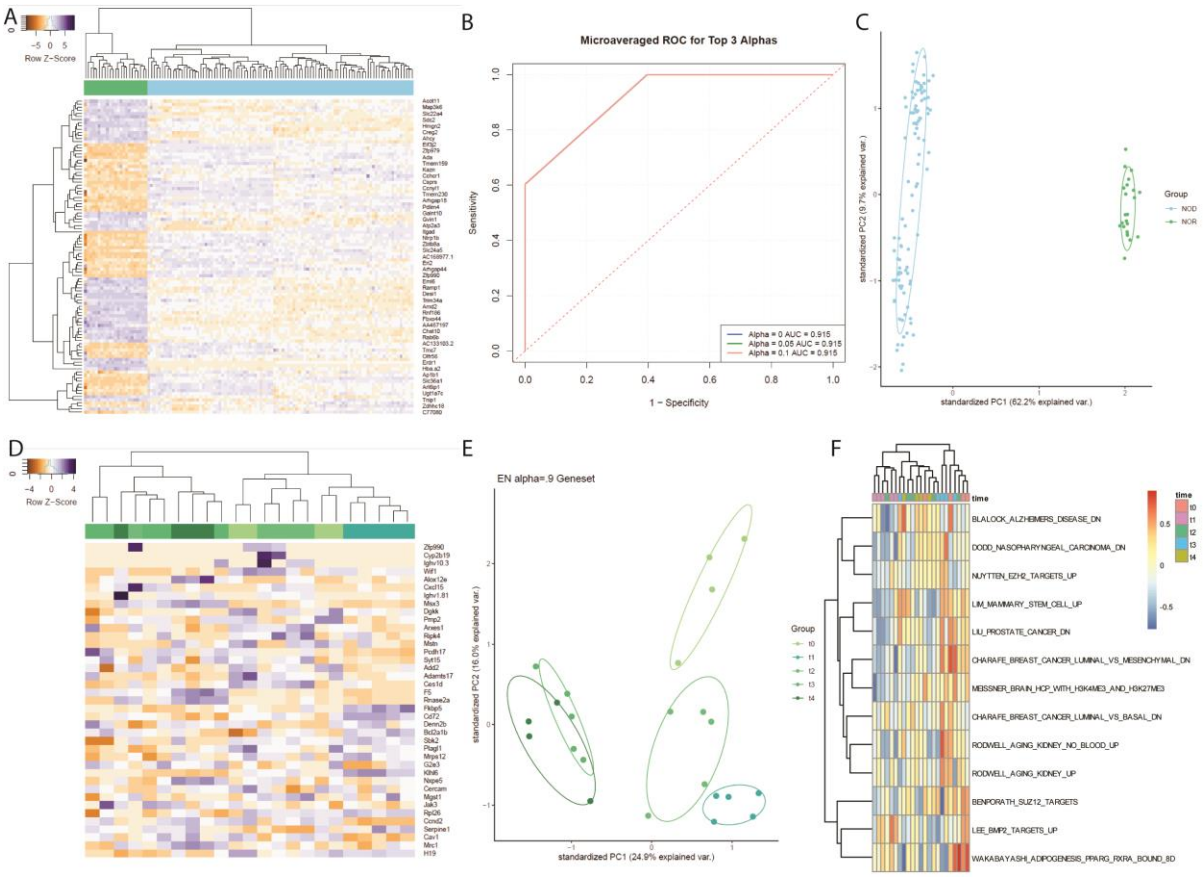


Figure 4.2: IN analysis separates all NOD mice from NOR controls regardless of disease progression. (A) All NOD mice (n=97) are separable from NOR controls (n=23) across timepoints using a 101 gene signature. (B) Group seperation has a ROC performance above 0.9 for 50 iterations of training/test data partitioning for fitting the elastic net model. (C) PCA of the samples using the 101 gene signature shows complete separation of the two groups. (D) Samples from NOR mice across six timepoints identify 39 genes that vary with age. (E) PCA of the NOR time signature shows separation of the diabetic and 1 week before onset timepoints from all earlier timepoints on PCA1, and separation of the earlier three timepoints on PC2. (F) GSVA of the NOR time course signature identified 13 genes from the curated mouse chemical and genetic gene sets that are related to the time course signature.

4.4.3 NOD progressors and non-progressors are separable as early as 6 weeks of age

We next analyzed the at-risk population to determine the ability to distinguish those that would progress to diabetes from those that would remain normoglycemic. Progressors were identified as mice that developed hyperglycemia, defined as two consecutive blood glucose readings above 250 mg/dL, and non-progressors maintained glucose control throughout the duration of the study (Figure 4.1D). Multiple partitioning of the elastic net regression on the week 6 samples from

progressors and non-progressors identified a 13 gene signature (Figure 4.3A) that separated the two

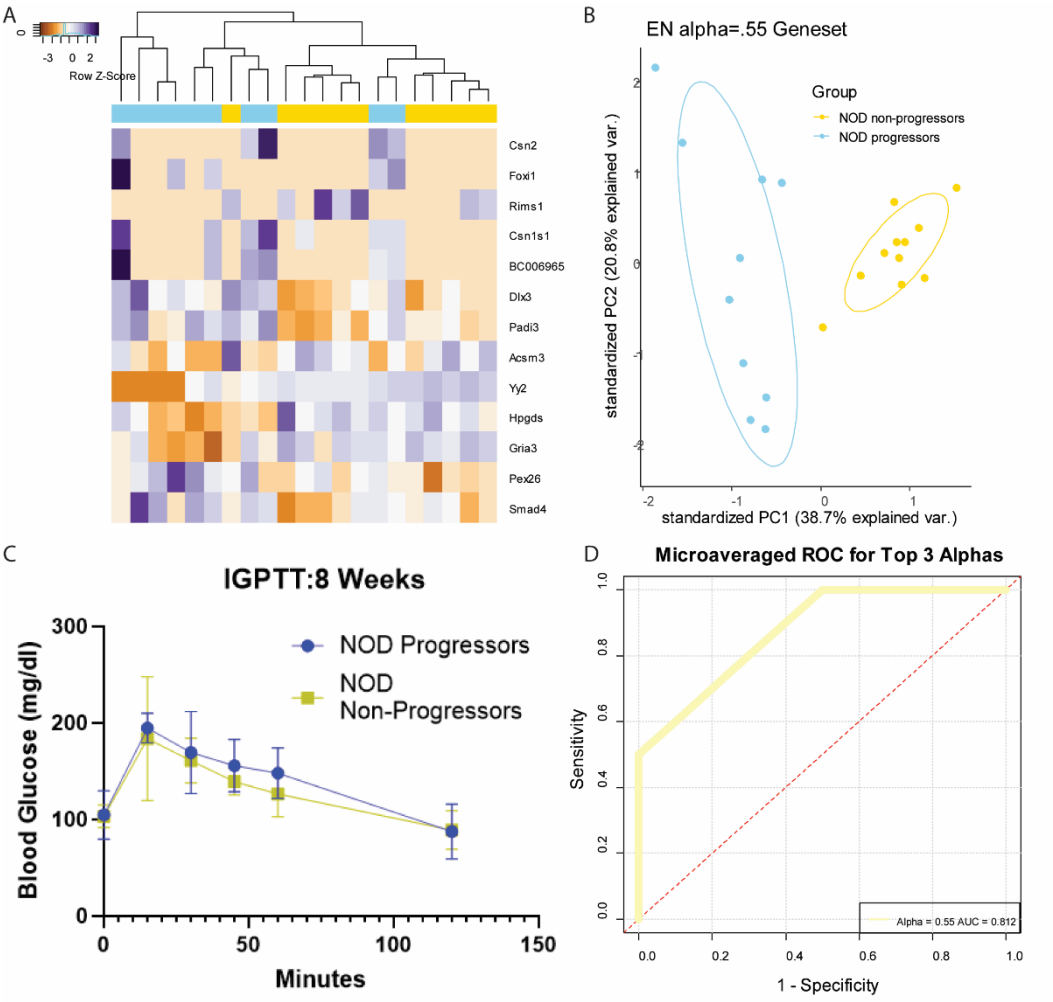


Figure 4.3: NOD progressors and non-progressors are separable as early as 6 weeks of age (A) Elastic net regression performed on week six samples from NOD progressors (n=10) and NOD non-progressors (n=11) identified a 13 gene signature. (B) PCA of the 13 gene signature results in group separation, with no overlap of the two groups. (C) IPGTT of a separate group of progressors and non-progressors (n=4 per group) showed no significant difference in glucose tolerance at 8 weeks of age. (D) Five iterations of train and test partitioning validation performed with ROC>0.8 for alpha=0.55, showing predictive power not shown by the IPGTT functional test.

groups (Figure 4.3B). Current clinical practice for identifying T1D progression in patients is by dysglycemia as indicated by a glucose tolerance test. For NOD mice, an IPGTT can be performed to identify dysglycemia at approximately 14 weeks of age.[24] We performed an IPGTT at 8 weeks, which showed no differences between progressors and non-progressors that have received IN implants (Figure 4.3C), indicating that our gene signature identifies disease prior to the clinical

standard equivalent in mice. Five iterations of train and test partitioning were performed with ROC>0.8 when comparing progressors and non-progressors at week 6 (Figure 4.3D). We next performed train and test validation on week 6 progressors compared to non-progressors at all time points. We identified an eight gene signature, Dlx3, Padi3, Sh3gl3, Gnasas1, Sox11, Marco, F2rl1, and Dlk1, that separates week 6 progressor samples from all non-progressor timepoints (Figure 4.4A, 4.4C). This signature performs with ROC>0.8 across 50 train and test iterations (Figure 4.4B). We next used a published data set of single cell RNA sequencing of immune, mesenchymal, and endothelial components of NOD pancreatic islets to identify which of these signature genes being captured by the IN are present at the pancreas (Figure 4.6A).[25] Six of the eight signature genes were found in the sequenced cells, Padi3, Sh3gl3, Sox11, Marco, F2rl1, and Dlk1, and Sox 11 was expressed by the greatest number of cells (Figure 4.4C). Dot plot analysis shows the highest expression of Sox11 in endothelial cells at 4 weeks, as well as Dlk1 in non-specific lymphoid cells at 8 weeks (Figure 4.4E). This analysis indicates that genes that are changing expression levels at the pancreas are also changing within the IN, suggesting that the IN serves as a distal site that can reflect changes occurring in the primary tissue.

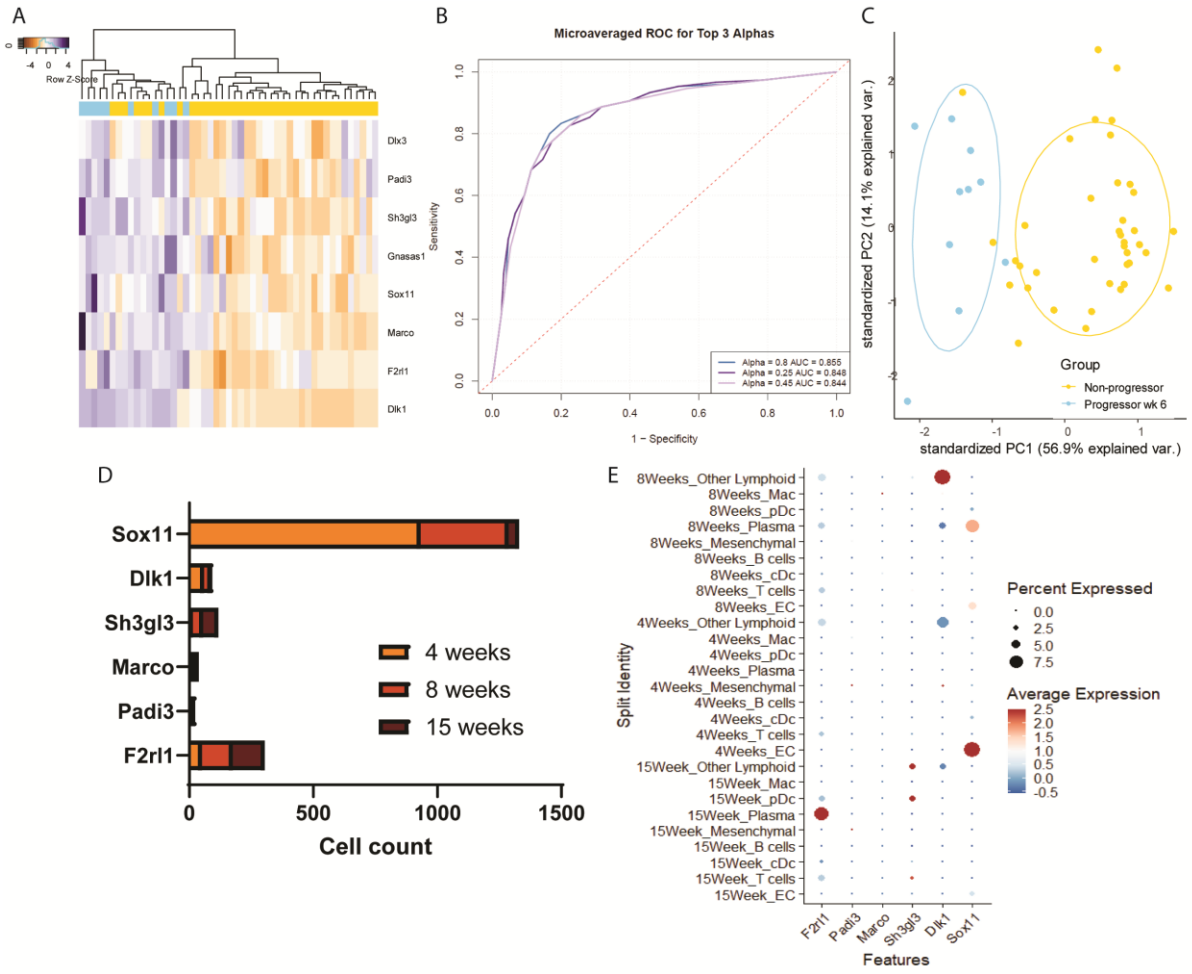


Figure 4.4: Six week signature can be applied to all time points in non-progressors, and relates to changes at the pancreas.(A) Elastic net regression performed on week six samples from NOD progressors (n=10) and NOD non-progressors from all time points (n=39) identified an eight gene signature. (B) The eight gene signature performed with ROC>0.8 across 50 iterations of train and test partitioning validation. (C) PCA of the eight gene signature results in group separation with two false positives, and no overlap of the two groups' confidence intervals. (D) Six of the eight signature genes are present in a single cell RNA sequencing data set performed on NOD islets at three timepoints: 4, 8, and 15 weeks of age. (E) A dot plot showing the average expression and percentage of cells expressing the signature genes identifies upregulation of Sox11 in islet endothelial cells at week 4, of Dlk1in lymphoid cells at week 8, and of F2rl1 in plasma at week 15.

4.4.4 IN analysis identifies pre-symptomatic disease 7 weeks before symptom onset

We next sought to identify changes over time within the mice that would progress to diabetes. Elastic net regression with multiple partitioning of all timepoints normalized to week 6 shows a shift in the groups from early to late times, with samples from symptom onset, one week before onset, and three weeks before onset all clustering together (Figure 4.5A). Seven weeks before onset (-7) and the three latest timepoints, 3 weeks before, 1 week before, and time of onset, separated

completely. Five weeks before (-5) onset spanned the difference between -7 and later timepoints (Figure 4.5A), indicated the -7 to -5 week time frame as a period of transition during disease progression. As a result, we ran an elastic net for the -7 and -5 timepoints, identifying a 13 gene signature that separates the two groups: Amd1, Chp1, Zfp760, Snca, Zc3h12a, Lipm, Lor, Adamts3, Ccdc85b, Erdr1, Rbfa, Mgat2, and H2ac88 (Figure 4.5B-C). This signature was employed to develop a scoring system for all samples using both a supervised Random Forest (RF) and unsupervised Singular Value Decomposition (SVD). Using these scoring systems, we show that the gene signature for the -7 to -5 transition separates all later timepoints from the -7 and week 6 timepoints (Figure 4.5D). When evaluated on a per mouse basis, the RF scores indicate a significant score increase between -7 and -5 weeks, with no significant changes between -5 weeks relative to disease onset and any later timepoints (Figure 4.5E). SVD indicates a significant change between 6 weeks and -7 weeks relative to disease onset, with no later significant changes (Figure 4.5F). Taken together, the scoring shows both a progression from the initial timepoint (Figure 4.5F), as well as a transitional point in disease progression (Figure 4.5E). When validated through 50 train and test iterations, elastic net regression of -7 weeks versus all later timepoints performs with ROC>0.85 (Figure 4.5G).

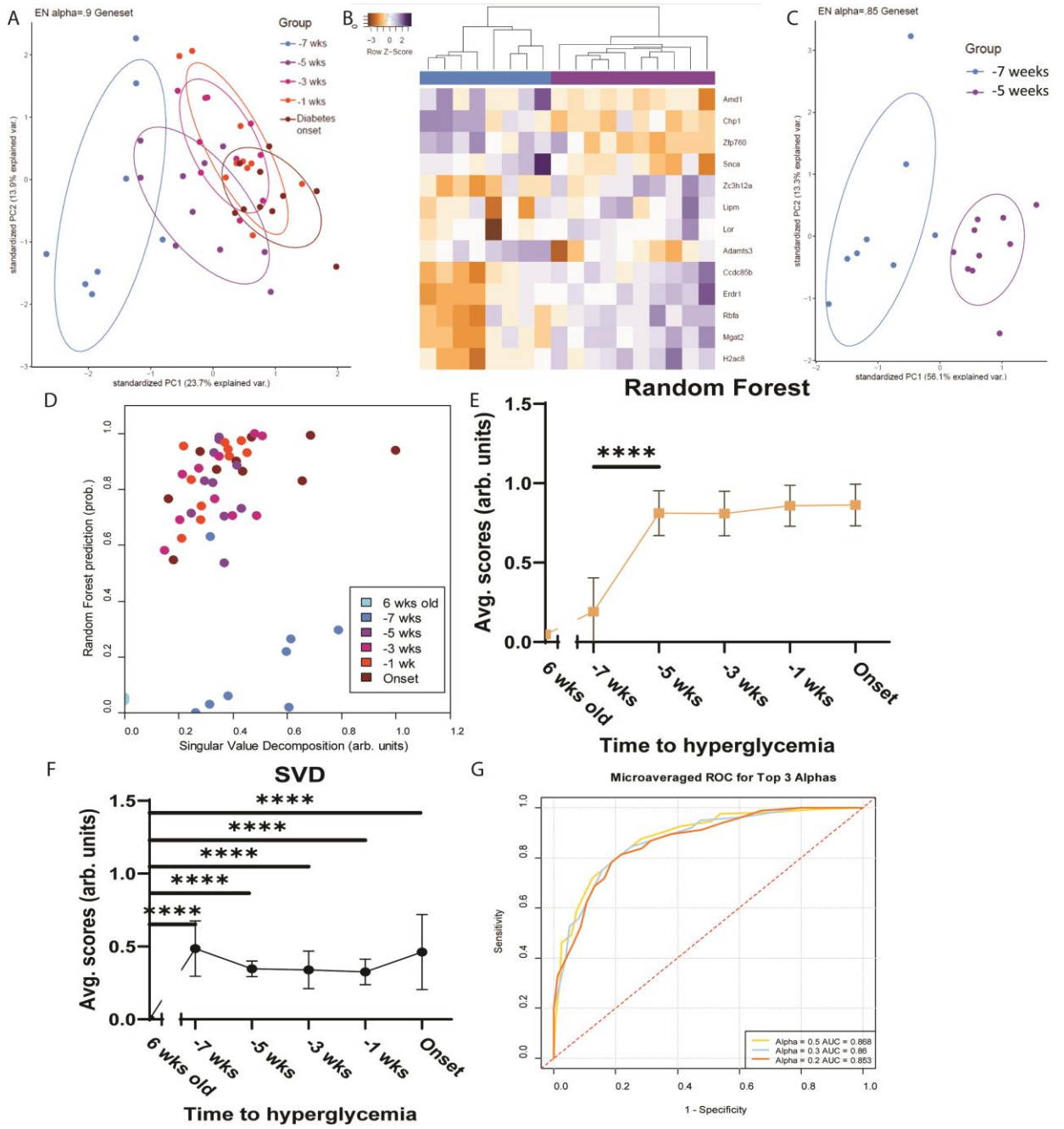


Figure 4.5: A 13 gene signature separates NOD progressors 7 weeks before onset from all later time points. (A) PCA of an elastic net regression run on all NOD progressor time points (n=8 for -7 weeks, n=10 all other groups) normalized to week 6 shows separation between -7 and -3 through onset, with -5 spanning the middle. (B) Elastic net regression of -7 versus -5 resulted in a 13 gene signature, and (C) PCA shows complete separation of the two groups according to the signature. (D) All time points were scored using random forest and singular value decomposition according to the 13 gene signature, showing separation of -7 and week 6 from the later time points. (E) The random forest scores on a per mouse basis show significant difference between -7 and -5, ($p<0.0001$) and no significant difference between -5 and later times. (F) SVD per mouse shows a significant difference between 6 weeks and all later time points ($p<0.0001$), and no significant difference between -7 and later time points. (G) Train and test partition validation of -7 versus all later time points performed with ROC>0.85 for 50 iterations.

4.4.5 Progression signature genes correspond to cell types found in the pancreas

We again employed single cell sequencing data to identify the cell types within the pancreas that are expressing the 13 genes in the progression signature. We found that 11 of the 13 signature genes are expressed in the immune, endothelial, or mesenchymal cells of NOD islets: Amd1, Chp1, Zfp760, Snca, Zc3h12a, Lor, Adamts3, Ccdc85b, Erdr1, Rbfa, and Mgat2, with dot plot analysis showing the expression of each gene across cell types and time (Figure 4.6B). When analyzing the expression of these genes over time, the number of cells expressing signature genes is greater at the 4 and 8 week time points in comparison to 15 weeks (Figure 4.6C). The greatest proportion of signature expressing cells comes from endothelial cells, with appreciable leukocyte populations present for 7 genes: Chp1, Rbfa, Zc3h12a, Mgat2, Amd1, Ccdc85b, and Erdr1 (Figure 4.6D).

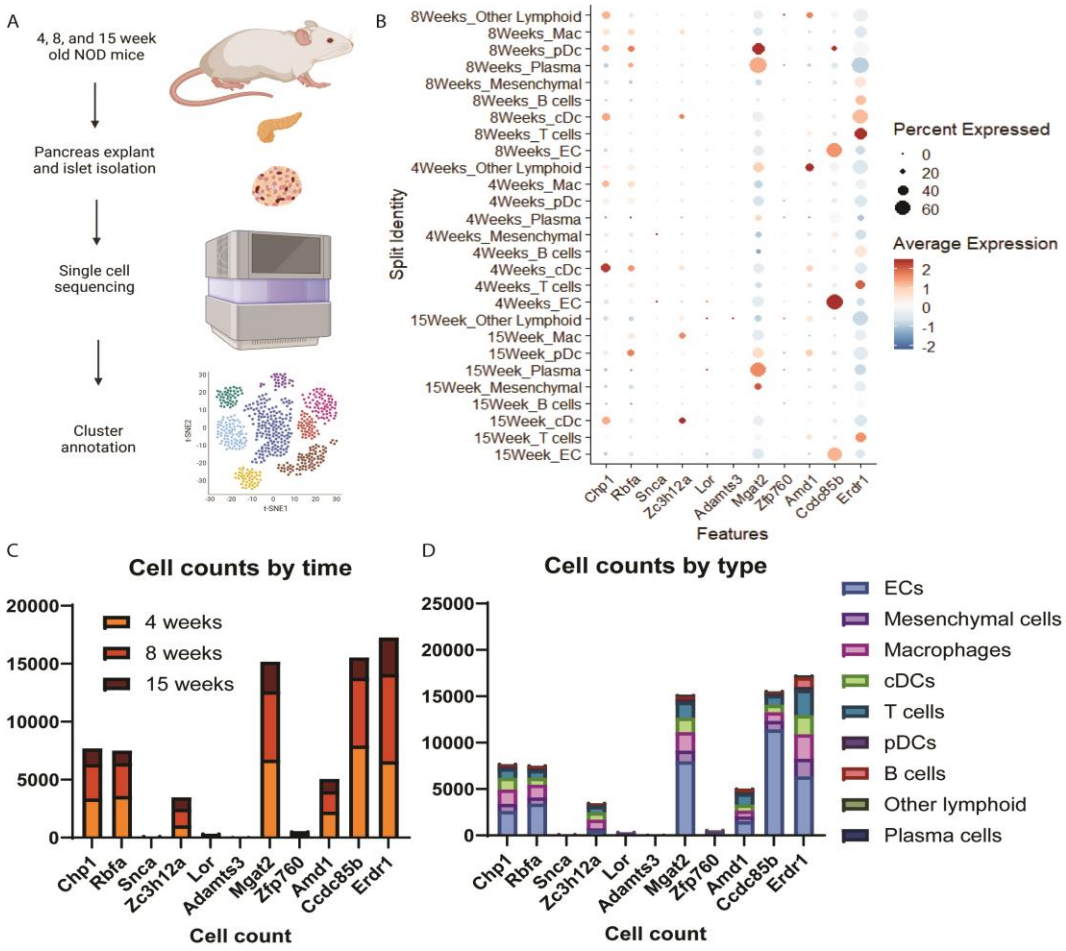


Figure 4.6: NOD progressor signature genes are found in the pancreatic islets. (A) A publicly accessible data set for single cell sequencing of the pancreatic islets of NOD at three time points was annotated to identify cell clusters during the time course of disease progression. (B) Dot plot analysis of the annotated data show that 11 of the 13 genes in the -7 versus -5 signature are expressed in immune, endothelial, or mesenchymal cells within pancreatic islets. (C) Quantification of the number of cells expressing each signature gene over time shows higher cell counts for signature expressing cells at weeks 4 and 8 compared to week 15 for 5 genes: Chp1, Rbfa, Mgat2, Ccdc85b, and Erdr1. (D) The number of cells expressing signature genes by cell type show the greatest number of endothelial cells for all cells expressing signature genes, with appreciable leukocyte populations present for 7 genes: Chp1, Rbfa, Zc3h12a, Mgat2, Amd1, Ccdc85b, and Erdr1.

4.5 Discussion

Advancements in immunotherapies for T1D have highlighted the lack of monitoring tools to identify disease progression prior to functional ß cell loss. Autoantibodies have utility as a screening tool when identifying candidates for immunotherapies, yet there is wide variability in time to disease progression within autoantibody positive groups. Efforts have been made to

identify other blood-based indicators for T1D, with success in identifying biomarkers of disease development independent of autoantibody presence.[26] However, these antibody independent biomarkers are similar to the antibody biomarkers in that they predict the risk of eventual disease state and do not demonstrate disease changes over time. Another approach has been to identify the presence of diabetogenic T cells as lagging indicators of T1D progression,[27] yet this strategy does not account for the role of the innate immune response and insulitis that prompts β cell targeting and promotes T cell activation and would thus be an early indicator of T1D progression.[28–30] The IN offers a distinct approach by focusing on cell infiltration of a tissue surrogate, which reflect phenotypes associated with the tissue that can significantly differ from phenotypes in circulation. The IN has been shown to capture disease associated changes in models of T1D, EAE, cancer, and transplant rejection.[15–17,31,32] In these models, the IN offers a minimally invasive option for long-term monitoring of a tissue specific immune response without perturbing the already stressed tissue or organ. In the case of T1D, the IN enables monitoring of specific transcriptomic changes that indicate progression of disease, rather than relying on functional loss indicated by dysglycemia, or autoimmune targeting identified by the presence of diabetogenic T cells. The IN's ability to capture broad systemic changes offers a comprehensive approach to disease monitoring.

Our transcriptomic analysis of the IN discerns disease progression from background processes. NOR mice act as a control population without diabetic risk capable of accounting for disease agnostic immunological changes. The NOD and NOR mice in the study were treated as at-risk, and non-risk groups respectively, similar to the delineation between autoantibody positive and autoantibody negative populations. Isolating the at-risk group allowed identification of changes in NOD specific to T1D, which could then be related to immunological changes at the pancreas. For example, time dependent changes in the NOR group showed connections to aging and cancer

related pathways (Figure 4.2F), which isolates transcriptomic changes on the background that are independent of T1D progression. The ability to account for background processes will facilitate translation, as patients may experience other illnesses while being monitored for T1D progression. While the genetic background match used here is not possible for a heterogenous human population, the use of a T1D risk-free group could control for non-disease specific changes. IN specificity to disease has been established in a model of transplant rejection, showing distinct transcriptomic changes when comparing rejection to respiratory infection.[17] Similarly to how the time dependent changes herein were filtered out to identify T1D specific changes, genetic signatures for other diseases can be used to account for non-T1D illnesses that arise throughout the course of monitoring.

Through IN monitoring, T1D progressors can be identified from the at-risk population as early as 6 weeks of age. Within the autoantibody positive population, a proportion of individuals will never progress to symptomatic T1D.[33] Our analysis aimed to separate the group of non-progressors from the earliest time point of progressors in order to focus our longitudinal analysis on the changes associated with disease progression and identify candidates who need more frequent monitoring. Identifying those individuals that are unlikely to progress would alleviate the burden of frequent monitoring for this group, while also indicating the need for additional surveillance and potential intervention in the progressing group. The signature also identifies progressors at a time when no significant differences in glucose tolerance test results are observed for progressing and non-progressing groups (Figure 4.3C), indicating that signature changes precede a functional loss in glucose responsiveness. The signature itself, Dlx3, Padi3, Sh3gl3, Gnasas1, Sox11, Marco, F2rl1, and Dlk1, offers insight into the biological differences between progressors and non-progressors. Marco for example, encodes a macrophage receptor and is upregulated in progressors.

Macrophages are part of the early innate immune response responsible for insulitis,[34] so an increase in their abundance relative to non-progressors indicates that changes in the innate immune response are an early sign of disease progression. F2rl1, also known as Par2, encodes a receptor found on several immune cell populations and is a regulator of inflammation and metabolism.[35] Investigation into its role in T1D has shown that F2rl1 activation has a protective effect on β cells locally, but when elevated in the immune system increases autoimmunity.[36] When compared across time in single cell data from NOD islets, F2rl1 expression is low in cells at the islets for weeks 4 and 8 (Figure 4.4E), yet these genes are highly expressed at the IN. The expression F2rl1 at sites distant to the pancreas demonstrates the utility of the IN for identifying immune specific changes independent of islet infiltration, and its capability of identifying early indicators of disease. Dlk1 is essential to glucose metabolism and has also been associated with inherited risk of T1D.[37,38] Sh3gl3 has been linked to insulin resistance,[39] while Gnasas1 is the antisense strand to GNAS, which is needed for insulin secretion.[40] Sox11 has been indicated as a regulator of β cell regeneration, which could indicate that the increased Sox11 in progressors is an attempted compensatory response to early disease progression.[41] Taken together, the eight gene signature delineating 6-week-old progressors from non-progressors demonstrates the IN's capabilities for identifying disease before functional loss, as well as biomarkers that point to underlying mechanisms of early disease.

IN monitoring distinguishes disease specific changes over time within the progressors. Disease progression is identifiable 7 weeks before symptom onset, with scoring on the 13 gene signature for the transition from -7 to -5 successfully separating all later time points from 7 weeks pre-onset. As this signature precedes significant changes shown by IPGTT, the signature offers a predictive indicator for therapy prior to functional loss. Of the 13 gene signature, 11 are expressed in the

pancreatic islets of NOD mice (Figure 4.6B). Of the expressed genes, Amd1, Mgat2, and Snca have been associated with type 2 diabetes in the literature, with Mgat2 functioning as a regulator of lipid metabolism, and Snca expression being shown to have an inverse relationship to insulin resistance.[42–44] Chp1 is also involved in lipid metabolism,[45] and Zc3h12a expression is upregulated in β cells in models of type 1 and type 2 and has an inhibitory effect on downstream insulin secretion mechanisms.[46] The finding of metabolic pathways being altered may reflect recent work suggesting that metabolic differences in the microbiomes of autoantibody positive individuals are associated with the rate of T1D progression.[47,48] A mutation in the Adamts3 gene is related to higher risk of T1D,[49] while Rbfa is the gene for a ribosome binding protein, the family of which have been shown to not function properly in diseased states including diabetes.[50] While not directly to diabetes or metabolism, Erdr1 is a regulator of T cell and NK cell activation and has been implicated in macrophage polarization.[51] Notably, Erdr1 has the highest cell count in our single cell analysis of the signature genes (Figure 4.6C), indicating Erdr1's presence in the IN signature may be indicating its immune activating role at the pancreas. Additionally, the ability to delineate between an early disease time point, -7 weeks, and all later time points using a signature trained on only two points, which may reflect an inflection point within disease progression. In practice, monitoring all patients at the exact same proximity to disease is implausible. Our results show that regardless of the exact timing, unsupervised scoring by SVD shows a significant difference between an initial baseline and any disease progression (Figure 4.5F). The supervised method can then be used to identify whether that change corresponds to an early or late progression, in this model corresponding to more than seven or less than five weeks from onset respectively (Figure 4.5E). This dual approach enables an early versus late progression categorization without the need to wait for measurable glucose dysregulation.

In conclusion, transcriptomic analysis of the IN is capable of stratifying at-risk and non-risk groups, progressors from non-progressors, and timeframe of progression in the NOD model of T1D. These results provide the basis for a monitoring strategy at a subcutaneous site for a disease that is currently dependent on functional loss for clinical diagnosis. By identifying individuals who will progress to symptomatic disease, we would be able to administer preventive therapies at a time to preserve the greatest cellular function. Additionally, the genetic signatures derived for disease progression may have the potential to inform future targets for treatment and elucidate currently unknown mechanisms of disease.

4.6 Methods

4.6.1 IN fabrication

INs were prepared by pressing a mixture of PCL microspheres and 250-425 μm NaCl in a 5mm die at 1500 psi for 30 seconds and heated each side at 60 ˚C for 5 minutes as previously described[52,53]. A deionized water bath was used to remove the salt from the IN, and the resulting porous scaffolds were sterilized with 70% ethanol and sterile PBS rinses. INs were dried on sterile gauze, and then stored at -80 ˚C until use.

4.6.2 Glucose monitoring

Non-fasted blood glucose measurements were taken on Monday, Wednesday and Friday via tail-vein prick. Measurements were taken with an Accu-Chek Aviva Plus blood glucose monitor and strips (Roche Cat. Nos. 6908373001). Measurements were taken until diabetes incidence defined as two consecutive readings above 250 mg/dL, or the conclusion of the study at 30 weeks of age.

4.6.3 IN implantation

All animal work was conducted under approved protocols and regulations of the Institutional Animal Care and Use Committee of the University of Michigan. Four week old NOD/ShiltJ (strain #001976) and NOR/LtJ (strain # 002050) mice were purchased from Jackson Laboratory. Blood glucose measurements were taken prior to surgery, and 5 mg/kg carprofen analgesic was given before implantation. INs were implanted into the subcutaneous space under 2% inhaled isoflurane anesthesia. Additional analgesic was administered 24 hours after surgery.

4.6.4 IN explantation

IN explantation followed the same anesthesia and analgesic administration as implantation and began at 6 weeks for all mice. INs were explanted via an incision in the skin, and the removed INs were replaced with an additional IN implant into the same space. The removal and replacement surgeries were conducted weekly until the time of diabetes onset in progressors, or 30 weeks of age in NOR and non-progressors. INs were flash frozen in isopentane immediately after explantation, and stored on dry ice until all samples were transported to a -80 ˚C freezer for long-term storage.

4.6.5 RNA sequencing

Scaffolds were lysed in 800ul TRIzol reagent (Fisher Scientific, Cat. No. 15596026) and homogenized at 15000 RPM. The homogenized scaffold solution was centrifuged to pellet any remaining scaffold debris, and the supernatant was taken for RNA isolation. RNA isolation was performed using the Zymo Direct-zol RNA miniprep kit (Fisher Scientific, Cat. No. NC1047980), and the Zymo DNase 1 set with DNA digestion buffer (Fisher Scientific, Cat. No. NC0847937). Concentration of the isolated RNA was measured using a NanoDrop, and RNA was stored at -80 ˚C until being submitted for sequencing. Sequencing was performed by the Advanced Genomics

Core at the University of Michigan. Ribo depletion was used for a total RNA library preparation. Sequencing was run on the Illumina NovaSeq S4 with 300 cycles.

4.6.6 Computational analysis

Full code for computational analysis of RNA sequencing data can be found at https://github.com/shea-lab/INforT1Dprogression. Briefly, count data from two batches of sequencing was read into R and categorized according to disease state and time. The combined data sets were batch corrected, and genes with low expression and/or variance across samples. Filtered data was then passed through an elastic net regression to identify the genes most contributing to inter condition variance (the gene signature). For train and test validation, the elastic net regression was performed on 60% of the data for each group, and the resulting signature performance on the remaining 40%. Gene set variation analysis was performed using the GSVA package in R.[23] Singular value decomposition (SVD) and random forest (RF) were used to test the robustness of the signatures to other analysis, and the combination of SVD and RF performance was used to determine the signature score per mouse. Single cell data was annotated using scanpy in Python, and then transformed to a Seurat object to identify cells expressing the signature genes in R.

4.7 Acknowledgements

Support for this work was provided by JDRF, the JDRF Center of Excellence at the University of Michigan, the Caswell Diabetes Center, and NIH grants 1R01DK121462 and 1R01CA272940-01A1. J.L.K. was supported by the National Science Foundation Graduate Research Fellowship under Grant No. DGE-2241144. Figures were created in Biorender.com and Adobe Illustrator.

4.8 References

1. Gregory, G. A. *et al.* Global incidence, prevalence, and mortality of type 1 diabetes in 2021 with projection to 2040: a modelling study. *Lancet Diabetes Endocrinol* **10**, (2022).
2. Parums, D. V. Editorial: First Regulatory Approval for Allogeneic Pancreatic Islet Beta Cell Infusion for Adult Patients with Type 1 Diabetes Mellitus. *Medical Science Monitor* vol. 29 Preprint at https://doi.org/10.12659/MSM.941918 (2023).
3. Qi, M. *et al.* Five-year follow-up of patients with type 1 diabetes transplanted with allogeneic islets: the UIC experience. *Acta Diabetol* **51**, (2014).
4. Kramer, V. Expanded FORWARD Trial Demonstrates Continued Potential for Stem Cell-Derived Islet Cell Therapy to Eliminate Need for Insulin for People with T1D. *American Diabetes Association* (2024).
5. Stegall, M. D., Lafferty, K. J., Kam, I. & Gill, R. G. Evidence of recurrent autoimmunity in human allogeneic islet transplantation. *Transplantation* **61**, (1996).
6. Yue, L. *et al.* Cutting edge of immune response and immunosuppressants in allogeneic and xenogeneic islet transplantation. *Front Immunol* **15**, (2024).
7. Taplin, C. & Barker, J. Autoantibodies in type 1 diabetes. *Autoimmunity* **41**, 11–18 (2008).
8. Ziegler, A. G. *et al.* Seroconversion to Multiple Islet Autoantibodies and Risk of Progression to Diabetes in Children. *JAMA* **309**, 2473–2479 (2013).
9. Peters, A. Screening for Autoantibodies in Type 1 Diabetes: A Call to Action. *J Fam Pract* **70**, (2021).
10. Jacobsen, L. M. *et al.* The risk of progression to type 1 diabetes is highly variable in individuals with multiple autoantibodies following screening. *Diabetologia* **63**, (2020).
11. Ramos, E. L. *et al.* Teplizumab and β-Cell Function in Newly Diagnosed Type 1 Diabetes. *New England Journal of Medicine* **389**, 2151–2161 (2023).

12. Herold, K. C. *et al.* An Anti-CD3 Antibody, Teplizumab, in Relatives at Risk for Type 1 Diabetes. *New England Journal of Medicine* **381**, 603–613 (2019).
13. Sims, E. K. *et al.* Teplizumab improves and stabilizes beta cell function in antibody-positive high-risk individuals. *Sci Transl Med* **13**, (2021).
14. Keam, S. J. Teplizumab: First Approval. *Drugs* **83**, (2023).
15. King, J. L. *et al.* Polymer scaffolds delineate healthy from diseased states at sites distal from the pancreas in two models of type 1 diabetes. *Biotechnol Bioeng* **121**, 3600–3613 (2024).
16. Morris, A. H. *et al.* Engineered immunological niches to monitor disease activity and treatment efficacy in relapsing multiple sclerosis. *Nat Commun* **11**, (2020).
17. Urie, R. R. *et al.* Biomarkers from subcutaneous engineered tissues predict acute rejection of organ allografts. *Sci. Adv* **10**, 6178 (2024).
18. Prochazka, M., Serreze, D. V., Frankel, W. N. & Leiter, E. H. NOR/Lt mice: MHC-matched diabetes-resistant control strain for NOD mice. *Diabetes* **41**, (1992).
19. Pozzilli, P., Signore, A., Williams, A. J. K. & Beales, P. E. NOD mouse colonies around the world- recent facts and figures. *Immunol Today* **14**, (1993).
20. Subramanian, A. *et al.* Gene set enrichment analysis: A knowledge-based approach for interpreting genome-wide expression profiles. *Proc Natl Acad Sci U S A* **102**, (2005).
21. Castanza, A. S. *et al.* Extending support for mouse data in the Molecular Signatures Database (MSigDB). *Nature Methods* vol. 20 Preprint at https://doi.org/10.1038/s41592-023-02014-7 (2023).
22. Liberzon, A. *et al.* Molecular signatures database (MSigDB) 3.0. *Bioinformatics* **27**, (2011).
23. Hänzelmann, S., Castelo, R. & Guinney, J. GSVA: Gene set variation analysis for microarray and RNA-Seq data. *BMC Bioinformatics* **14**, (2013).

24. Ize-Ludlow, D. *et al.* Progressive erosion of β-cell function precedes the onset of hyperglycemia in the NOD mouse model of type 1 diabetes. *Diabetes* **60**, (2011).
25. Zakharov, P. N., Hu, H., Wan, X. & Unanue, E. R. Single-cell RNA sequencing of murine islets shows high cellular complexity at all stages of autoimmune diabetes. *Journal of Experimental Medicine* **217**, (2020).
26. Nakayasu, E. S. *et al.* Plasma protein biomarkers predict the development of persistent autoantibodies and type 1 diabetes 6 months prior to the onset of autoimmunity. *Cell Rep Med* **4**, (2023).
27. Schroderus, A.-M. *et al.* Temporal Alterations in CD8+ T Cells During the Progression From Stage 1 to Stage 3 Type 1 Diabetes. *Diabetes* **73**, 1705–1715 (2024).
28. Jun, H. S., Yoon, C. S., Zbytnuik, L., Van Rooijen, N. & Yoon, J. W. The role of macrophages in T cell-mediated autoimmune diabetes in nonobese diabetic mice. *Journal of Experimental Medicine* **189**, (1999).
29. Petrelli, A. *et al.* The Contribution of Neutrophils and NETs to the Development of Type 1 Diabetes. *Frontiers in Immunology* vol. 13 Preprint at https://doi.org/10.3389/fimmu.2022.930553 (2022).
30. Price, J. D. & Tarbell, K. V. The role of dendritic cell subsets and innate immunity in the pathogenesis of type 1 diabetes and other autoimmune diseases. *Front Immunol* **6**, (2015).
31. Wang, J. *et al.* A synthetic metastatic niche reveals antitumor neutrophils drive breast cancer metastatic dormancy in the lungs. *Nat Commun* **14**, (2023).
32. Oakes, R. S. *et al.* Metastatic conditioning of myeloid cells at a subcutaneous synthetic niche reflects disease progression and predicts therapeutic outcomes. *Cancer Res* **80**, 602–612 (2020).

33. Hanna, S. J. *et al.* Slow progressors to type 1 diabetes lose islet autoantibodies over time, have few islet antigen-specific CD8+ T cells and exhibit a distinct CD95hi B cell phenotype. *Diabetologia* **63**, (2020).
34. Carrero, J. A. *et al.* Resident macrophages of pancreatic islets have a seminal role in the initiation of autoimmune diabetes of NOD mice. *Proc Natl Acad Sci U S A* **114**, (2017).
35. Heuberger, D. M. & Schuepbach, R. A. Protease-activated receptors (PARs): Mechanisms of action and potential therapeutic modulators in PAR-driven inflammatory diseases. *Thrombosis Journal* vol. 17 Preprint at https://doi.org/10.1186/s12959-019-0194-8 (2019).
36. Reches, G., Khoon, L., Ghanayiem, N., Malka, A. & Piran, R. Controlling autoimmune diabetes onset by targeting Protease-Activated Receptor 2. *Biomedicine & Pharmacotherapy* **175**, 116622 (2024).
37. Abdallah, B. M., Ditzel, N., Laborda, J., Karsenty, G. & Kassem, M. DLK1 regulates whole-body glucose metabolism: A negative feedback regulation of the osteocalcin-insulin loop. *Diabetes* **64**, (2015).
38. Wallace, C. *et al.* The imprinted DLK1-MEG3 gene region on chromosome 14q32.2 alters susceptibility to type 1 diabetes. *Nat Genet* **42**, (2010).
39. Tim, B., Kouznetsova, V. L., Kesari, S. & Tsigelny, I. F. Targeting of insulin receptor endocytosis as a treatment to insulin resistance. *J Diabetes Complications* **37**, (2023).
40. Taneera, J. *et al.* GNAS gene is an important regulator of insulin secretory capacity in pancreatic β-cells. *Gene* **715**, (2019).
41. Khurana, I. *et al.* DNA methylation status correlates with adult β-cell regeneration capacity. *NPJ Regen Med* **6**, (2021).

42. Zhou, X. *et al.* Whole exome sequencing study in a family with type 2 diabetes mellitus. *Int J Gen Med* **14**, (2021).
43. Mochida, T. *et al.* Inhibition of MGAT2 modulates fat-induced gut peptide release and fat intake in normal mice and ameliorates obesity and diabetes in ob/ob mice fed on a high-fat diet. *FEBS Open Bio* **10**, (2020).
44. Rodriguez-Araujo, G. *et al.* Low alpha-synuclein levels in the blood are associated with insulin resistance. *Sci Rep* **5**, (2015).
45. Zhu, X. G. *et al.* CHP1 Regulates Compartmentalized Glycerolipid Synthesis by Activating GPAT4. *Mol Cell* **74**, (2019).
46. Tyka, K. *et al.* MCPIP1 is a novel link between diabetogenic conditions and impaired insulin secretory capacity. *Biochim Biophys Acta Mol Basis Dis* **1867**, (2021).
47. Vatanen, T. *et al.* The human gut microbiome in early-onset type 1 diabetes from the TEDDY study. *Nature* **562**, (2018).
48. Lamichhane, S. *et al.* Circulating metabolic signatures of rapid and slow progression to type 1 diabetes in islet autoantibody-positive children. *Front Endocrinol (Lausanne)* **14**, (2023).
49. Jambaljav, B. *et al.* Whole-exome sequencing in a Japanese family with highly aggregated diabetes identifies a candidate susceptibility mutation in ADAMTSL3. *Diabetes Res Clin Pract* **135**, (2018).
50. Nutter, C. A. & Kuyumcu-Martinez, M. N. Emerging roles of RNA-binding proteins in diabetes and their therapeutic potential in diabetic complications. *Wiley Interdisciplinary Reviews: RNA* vol. 9 Preprint at https://doi.org/10.1002/wrna.1459 (2018).

51. Wang, Y. Erdr1 orchestrates macrophage polarization and determines cell fate via dynamic interplay with YAP1 and Mid1. *bioRxiv* 2023.09.17.557960 (2023) doi:10.1101/2023.09.17.557960.

52. Rao, S. S. *et al.* Enhanced survival with implantable scaffolds that capture metastatic breast cancer cells in vivo. *Cancer Res* **76**, 5209–5218 (2016).

53. Bushnell, G. G. *et al.* Biomaterial scaffolds recruit an aggressive population of metastatic tumor cells in vivo. *Cancer Res* **79**, (2019).

.

Chapter 5 Metabolic Network Reconstruction of SC-Islets Enables Simulation of Metabolic Treatments *In Silico*

5.1 Authors

Jessica L. King, Anne Lietzke, Elizabeth Bealer, Kelly Crumley, Scott A. Soleimanpour, and Lonnie D. Shea

5.2 Abstract

Cell replacement therapies offer the possibility of restoring native function for patients with type 1 diabetes (T1D), but with high cell demands per patient, and limited availability of donor islets, a renewable source is needed. Human pluripotent stem cell derived islets (sc-islets) offer a limitless source for cell therapies, but current protocols generate metabolically immature cells that have functional deficits compared to human islets. In these studies, we develop a metabolic network reconstruction of sc-islets as a tool to investigate differences in metabolic flux activity between sc-islets and mature islets *in silico*. Transcriptomic data from mature and sc-islets was used to generate cell specific models for each group. This reconstruction recapitulates changes seen *in vitro* for sc-islet function following PPAR agonist treatment, validating our model as a screening tool for treatment effects. We also implemented the reconstruction to perform a knock-in screen of the 443 genes down regulated in sc-islets compared to mature islets. A pilot *in vitro* validation suggests that targeting the gene identified in the knock-in screen improves ATP metabolism efficiency in sc-islets. This result supports the utility of metabolic reconstruction modeling as a tool to inform sc-islet treatments to improve metabolic maturation.

5.3 Introduction

Type 1 diabetes (T1D) is an autoimmune disease characterized by glucoses dysregulation brought about by the destruction of the pancreatic islets. Islets, specifically β-cells, are responsible for insulin production and secretion to regulate blood glucose levels. People living with T1D are unable to produce their own insulin due to the destruction of their islets, and the current standard of care relies on exogenous insulin therapy. While exogenous insulin therapy can effectively keep blood glucose levels from reaching critical levels, the therapy has a significant burden of care and still lacks the tight control of blood glucose levels provided by native healthy islets, which puts patients at risk for long-term complications.[1–3] Cell replacement therapies offer the potential for a new gold standard, as functional cells would lessen the burden of care from constant glucose monitoring. Lantrida is an FDA approved cell replacement therapy which utilizes cadaveric islets, but restoration of euglycemia is not long lasting, and this approach relies on a limited supply of donor islets.[4,5]

Several differentiation protocols have been developed for human pluripotent stem cell (hPSC) derived islets as a limitless manufacturable source for cell replacement therapy.[6–9] Current protocols have shown success in restoring euglycemia, with cell replacement therapies from Vertex Pharmaceuticals progressing to clinical trials.[10] However, stem cell derived islets have been shown to require an *in vivo* maturation period following transplantation before exhibiting full metabolic function.[7] This maturation period results in longer times to euglycemia compared to human islet transplants in animal models.[11] In order to bridge the gap between metabolic function of sc-islets and mature islets, protocols need to be adapted to promote greater metabolic maturation *in vitro*.

In these studies, we establish a metabolic network model for identifying candidates for differentiation modification to improve sc-islet metabolic maturation. Metabolic reconstructions

account for all genes, reactions, and metabolites involved in metabolism, and can be constrained to generate cell or organism specific models.[12] We use the RECON1 human metabolic network reconstruction[13,14] in conjunction with the COBRA toolbox[15] to generate sc-islet specific models based on transcriptomic data. Metabolic reconstruction analysis of our sc-islet and mature islet models enables *in silico* testing of drug treatments and screening for potential drug targets.[16–18] Implementing metabolic network modeling as a first step in identifying factors to improve sc-islet maturation has the potential to streamline differentiation improvements, and possibly accelerate clinical impacts.

5.4 Results

5.4.1 Transcriptomic data identifies metabolic flux differences between mature and sc-islets when implemented in a metabolic reconstruction

We implemented a six-stage differentiation protocol[7] to generate metabolically immature stem cell derived islets (sc-islets) from human pluripotent stem cells (hPSCs), with samples taken for RNA sequencing (RNAseq) at each stage of differentiation (Figure 5.1A). We then performed differential gene expression analysis on the sequencing data, with mature human islets used as the control. The differential expression results were integrated with the human metabolic reconstruction RECON1,[13] with differential expression providing the reaction weights for flux balance analysis (Figure 5.1B). A principal component analysis of the RNAseq data for stages 4 (S4), 5 (S5), and 6 (S6) of differentiation and human islets shows a shift towards human islets, but still a large gap, as cells enter stage 6 (Figure 5.1C). Unbounded flux balance analysis of stage 6, or sc-islets, compared to human islets identified 20 reactions with a flux difference greater than |0.01|, with 8 of the 20 reactions playing a role in NAD/NADH or NADP/NADPH metabolism, which are precursors needed for mitochondrial respiration (Figure 5.1D).[19,20]

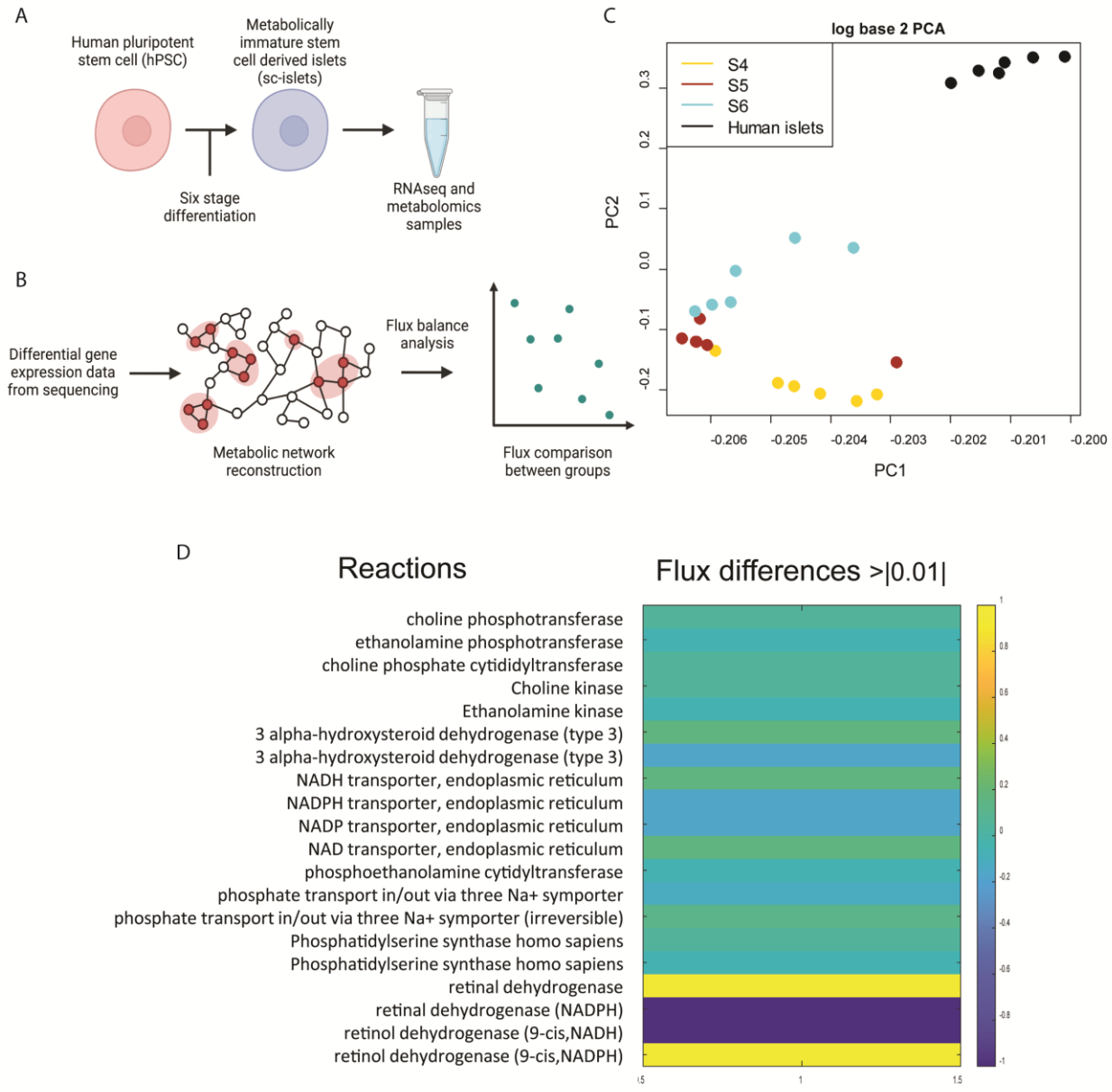


Figure 5.1: Transcriptomic data identifies metabolic flux differences between mature and sc-islets when implemented in a metabolic reconstruction. (A) RNA sequencing (RNAseq) samples were generated from each stage of a six stage differentiation protocol for the differentiation of hPSCs into sc-islets. (B) The sequencing data were analyzed for differential gene expression, and these results were used to generate stage specific constraints in a human metabolic network reconstruction. The reconstruction was used to perform flux balance analysis of stage 6, or sc-islets, versus human islet controls. (D) Of the 3744 reactions in the reconstruction, 20 were identified with a flux difference between stage 6 and human islets >0.01. 8 of the 20 reactions are related to NAD/NADH or NADP/NADPH metabolism, which are needed as electron donors for mitochondrial respiration.

5.4.2 Model sensitivity to differentiation efficiency is dependent on objective function selection

Setting model constraints to account for differentiation variability enables us to connect metabolic maturity outputs to the target cell population. Stem cell differentiations are subject to variability, with not all cultures resulting in the same efficiency of target cell production. Differentiation variability can be shown via PCA of the sequencing results, with poor differentiation clustering further from the human islet samples, and good differentiations clustering closer to human islets (Figure 5.2A). We also measured differentiation efficiency of the sequenced differentiations via flow, with a higher co-positivity for NKX6.1 and C-peptide demonstrating a good differentiation (Figure 5.2B), and low co-positivity demonstrating poor efficiency (Figure 5.2C). We performed flux balance analysis of S6 versus human islets with S6 samples separated into good and poor efficiency groups. We tested two objective functions, ATP exchange, as an indicator of mitochondrial respiration (Figure 5.2D), and calcium ion transport, as a surrogate for insulin secretion, as calcium influx triggers the release of insulin granules (Figure 5.2E).[21,22] In both analyses, there was some separation between the good and poor differentiation groups, but only for the calcium transport objective did the good differentiation group show a decreased Euclidean distance from the human islet condition (Figure 5.2F).

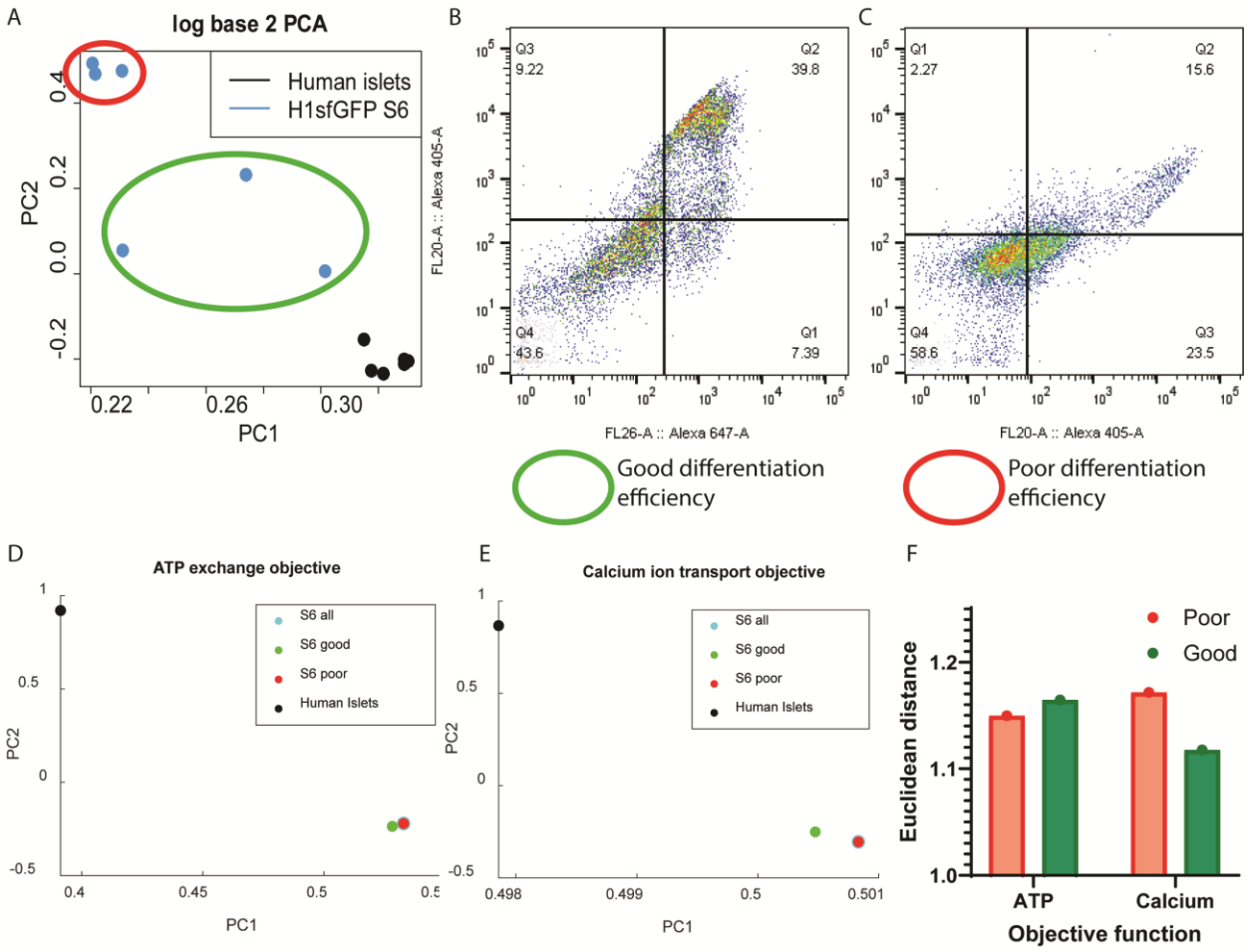


Figure 5.2: Model sensitivity to differentiation efficiency is dependent on objective function selection. (A) PCA of gene expression data for stage 6 and human islet samples shows separate sub-populations within the stage 6 group. (B) A representative example of flow cytometry from one of the differentiations in the group closer to human islets in the PCA show good differentiation efficiency. (C) A representative flow cytometry result for a differentiation further from human islets in PCA, with poor differentiation efficiency. (D) PCA of the flux results for the metabolic reconstruction with ATP transport set as the objective function has minimal separation between good and poor differentiations. (E) PCA of flux results for the same model with calcium ion transport set as the objective has greater separation between the good and poor differentiations. (F) Euclidean distances calculated for good and poor stage 6 groups to human islets show the smallest Euclidean distance for good differentiations, using calcium transport as the objective function.

5.4.3 PPAR agonist treatment simulation recapitulates sc-islet improvements found via in vitro testing

We next looked to validate the model's utility as a tool to screen potential treatments by comparing modeling results to the results of an *in vitro* study that improved sc-islet function. Previous analysis of the sequencing data identified PPARα and PPARγ as potential targets to improve sc-islet

function (Figure 5.3A).[23] From that analysis the PPARα agonist WY14643 was chosen to test in sc-islet differentiations, which showed improved maturation *in vitro*.[23,24] In order to simulate treatment in the modeling, the downstream genes of PPARα in humans and their regulation relationships were identified from the literature (Figure 5.3B).[25] Of the 42 downstream genes identified, 19 were present in the RECON1 reconstruction (Figure 5.3C). The 19 downstream genes were added into the reaction weights of stage 6 cells, and a 20% increase or decrease was added for upregulated and downregulated genes respectively. PCA of the flux balance analysis for human islets compared to treated and untreated stage 6 cells shows a shift in the treated group to more mature islet-like flux results (Figure 5.3D). In comparison, an *in vitro* glucose stimulated insulin secretion study also shows improved function in treated cells compared to untreated controls (Figure 5.3E).[23] The improvements shown in both *in silico* flux results and an *in vitro* functional assay demonstrate the model's ability to capture functional differences in simulated treatments.

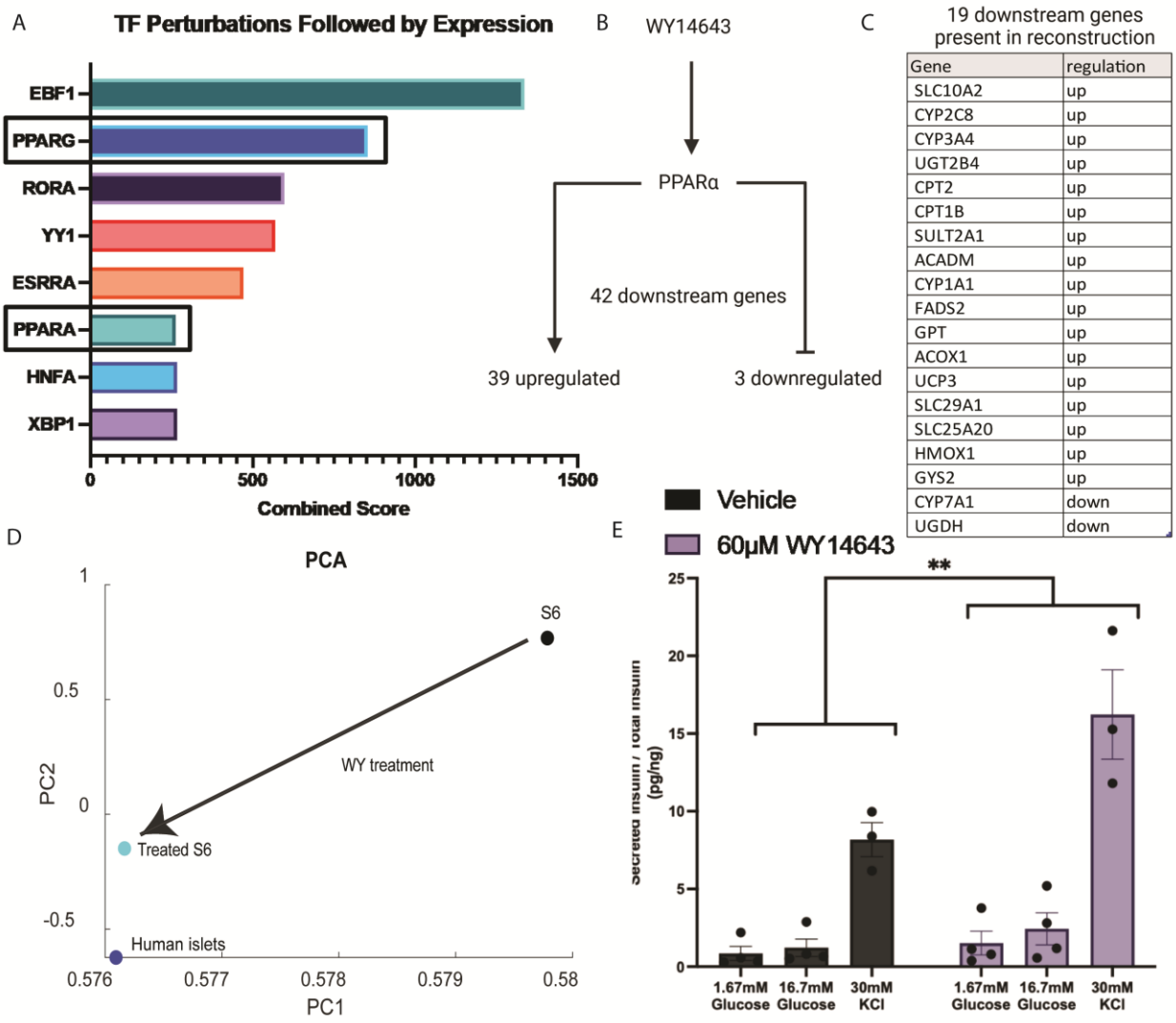


Figure 5.3: Simulation of PPAR agonist treatment recapitulates beta cell improvements found via in vitro testing. (A) Transcription factor analysis of the RNAseq data identified PPARα and PPARγ as having high perturbation in stage 6 compared to human islets. (B) WY14643 is a PPARα agonist, with some gamma effects. 42 downstream genes for PPARα in humans have been identified in the literature: 39 upregulated, and 3 downregulated. (C) Comparing the PPARα downstream genes to the genes in the metabolic reconstruction, 19 are present: 17 upregulated, 2 downregulated. (D) WY14643 treatment of stage 6 cells was simulated in the metabolic reconstruction by adding the PPARα downstream genes to the arrays of weighted reactions for stage 6 cells and adding a 20% increase or decrease to their reaction weights according to their regulation. PCA of the treatment simulation shows an increase in the similarity of the treated group to human islets compared to untreated. (E) The improvement in stage 6 cells following WY treatment is also demonstrated in vitro, with glucose stimulated insulin secretion being significantly increased in the treated group compared to untreated. (Panel E adapted from Lietzke, Bealer, Crumley, King et al. doi: https://doi.org/10.1101/2024.07.26.605318)

5.4.4 Knock-in simulation of downregulated genes identifies target for improving stage 6 cells

Following validation of the model for recapitulating effects of pre-tested factors, we next sought to use the model to identify new targets for improving sc-islets. We performed a knock-in simulation of the 443 genes shown to be downregulated in sc-islets compared to human islets in the differential gene expression analysis. PCA of the flux results for these 443 knock-ins identified NMNAT3 as the single gene knock-in resulting in the greatest flux similarity to human islets (Figure 5.4A). NMNAT3 is a gene that encodes a metabolic enzyme involved in nicotinamide adenine dinucleotide (NAD^+) production from nicotinamide mononucleotide (NMN) in the mitochondria, which is then used to form NADH in the citric acid cycle (Figure 5.4B).[19,26,27] We also investigated if simulating NAD^+ supplementation resulted in the same improvement in sc-islets, but there was no change in flux between the treated and untreated groups (Figure 5.4C).

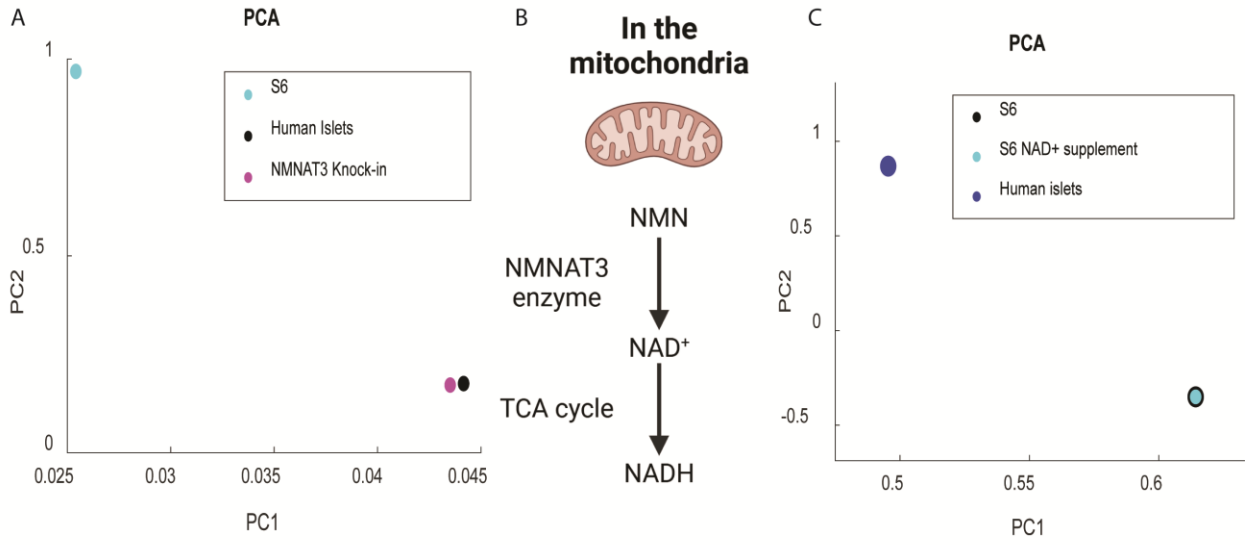


Figure 5.4: Knock-in simulation of downregulated genes identifies target for improving stage 6 cell. (A) A knock-in simulation was run by removing the downregulated reaction weight for each of the 443 genes downregulated between stage 6 cells and human islets. This screen identified NMNAT3 as the gene with the greatest flux similarity to human islets following knock-in. (B) NMNAT3 encodes an enzyme that regulates the production of nicotinamide adenine dinucleotide (NAD^+) from nicotinamide mononucleotide. (C) An additional simulation of supplementing stage 6 cells with NAD^+ shows no difference between treated and untreated groups, indicating that the knock-in improvement is not based solely on increased production of NAD^+.

5.4.5 In vitro testing of elements of the NMNAT3 pathway suggest this target may improve metabolism

We performed a pilot study of treating stage 6 cells with factors targeting the NMNAT3 pathway to validate our knock-in results. We identified FK866 as a treatment, as it has been shown to recover NMNAT3 function in other disease models.[28] FK866 works as a nicotinate phosphoribosyltransferase (NAPRT) inhibitor, which is an enzyme needed for NAD^+ production from nicotinic acid.[29] Since NAD^+ is essential to cellular metabolism, it is thought that the other production pathways, such as from NMN via NMNAT3 activity, are indirectly upregulated to compensate for the NAPRT inhibition (Figure 5.5A). To test the effect on stage 6 cultures, cells were treated 50nM FK866, 10mM NMN, or a combination of both on days 3, 5, 7, and 9 of stage 6 (Figure 5.5B). Cells were lifted from planar culture and reaggregated into sc-islet cluster on day 7, and samples were taken for ATP and ADP assessments on day 10 (Figure 5.5B). ATP concentration was highest for the control sample (Figure 5.5C), but it also had the highest ADP concentration (Figure 5.5D), indicating poor ADP to ATP conversion. ATP to ADP ratio was highest for the FK866 condition at both low (2mM) and high (20 mM) glucose levels, and the NMN treatment group had the highest fold change in ATP/ADP from low to high glucose (Figure 5.5E). The combination group had the highest ATP concentration of the treatment groups (Figure 5.5C), and the highest ratio at low glucose, but had a decreased ratio at high glucose (Figure 5.5E).

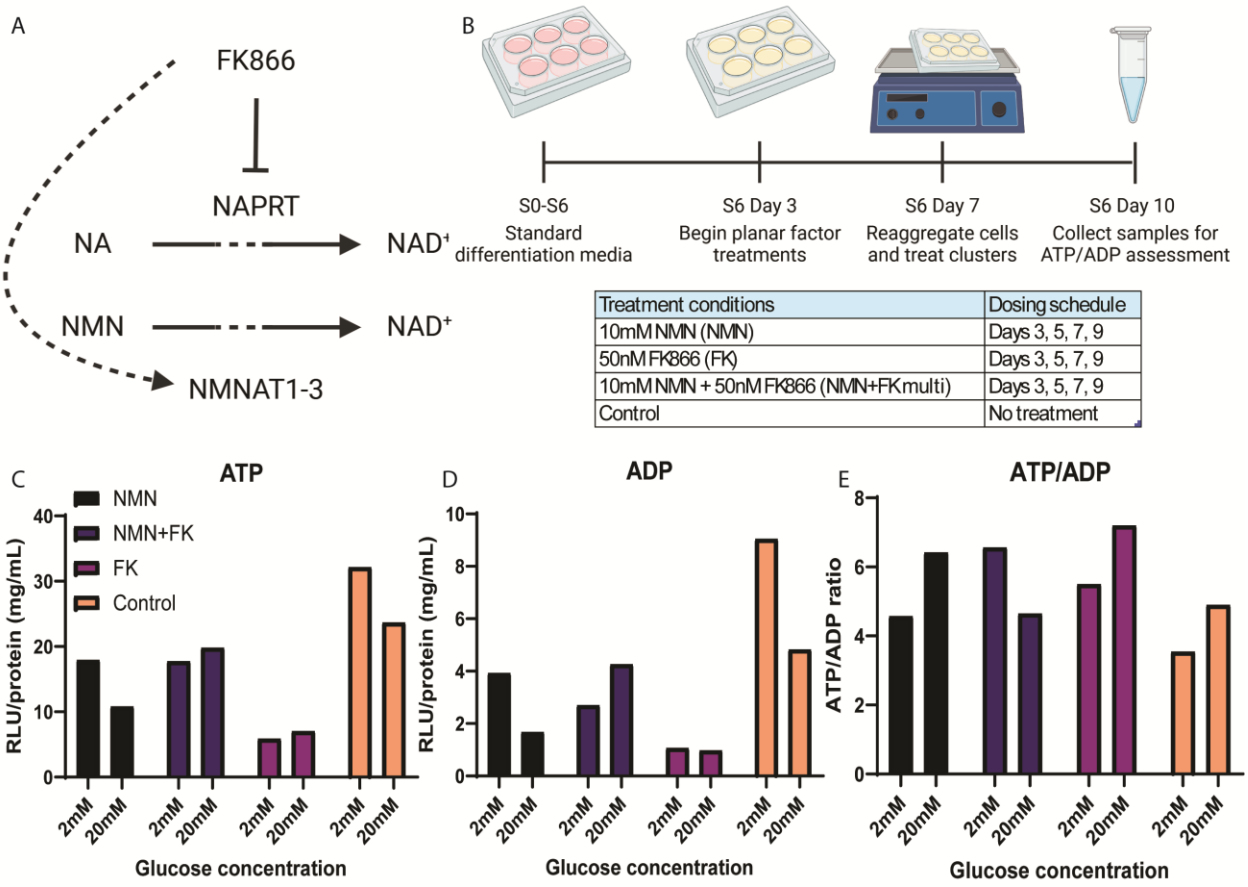


Figure 5.5: In vitro testing of elements of the NMNAT3 pathway suggest this target may improve metabolism. (A) FK866 is an inhibitor of NAMPT, which is needed to produce NAD^+ from nicotinic acid. It is possible that this inhibition has an indirect upregulation of NMNAT3 activity as a compensatory effect to produce NAD^+ via alternative pathways. (B) Stage 6 cells were treated with 50nM FK866, 10mM NMN, or a combination of the two between days three and ten of stage 6 differentiation. At day 7, cells were taken out of planar culture and reaggregated as clusters until the time of assessment. (C-D) ATP and ADP concentrations were measured at low (2mM) and high (20mM) glucose concentrations. (C) ATP concentration was higher for control and singly treated samples, but these groups also had the highest ADP concentration (D) indicating poor efficiency in ADP to ATP conversion. (E) ATP to ADP ratios show trends of higher performance in the groups that received multiple treatments (n=1).

5.5 Discussion

Advancements in cell replacement therapies for T1D have the potential to alleviate the daily burden of care for millions of patients, but challenges in the production of a high quality, limitless cell source remain. Current protocols have progressed to clinical trials and shown success in restoring euglycemia in patients,[10] but current protocols still generate metabolically immature sc-islets that require an *in vivo* maturation period.[7,30,31] Other groups have taken computational approaches to identify specific differences between mature and sc-islets, largely focused on

sequencing datasets.[32–34] While this approach has had success in identifying transcriptional markers of sc-islet immaturity, they do not examine the implications of these immaturity markers on functional metabolic reactions, or strategies to improve maturation *in vitro*. Metabolic modeling using network reconstruction allows for the integration of sequencing data in a way that accounts for metabolic reactions, not just gene expression.[35,36] Experimentally, metabolic reaction rates can be measured via fluxomics, but this approach would be time and material intensive to screen a large number of drug or metabolic factor treatments when cultures to produce sc-islet take 30 days.[37] The computational metabolic reconstruction approach allows for identification of the key reactions driving metabolic function, and to screen a large number of factors, without the demands on time and cell material required by a flux metabolomics study.

Our analysis demonstrates that differentiation efficiency between groups can be identified by flux analysis independently of metabolic function. A constraining factor in the performance of metabolic models is the objective function selected. By design, flux balance analysis optimizes the model to maximize the objective function.[38] In our case, ATP was initially chosen as the objective to represent metabolic maturity, as sc-islets have been shown to have mitochondrial insufficiencies compared to human islets, and ATP transport is needed to maintain oxidative phosphorylation.[39] While this objective acts as a functional surrogate for metabolic maturity, it is not cell type specific, as cellular metabolism is not exclusive to the endocrine cells found in sc-islets. In order to test the model's sensitivity to differentiation efficiency, we sought an additional objective function that would act as a surrogate of insulin secretion, a process specific to islet β-cells. Insulin granule secretion is triggered by calcium ion influx.[22] Given this mechanism, calcium ion transport was chosen as the objective function for evaluating differentiation efficiency. Our results show that the calcium transport objective outperforms ATP exchange when evaluating similarity of good

differentiations to human islets (Figure 5.2F). The lack of improvement in flux similarity to human islets for good differentiations with the ATP objective suggests that while good differentiations have more β-cells present in the final sc-islets, the metabolic maturity of these cells is not better than those present in the lower efficiency differentiations.

When compared to *in vitro* results, simulated treatments show the same trends in sc-islet improvements. Prior to using the model to screen for targets to improve sc-islet maturity, we first wanted to validate it against a treatment shown to improve sc-islet function *in vitro*. We have previously shown that sc-islets treated with the PPAR agonist WY14643 during stage 6 results in improved sc-islet function (Figure 5.3E) and maturity compared to untreated controls.[23] Similarly to the way we incorporated differential gene expression data to compare stage 6 sc-islets to mature human islets, we were able to simulate PPAR targeting by adding reaction weights to the downstream genes. The resulting flux analysis shows a shift in flux performance of the simulated treatment group towards human islets compared to the untreated group (Figure 5.3D), validating that our model captures functional differences present *in vitro*. This validation lends support to this approach as a screening tool for future drug candidates. While treatment efficacy will always need to be validated *in vitro* and *in vivo* prior to clinical testing to account for toxicity and off target effects, a validated *in silico* model allows for high throughput screening so only the most promising treatments are tested experimentally.

After validating the model, a knock-in screen of 443 genes identified a treatment target that generates the most mature islet-like flux *in silico*. While validating the model with an established treatment lends support to our model's accuracy, the ultimate goal is to implement this modeling to identify new treatments. We performed a knock-in screen of the 443 genes downregulated in S6 compared to human islets in order to identify a target gene, and identified NMNAT3 as our best

performing knock-in. NMNAT3 is an enzyme involved in mitochondrial NAD^+ metabolism, an element of respiration also indicated as a deficiency in stage 6 by differences in reaction flux (Figure 5.1D). As there are multiple pathways involved in NAD^+ metabolism[19,20], we also performed a simulation of NAD^+ supplementation. This simulation did not show any changes in flux from the untreated group, indicating the NMNAT3 upregulation is having an effect independent of NAD^+ concentration. As an initial *in vitro* validation, we treated stage 6 cells with FK866, a drug that inhibits NAD^+ metabolism via a NMNAT3 independent pathway[29], and with NMN, a precursor to NAD^+ in the NMNAT3 pathway (Figure 5.5A). As with using ATP exchange as the objective function to measure metabolic maturity *in silico*, ATP/ADP ratio was measured to assess metabolic maturity in this *in vitro* study. ATP/ADP ratio was the highest for the FK866 treatment group, indicating that our modeling results are recapitulated *in vitro* (Figure 5.5E). However, the mechanism of FK866 can lead to depletion of NAD^+ and apoptosis if cells don't compensate via other mechanisms.[29] In our case, this was seen as a lower cell number and worse flow results compared to control and NMN supplemented groups (Figure 5.6). NMN supplementation was used to account for the apoptotic potential of FK866. We found that NMN supplementation alone performed better than control at both low and high glucose levels, but the combination of NMN and FK866 only outperformed control at the low glucose concentration (Figure 5.1E). While this was a pilot study and additional samples are needed to ensure that this is a significant result rather than an outlier, it is possible that the combination treatment is less effective at high glucose levels. A possible explanation for this is that NMN is a precursor to the NAD^+ used in glycolysis, and the decrease in overall NAD^+ concentration from FK866 may lead to a stressed state favoring the glycolytic pathway at high glucose.[40]

In conclusion, metabolic network reconstruction enables *in silico* treatment simulation to target metabolic maturity of sc-islets. Our modeling results provide the framework for a screening tool to identify high potential treatments, without the time and resource demands of *in vitro* cultures. High throughput screening would enable us to improve sc-islet quality with greater efficiency, and across more conditions, expediting the timeline for translation. Greater screening capabilities ultimately move us towards generating more mature sc-islets, with the potential for greater therapeutic efficacy.

5.6 Methods

5.6.1 hPSC culture

An H1 hPSC cell line was cultured according to a previously reported six-stage differentiation protocol.[7] Samples were taken at the end of stages 1-5 of differentiation, and on day ten of stage 6 for RNA sequencing. Flow cytometry samples were also taken to monitor differentiation progression and efficiency.For treatment testing, stage 6 cells were dissociated from the plate with trypsin and reaggregated into clusters on day seven.[6]

5.6.2 RNA sequencing

RNA samples were isolated and sequenced by the University of Michigan Advanced genomics core, as described in Lietzke et al., and data will be available at GEO (GSE270220) following publication.[23]

5.6.3 Metabolic reconstruction

Full code for differential gene expression analysis and flux balance analysis can be found at https://github.com/shea-lab/scisletRECON. In brief, RNAseq data was filtered to remove low expression genes, and differential gene expression was analyzed using DEseq2 in R. Differential

expression results were then exported and read into the RECON1 model[13] as reaction weights in MATLAB. The COBRA toolbox was used to set objectives and run flux balance analysis in combination with flux constraint functions developed by the Chandrasekaran lab at the University of Michigan.[15,41]

5.7 Acknowledgements

Support for this work was provided by JDRF, the JDRF Center of Excellence at the University of Michigan, the Caswell Diabetes Center, and NIH grants 1R01DK121462 and 1R01CA272940-01A1. J.L.K. was supported by the National Science Foundation Graduate Research Fellowship under Grant No. DGE-2241144. Figures were created in Biorender.com and Adobe Illustrator.

5.8 Supplemental information

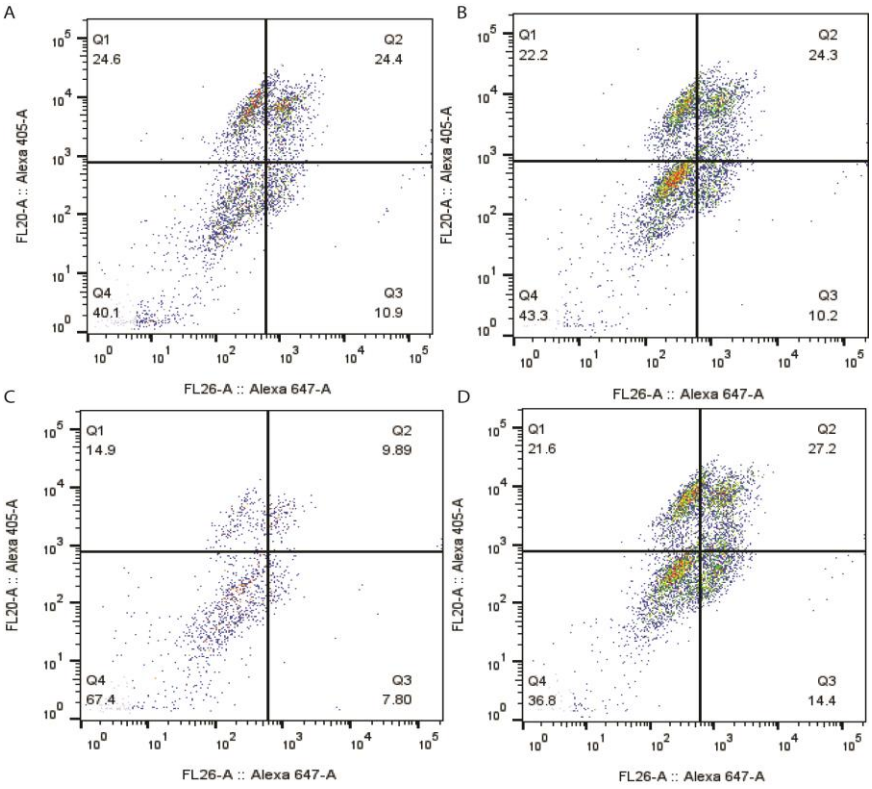


Figure 5.6: Flow cytometry results for sc-islet samples taken on the day of reaggregation and stained for NKX6.1 (Alexa 405) and C-peptide (Alexa 647). Analysis was performed for treatment groups: (A) control, (B) 10mM NMN, (C) 50nM FK866, and (D) 10mM NMN and 50nM FK866.

5.9 References

1. Tamborlane, W. V. *et al.* Continuous glucose monitoring and intensive treatment of type 1 diabetes. *New England Journal of Medicine* 359, 1464–1476 (2008).

2. Commissariat, P. V. *et al.* "I'm essentially his pancreas": Parent perceptions of diabetes burden and opportunities to reduce burden in the care of children <8 years old with type 1 diabetes. *Pediatr Diabetes* 21, (2020).

3. Balcázar-Hernández, L. *et al.* Burden in primary informal caregivers of children and adolescents with type 1 diabetes: Is it associated with depression, family dysfunction, and glycemic control? *Front Endocrinol (Lausanne)* 13, (2023).

4. Parums, D. V. Editorial: First Regulatory Approval for Allogeneic Pancreatic Islet Beta Cell Infusion for Adult Patients with Type 1 Diabetes Mellitus. *Medical Science Monitor* vol. 29 Preprint at https://doi.org/10.12659/MSM.941918 (2023).

5. Qi, M. *et al.* Five-year follow-up of patients with type 1 diabetes transplanted with allogeneic islets: the UIC experience. *Acta Diabetol* 51, (2014).

6. Hogrebe, N. J., Maxwell, K. G., Augsornworawat, P. & Millman, J. R. Generation of insulin-producing pancreatic β cells from multiple human stem cell lines. *Nature Protocols* vol. 16 Preprint at https://doi.org/10.1038/s41596-021-00560-y (2021).

7. Hogrebe, N. J., Augsornworawat, P., Maxwell, K. G., Velazco-Cruz, L. & Millman, J. R. Targeting the cytoskeleton to direct pancreatic differentiation of human pluripotent stem cells. *Nat Biotechnol* (2020) doi:10.1038/s41587-020-0430-6.

8. Velazco-Cruz, L. *et al.* Acquisition of Dynamic Function in Human Stem Cell-Derived β Cells. *Stem Cell Reports* 12, 351–365 (2019).

9. Pagliuca, F. W. *et al.* Generation of functional human pancreatic β cells in vitro. *Cell* 159, 428–439 (2014).

10. Kramer, V. Expanded FORWARD Trial Demonstrates Continued Potential for Stem Cell-Derived Islet Cell Therapy to Eliminate Need for Insulin for People with T1D. *American Diabetes Association* (2024).

11. Augsornworawat, P., Maxwell, K. G., Velazco-Cruz, L. & Millman, J. R. Single-Cell Transcriptome Profiling Reveals β Cell Maturation in Stem Cell-Derived Islets after Transplantation. *Cell Rep* 32, 108067 (2020).

12. Thiele, I. & Palsson, B. A protocol for generating a high-quality genome-scale metabolic reconstruction. *Nat Protoc* 5, 93–121 (2010).

13. Duarte, N. C. *et al.* Global reconstruction of the human metabolic network based on genomic and bibliomic data. *Proc Natl Acad Sci U S A* 104, 1777–1782 (2007).

14. Rolfsson, O., Palsson, B. T. & Thiele, I. The human metabolic reconstruction Recon 1 directs hypotheses of novel human metabolic functions. *BMC Syst Biol* 5, 1–16 (2011).

15. Heirendt, L. *et al.* Creation and analysis of biochemical constraint-based models using the COBRA Toolbox v.3.0. *Nat Protoc* 14, 639–702 (2019).

16. Shaked, I., Oberhardt, M. A., Atias, N., Sharan, R. & Ruppin, E. Metabolic Network Prediction of Drug Side Effects. *Cell Syst* 2, (2016).

17. Ma, H. & Goryanin, I. Human metabolic network reconstruction and its impact on drug discovery and development. *Drug Discovery Today* vol. 13 Preprint at https://doi.org/10.1016/j.drudis.2008.02.002 (2008).

18. Rawls, K., Dougherty, B. V. & Papin, J. Metabolic network reconstructions to predict drug targets and off-target effects. in *Methods in Molecular Biology* vol. 2088 (2020).

19. Xie, N. *et al.* NAD+ metabolism: pathophysiologic mechanisms and therapeutic potential. *Signal Transduction and Targeted Therapy* vol. 5 Preprint at https://doi.org/10.1038/s41392-020-00311-7 (2020).

20. Covarrubias, A. J., Perrone, R., Grozio, A. & Verdin, E. NAD+ metabolism and its roles in cellular processes during ageing. *Nature Reviews Molecular Cell Biology* vol. 22 Preprint at https://doi.org/10.1038/s41580-020-00313-x (2021).

21. Hauke, S., Rada, J., Tihanyi, G., Schilling, D. & Schultz, C. ATP is an essential autocrine factor for pancreatic β-cell signaling and insulin secretion. *Physiol Rep* 10, (2022).

22. Fu, Z., R. Gilbert, E. & Liu, D. Regulation of Insulin Synthesis and Secretion and Pancreatic Beta-Cell Dysfunction in Diabetes. *Curr Diabetes Rev* 9, (2012).

23. Lietzke, A. C. *et al.* Limitations in mitochondrial programming restrain the differentiation and maturation of human stem cell-derived β cells. *bioRxiv* 2024.07.26.605318 (2024) doi:10.1101/2024.07.26.605318.

24. Bernardes, A. *et al.* Molecular mechanism of peroxisome proliferator-activated receptor α activation by WY14643: A new mode of ligand recognition and receptor stabilization. *J Mol Biol* 425, (2013).

25. Fang, L. *et al.* PPARgene: A Database of Experimentally Verified and Computationally Predicted PPAR Target Genes. *PPAR Res* 2016, (2016).

26. Wang, T. *et al.* Overexpression of NMNAT3 improves mitochondrial function and enhances antioxidative stress capacity of bone marrow mesenchymal stem cells via the NAD+-Sirt3 pathway. *Biosci Rep* 42, (2022).

27. Hikosaka, K. *et al.* Deficiency of nicotinamide mononucleotide adenylyltransferase 3 (Nmnat3) causes hemolytic anemia by altering the glycolytic flow in mature erythrocytes. *Journal of Biological Chemistry* 289, (2014).

28. Parsons, R. B. *et al.* Alpha-synucleinopathy reduces NMNAT3 protein levels and neurite formation that can be rescued by targeting the NAD+ pathway. *Hum Mol Genet* 31, (2022).

29. Hasmann, M. & Schemainda, I. FK866, a Highly Specific Noncompetitive Inhibitor of Nicotinamide Phosphoribosyltransferase, Represents a Novel Mechanism for Induction of Tumor Cell Apoptosis. *Cancer Res* 63, (2003).

30. Diane, A., Al-Shukri, N. A., Bin Abdul Mu-u-min, R. & Al-Siddiqi, H. H. β-cell mitochondria in diabetes mellitus: a missing puzzle piece in the generation of hPSC-derived pancreatic β-cells? *Journal of Translational Medicine* vol. 20 Preprint at https://doi.org/10.1186/s12967-022-03327-5 (2022).

31. Maxwell, K. G., Kim, M. H., Gale, S. E. & Millman, J. R. Differential Function and Maturation of Human Stem Cell-Derived Islets after Transplantation. *Stem Cells Transl Med* 11, (2022).

32. Schmidt, M. D., Ishahak, M., Augsornworawat, P. & Millman, J. R. Comparative and integrative single cell analysis reveals new insights into the transcriptional immaturity of stem cell-derived β cells. *BMC Genomics* 25, (2024).

33. Augsornworawat, P. *et al.* Single-nucleus multi-omics of human stem cell-derived islets identifies deficiencies in lineage specification. *Nat Cell Biol* 25, (2023).

34. Davis, J. C. *et al.* IAPP Marks Mono-hormonal Stem-cell Derived β Cells that Maintain Stable Insulin Production in vitro and in vivo *bioRxiv* 2024.04.10.587726 (2024) doi:10.1101/2024.04.10.587726.

35. Bordbar, A. & Palsson, B. O. Using the reconstructed genome-scale human metabolic network to study physiology and pathology. *J Intern Med* 271, 131–141 (2012).

36. Geng, J. & Nielsen, J. In silico analysis of human metabolism: Reconstruction, contextualization and application of genome-scale models. *Current Opinion in Systems Biology* vol. 2 Preprint at https://doi.org/10.1016/j.coisb.2017.01.001 (2017).

37. Emwas, A. H., Szczepski, K., Al-Younis, I., Lachowicz, J. I. & Jaremko, M. Fluxomics - New Metabolomics Approaches to Monitor Metabolic Pathways. *Frontiers in Pharmacology* vol. 13 Preprint at https://doi.org/10.3389/fphar.2022.805782 (2022).

38. García Sánchez, C. E. & Torres Sáez, R. G. Comparison and analysis of objective functions in flux balance analysis. *Biotechnol Prog* 30, (2014).

39. Bonora, M. *et al.* ATP synthesis and storage. *Purinergic Signalling* vol. 8 Preprint at https://doi.org/10.1007/s11302-012-9305-8 (2012).

40. González, P., Lozano, P., Ros, G. & Solano, F. Hyperglycemia and Oxidative Stress: An Integral, Updated and Critical Overview of Their Metabolic Interconnections. *International Journal of Molecular Sciences* vol. 24 Preprint at https://doi.org/10.3390/ijms24119352 (2023).

41. Chandrasekaran, S. *et al.* Comprehensive Mapping of Pluripotent Stem Cell Metabolism Using Dynamic Genome-Scale Network Modeling. *Cell Rep* 21, 2965–2977 (2017).

Chapter 6 Engineering a Translatable, Retrievable Islet Transplant Site with Microporous Scaffolds to Treat Type 1 Diabetes

6.1 Authors

Jessica L. King[+], Christopher Spencer[+], Richard Youngblood, Kelly Crumley, Elizabeth Bealer, Peter Rios, Ira Joshi, Sofia Ghani, Douglas Isa, James McGarrigle, David Cook, Conor Locke, Adam Abraham, Andrea Clark, José Oberholzer, and Lonnie D. Shea

[+]These authors contributed equally to this work

6.2 Abstract

Clinical islet transplantation has long been investigated as a potential cure for type 1 diabetes, yet the standard intrahepatic approach leaves islets prone to an aggressive inflammatory response and necessitates systemic immunosuppression. Herein, we investigated microporous poly(D,L-lactide-co-glycolide) (PLG) scaffolds for extrahepatic islet transplantation in a nonhuman primate (NHP) model. Acellular scaffolds did not elicit an undesirable inflammatory response in the omentum, and in three diabetic NHP transplant recipients we observed signs of islet survival, despite not achieving euglycemia. However, we observed fragility of irradiated scaffolds during seeding and implantation, motivating us to increase the PLG:NaCl ratio used in manufacturing to 1.25:30 w/w. These scaffolds exhibited no differences in porosity or interior geometry between sterilization conditions, and transplants in mice restored glycemic control. We therefore conducted a pilot study of the modified scaffold in a fourth NHP, and although the integrity of the scaffold was improved, there was no improvement in transplant outcomes. Thus, we tested two intermediate PLG:NaCl ratios in mice, finding that a 1.15:30 ratio achieved an

optimal balance of mechanical stability and islet compatibility. Overall, this investigation demonstrates the adaptability of the scaffold for improvement of islet transplant outcomes and future clinical translation.

6.3 Introduction

Type 1 diabetes (T1D) is an autoimmune disease characterized by the destruction of the insulin-producing β cells of the pancreas, affecting approximately 8.4 million people worldwide.[1,2] Patients must administer exogenous insulin through manual daily injections or an insulin pump, and even with diligent management, patients are at heightened risk of chronic cardiovascular and microvascular complications, in addition to acute conditions such as ketoacidosis and hypoglycemia.[3,4] With the global patient population expected to increase to 13.5-17.4 million by 2040,[1] there is a need to accelerate the clinical translation of regenerative therapies, such as islet transplantation.

Islet transplantation offers a promising alternative to current treatments due to its potential to functionally restore euglycemia with little or no exogenous insulin requirement. In 2023, Lantidra (donislecel) became the first FDA-approved allogeneic pancreatic islet cell therapy.[5,6] However, the therapy has several limitations, including proneness to the instant blood-mediated inflammatory reaction (IBMIR) in the liver, risks and side effects associated with immunosuppression, the scarcity of donor islets, and the irretrievability of the graft.[6-9] In Phase 1/2 clinical trials, 40% of Lantidra recipients did not have insulin independence 5 years post-transplant.[6] Vertex Pharmaceuticals and Sernova Corp have ongoing clinical trials employing intrahepatic infusion and macroencapsulation of cells, respectively.[10,11] Despite this progress, only a subset of the population living with T1D has a suitable risk-benefit profile to receive these treatments, underscoring the need to explore alternative transplant sites that offer minimal

invasiveness, maximal engraftment and survival of the cells, and superior retrievability.[5,6,10,11]

Several extrahepatic sites have been investigated for islet transplantation, such as the subcutaneous layer, bone marrow, skeletal muscle, gastric submucosa, anterior chamber of the eye, and intraperitoneal fat.[12,13] The omentum is of particular interest due to its superficial location relative to internal organs, as well as its rich vasculature and expansive volume. Several groups have transplanted allogeneic islets in the omentum.[14-19] Most recently, Deng *et al*. achieved euglycemia and insulin independence in a 1:1 donor to recipient model by distributing islets suspended in a plasma-thrombin gel across the omentum of cynomolgus monkeys.[19] While these findings demonstrate the suitability of the omentum as a transplant site, this and similar approaches are often limited by the poor tolerance of mechanical stress and reduced retrievability offered by hydrogels.[12,14-20] In principle, biomaterial platforms, manufactured with uniform and replicable characteristics, are preferable to amorphous tissue engineering approaches for clinically translatable, extrahepatic islet transplantation.

In this study, we investigate the safety and efficacy of microporous, poly(D,L-lactide-co-glycolide) (PLG) scaffolds for intra-omental islet transplantation in nonhuman primates (NHPs), a strategy we have previously validated in mice.[21-26] In healthy NHPs, we observed no significant immune response to acellular scaffolds at 30 days post-implantation. When we transplanted allogeneic islets on scaffolds into diabetic NHP recipients, we saw signs of islet survival despite not achieving euglycemia or insulin independence. However, we simultaneously discovered that the added step of sterilizing scaffolds with γ irradiation may adversely impact the structural integrity of the scaffold during seeding and implantation.[27-31] Therefore, we increased the w/w ratio of PLG to salt porogen (sodium chloride, NaCl) from 1:30 to 1.25:30 and pursued further material characterization and *in vivo* validation. In these studies, we demonstrated the tunability

of the scaffold architecture to compensate for the effects of γ irradiation while also enabling implant integration with the host tissue. Collectively, while these studies magnify the nontrivial aspects of the NHP model and hurdles to clinical-scale implementation in humans, they illustrate the adaptability of our manufacturing approach, supporting its appeal for further preclinical testing.

6.4 Results

6.4.1 Human islets and NHP islets on scaffolds effectively lower blood glucose in diabetic mice

We validated our established scaffold-islet transplantation approach using two sources of xenogeneic islets: humans and NHPs. Four STZ-induced diabetic NSG mice received a 2,000 IEQ total dose of human islets on two scaffolds in the EFPs, and two mice received a 2,000 IEQ total dose of NHP islets using the same approach. After transplantation, all transplant recipients had reduced fasting blood glucose levels, with recipients of NHP islets achieving sustained euglycemia (<200 mg/dL) beginning at day 10 (Fig. 6.1).

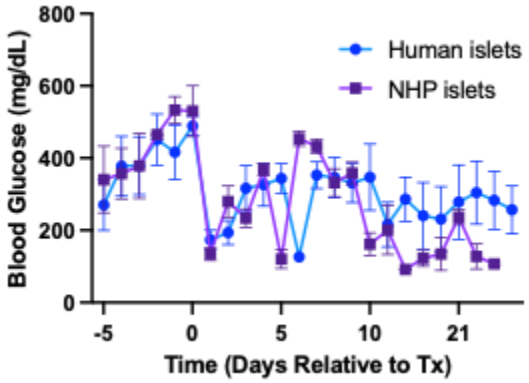


Figure 6.1: Comparison of glycemic control between mice transplanted with 2,000 IEQ human islets (n = 4) and nonhuman primate islets (n = 2) on non-irradiated scaffolds fabricated with a 1:30 w/w PLG:NaCl ratio.

6.4.2 Acellular, irradiated scaffolds elicit minimal immune response in NHPs after 30 days

Motivated by our success in the murine model, we proceeded to test the scaffold in a NHP model. We examined the immune response to acellular PLG scaffolds in three cynomolgus

monkeys. Scaffolds were fabricated with a 35 mm diameter and 1:30 PLG:NaCl ratio, sterilized by γ irradiation, and implanted in the omentum. Necropsy revealed no abnormal fibrotic tissue in the omentum, and the liver, gallbladder, and surrounding viscera appeared healthy in each animal (Fig. 6.2C). Immunofluorescent staining of explanted PLG scaffolds and the omentum revealed no significant differences in the presence of fibroblasts, innate immune cells, or cytotoxic T cells (Fig. 6.2D).

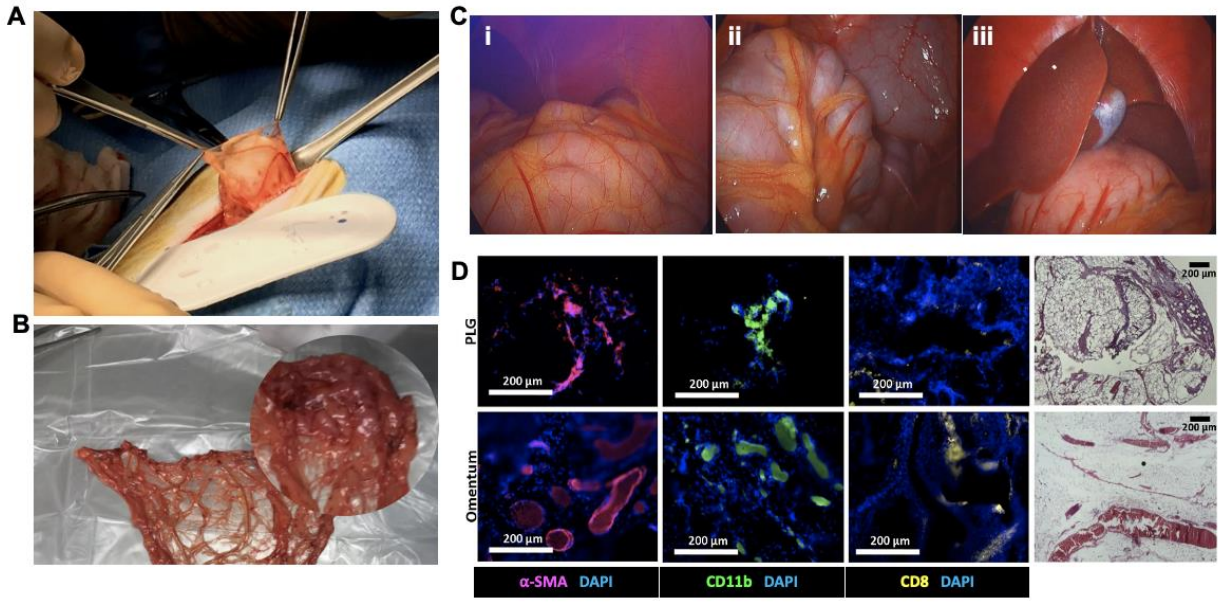


Figure 6.2: Immunoreactivity study of acellular, irradiated PLG scaffolds, fabricated with a 1:30 PLG:NaCl ratio, in cynomolgus monkeys. (A) Visualization of the scaffold being placed in the omentum. (B) Entire excised omentum, with the location of the PLG scaffold magnified. (C) Necropsy images. (i) Gross view of the omentum with no fibrotic tissue visible. (ii) Gross view of the omentum overlaying the colon. (iii) Gross view of the liver, gallbladder, and surrounding viscera. (D) Sections of the PLG scaffold and omentum were stained for α-SMA (fibroblasts), CD11b (macrophages), and CD8 (cytotoxic T cells). Hematoxylin and eosin staining was also performed to examine the tissues for signs of inflammation. All scale bars = 200 µm.

6.4.3 1:30 PLG:NaCl scaffolds support islet survival in NHPs, but do not immediately support restoration of euglycemia or insulin independence

Three STZ-induced diabetic cynomolgus monkeys were transplanted with allogeneic islets on 35 mm diameter, irradiated scaffolds, fabricated with a 1:30 PLG:NaCl ratio. Each transplant was treated as a pilot study, with adjustments to the insulin regimen made according to Tables 6.2

and 6.3.

Animal 1 (Fig. 6.3C, F, I) received 5,326 IEQ/kg on one scaffold, in tandem with exogenous insulin administered according to Tables 6.2 and 6.3. Euglycemia was not achieved in this animal, and serum C-peptide levels steadily declined from day 1 to day 12 (Fig. 6.3C, I). C-peptide was detected at levels of 0.2 ng/mL on day 26 and day 28 (the day of explant) before returning to 0 ng/mL on day 40 (Fig. 6.3I). However, post-transplant IVDTTs showed no significant improvement in glucose response compared to pre-transplant (Fig. 6.3F). During day 14 and day 28 IVDTTs, C-peptide was detected at levels of 0.1 ng/mL, demonstrating impaired, but not absent, implant function (Fig. 6.7).

Animal 2 (Fig. 6.3D, G, J) received 9,409 IEQ/kg on one scaffold, on a less aggressive insulin regimen (Tables 6.2, 6.3). Euglycemia was not achieved post-transplant (Fig. 6.3D), with no detectable C-peptide beyond day 8 (Fig. 6.3G, J). On day 41, the animal was euthanized, and the scaffold was explanted for sectioning and staining. Images showed evidence of islet survival, including colocalized insulin and DAPI (Fig. 6.3B).

Animal 3 (Fig. 6.3E, H, K) received 34,186 IEQ/kg on two scaffolds with a static insulin regimen (Table 6.2). This animal exhibited the lowest mean glucose throughout the study (135.5 ± 22.059 mg/dL pre-transplant, 171.4 ± 15.304 mg/dL post-transplant). Similarly to Animal 2, however, there was no detectable C-peptide after day 8 in routine labs or IVDTTs.

Scaffolds generally maintained their structural integrity during and after γ irradiation, with no change in color or overall appearance evident upon visual inspection prior to seeding. A few scaffolds were excluded from further use due to apparent damage during transit, such as compression in the transverse (short axis) direction, bulges or cracks on the edge of the scaffold, or surface debris. During seeding and implantation, we observed that the scaffolds had reduced

structural integrity, compared to the non-irradiated scaffolds used in our previous work and in the above mouse study.[21-26]

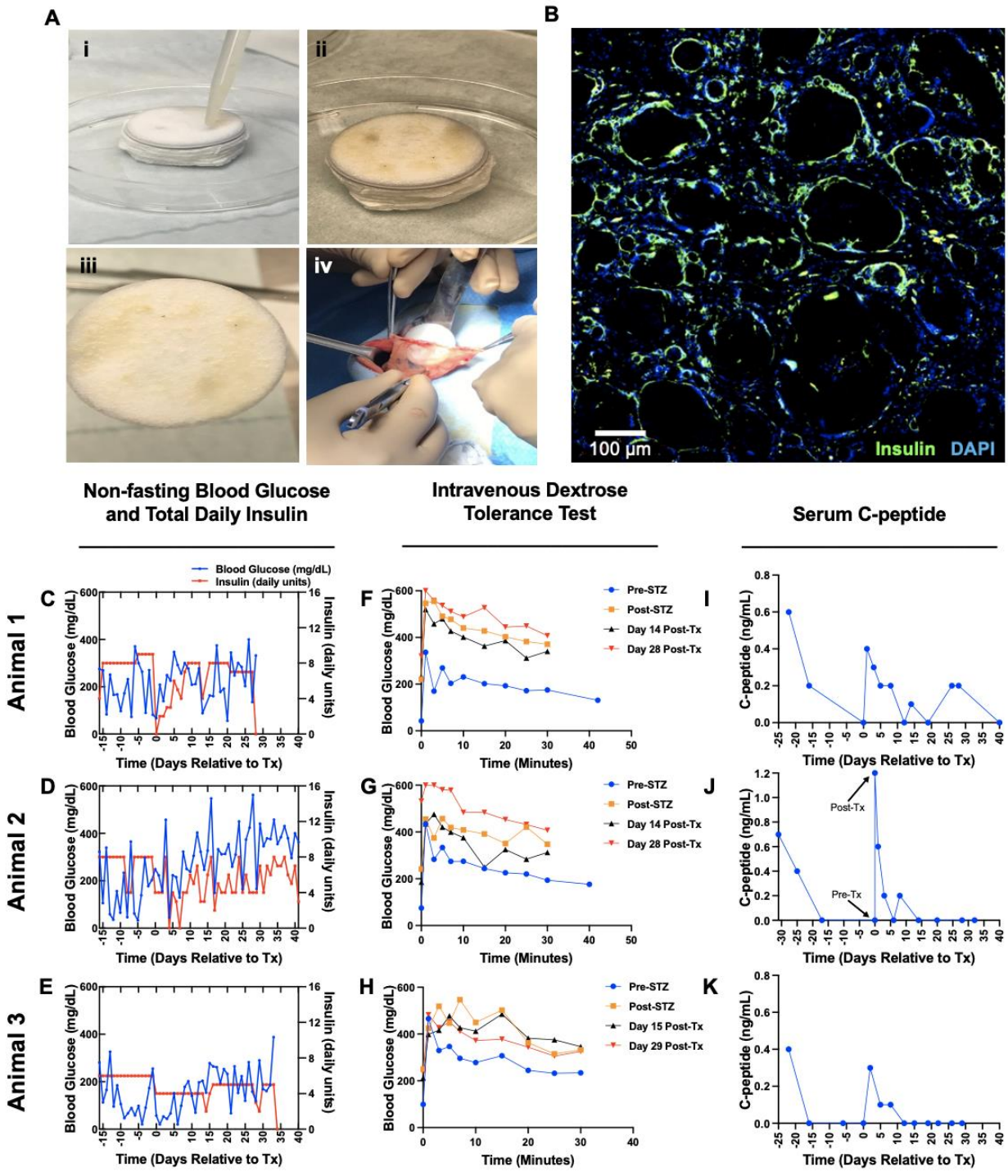


Figure 6.3: Allogeneic islet transplantation on irradiated scaffolds, fabricated with a 1:30 PLG:NaCl ratio, in the omentum of NHPs. (A) (i) Manual seeding of islets on the scaffold. (ii-iii) Scaffold after seeding with islets. (iv) Insertion of a cell-laden scaffold in the omentum. (B) Immunohistochemical staining of an explanted scaffold from

Animal 2, retrieved 41 days after transplantation. Insulin (green) and DAPI (blue) are colocalized throughout the image. Scale bar = 100 μm. (C-E) Timewise blood glucose and total daily exogenous insulin in diabetic NHP recipients. (F-H) IVDTTs were conducted before and after induction of diabetes with STZ, then again at serial timepoints after transplantation. (I-K) Serum C-peptide levels were measured before and after induction of diabetes, then again after transplantation until termination of the study.

6.4.4 Characterization of 1.25:30 PLG:NaCl scaffolds, and successful implementation in mice, suggests adequate compensation for effects of γ irradiation

Due to the fragility of scaffolds observed in our initial NHP studies, we increased the ratio of PLG:NaCl to 1.25:30 w/w and pursued further material characterization. After irradiation, scaffolds remained uniform in appearance (Fig. 6.4A), with interconnected pores of expected size visualized throughout the scaffold when observing cross-sections. Irradiated scaffolds required significantly higher compressive force to deform than non-sterilized scaffolds, implying an increase in stiffness of the scaffold (Fig. 6.4B). As expected, the scaffolds maintained porosity above 0.95 (Fig. 6.4C). The trabecular thickness, i.e. the thickness of PLG branches throughout the scaffold, was nearly identical before and after irradiation, averaging ~15 μm (Fig. 6.4D) with very low variance throughout the porous network.

Additionally, we compared NHP islet transplant outcomes between mice receiving irradiated and non-irradiated scaffolds, fabricated with the increased ratio. Each mouse (n = 2 per condition) received 4,000 IEQ, due to islet quality concerns. There was no significant difference in blood glucose levels over time between conditions, and all mice were euglycemic by day 12 post-transplantation (Figure 6.4E).

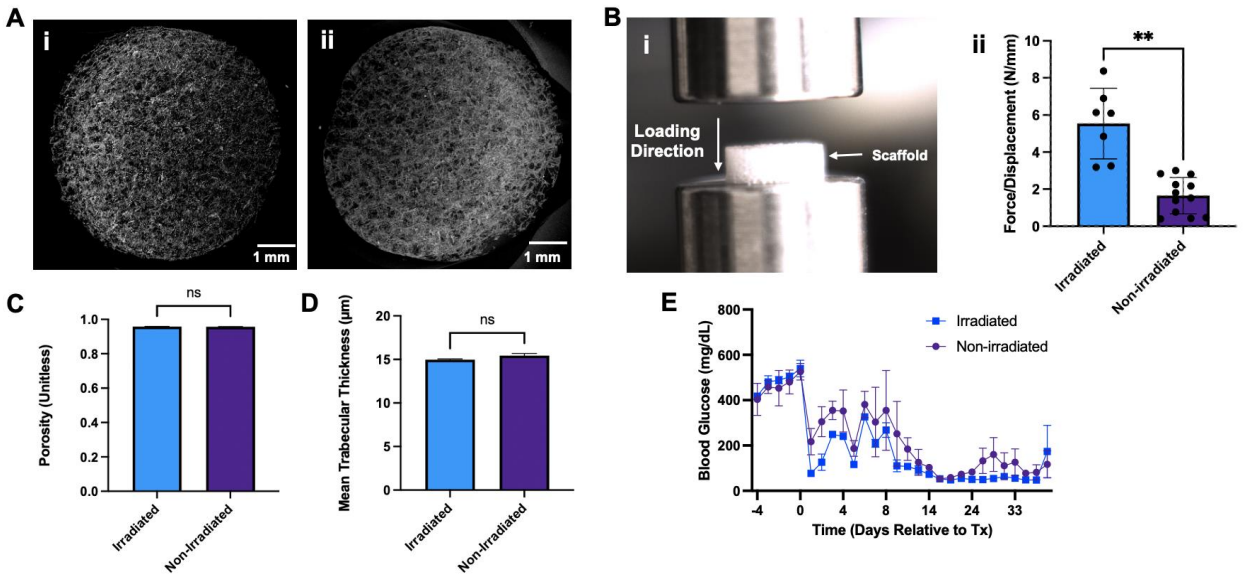


Figure 6.4: Characterization of γ-irradiated scaffolds versus non-sterilized scaffolds, fabricated with a 1.25:30 PLG:NaCl ratio. (A) Representative μCT images of (i) a γ-irradiated scaffold and (ii) a non-irradiated scaffold, visualized using the ImageJ2 3D Viewer. (B) Compressive testing of irradiated and non-irradiated PLG scaffolds. (i) Photograph of testing setup. (ii) The slope of the force-displacement curve was measured over a defined displacement interval (beginning at 0.1 mm) for each specimen, with statistical differences determined using a two-tailed t test with Welch's correction. (C) Porosity of γ-irradiated and non-irradiated scaffolds (n = 3 scaffolds per condition, each measured in triplicate). (D) Mean trabecular thickness (i.e. thickness of interior PLG branches) in γ-irradiated and non-irradiated scaffolds (n = 3 scaffolds per condition, each measured in triplicate).

6.4.5 1.25:30 PLG:NaCl scaffolds do not improve transplant outcomes in a NHP model

After validating the increased PLG:NaCl ratio in mice, we conducted a pilot study of the 1.25:30 PLG:NaCl scaffold in a fourth diabetic NHP transplant recipient (Animal 4). Exogenous insulin administration was adjusted according to Tables 6.2 and 6.3, with this animal being administered the most aggressive regimen. Animal 4 received a 22,083 IEQ/kg dose on one scaffold. Post-transplant, we observed high glucose variability similar to Animals 1-3, and insulin independence was not achieved. The post-transplant IVDTT showed no indications of implant function, and C-peptide was not detected in the blood after day 8 in routine labs.

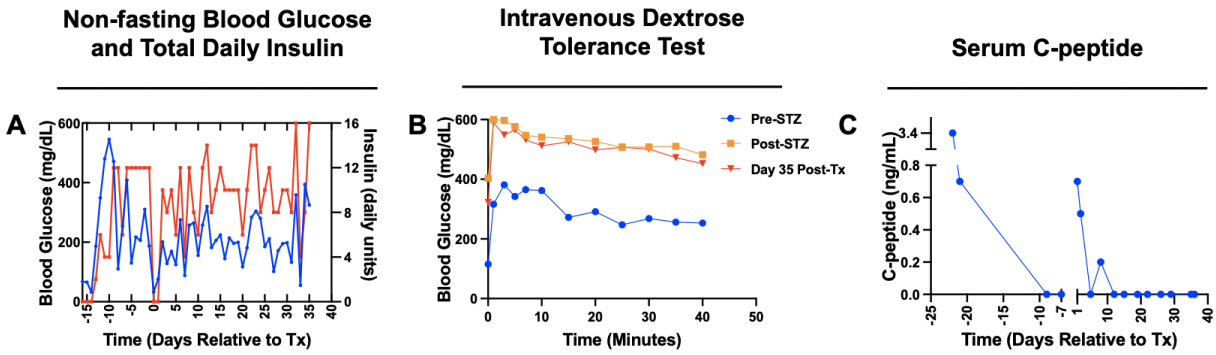


Figure 6.5: Pilot study of 1.25:30 PLG:NaCl scaffold for use in allogeneic islet transplantation in a NHP model. (A) Timewise blood glucose and total daily exogenous insulin. (B) IVDTTs. (C) Serum C-peptide.

6.4.6 Adjustment of the PLG:NaCl ratio compensates for irradiation without compromising islet survival and function

Lastly, we investigated the effects of two intermediate PLG:NaCl ratios in comparison to the 1.25:30 ratio. Four NSG mice per condition received a 2,000 IEQ total dose of human islets on irradiated scaffolds and were monitored for 40 days. If a mouse had two consecutive fasting blood glucose readings above 350 mg/dL, the transplant was considered to be unsuccessful, and the mouse was removed from the study. Mice receiving islets on 1.25:30 scaffolds exhibited the poorest maintenance of glucose below 350 mg/dL, with all four animals eliminated from the study by day 8 (Fig. 6.6C, D). Recipients of 1.05:30 scaffolds also exhibited relatively poor implant survival, though one mouse had complete restoration of euglycemia beginning approximately one week post-transplantation (Fig. 6.6A, D). The 1.15:30 condition achieved the highest implant survival rate, with three out of four mice having maintained glucose below 350 mg/dL for more than a month after transplantation (Fig. 6.6B, D). At least one mouse in this condition achieved euglycemia, with a second mouse exhibiting a trend towards long-term glycemic control (Fig. 6.6B).

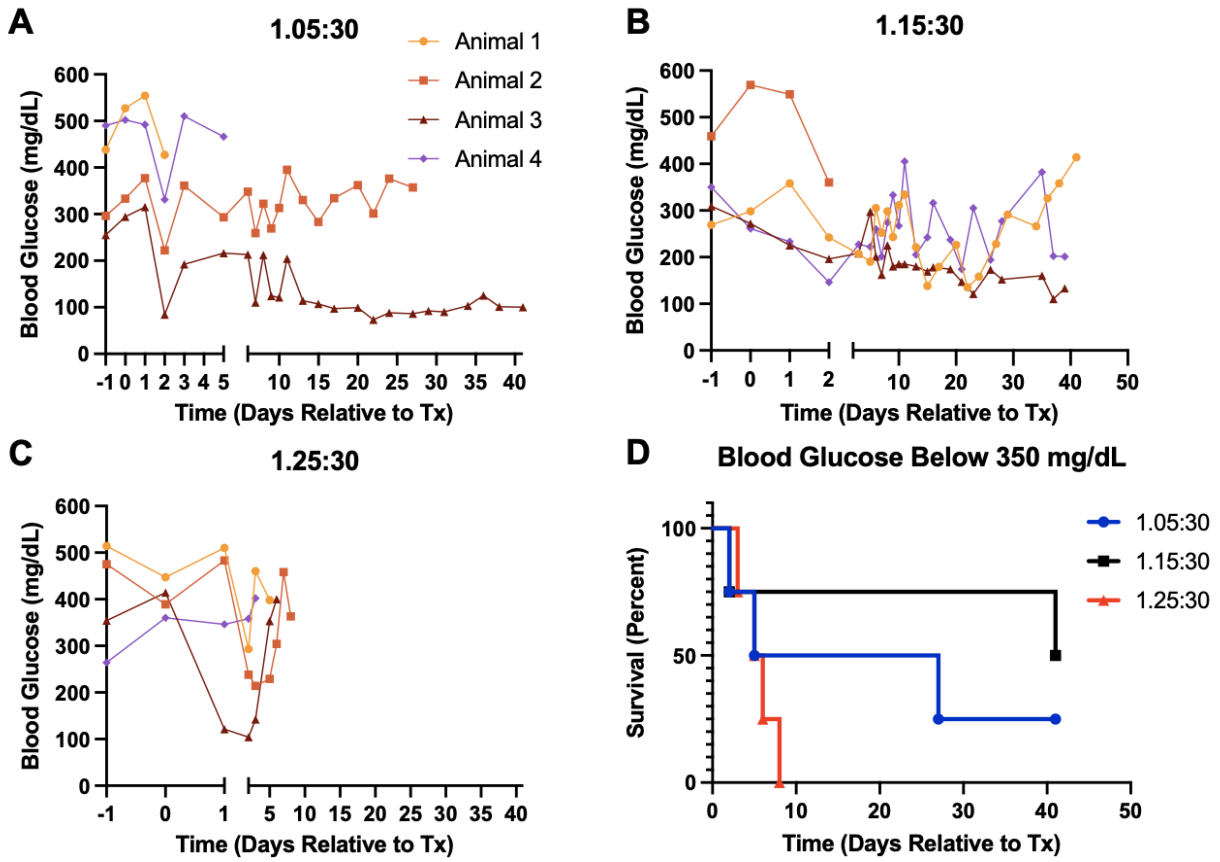


Figure 6.6: Further adjustment of PLG:NaCl ratio for xenogeneic islet transplants on irradiated scaffolds in NSG mice. (A-C) Timewise fasting blood glucose levels for individual mice, which received 2,000 IEQ of human islets on scaffolds fabricated with a (A) 1.05:30, (B) 1.15:30, or (C) 1.25:30 w/w PLG:NaCl ratio (n = 4 per condition). Once a mouse had two consecutive blood glucose readings ≥350 mg/dL, the mouse was eliminated from the study. (D) Reflecting this criterion, all mice are displayed in a Kaplan-Meier survival curve showing maintenance of fasting blood glucose below 350 mg/dL.

6.5 Discussion

The widespread use of T1D cell therapies is hindered by several factors, including the hostility of the intrahepatic site, the requirement of systemic immunosuppression, and the scarcity of donor islets.[5-8,12] We have previously shown that microporous PLG scaffolds seeded with islets can be implanted into the intraperitoneal fat, achieving euglycemia and insulin independence in murine models.[21-26] In this work, we demonstrated that the scaffold is well-tolerated by NHPs and adaptable to preserve islet survival and promote eventual engraftment, without compromising the structural integrity that is impacted by γ irradiation sterilization.

We determined that scaffold size and w/w PLG:NaCl ratio are among the most important

manufacturing parameters impacting scaffold mechanical properties and transplant outcomes. Comparing our experiences implanting scaffolds in mice, pigs, and NHPs across our past and present work, lower aspect ratio (diameter:thickness) improves the sturdiness of scaffolds upon hydration and surgical insertion.[21-26] In this study, during seeding and transplantation, 5 mm scaffolds held together better than 30 mm scaffolds fabricated at the same PLG:NaCl ratio. In pigs, we transplanted islets on 13 mm scaffolds into the omentum without losing scaffold intactness, achieving significant islet survival.[22] However, these comparisons are made before considering the molecular weight-reducing effects of γ irradiation, which we found impacted scaffold integrity in both 5 mm and 35 mm sizes.[27-31] Since increasing the thickness of the scaffold is an undesirable solution due to oxygen diffusion limits in tissue, we instead modulated the PLG:NaCl ratio. We initially showed that increasing the PLG:NaCl ratio to 1.25:30 compensated for the microstructural and macrostructural effects of γ irradiation, with parameters such as trabecular thickness, porosity, and glycemic control unaffected by sterilization (Fig. 4A, C, D, E). Later, after seeing no improved transplant outcomes in the NHP using the increased ratio (Fig. 5), we discovered that a more conservative increase to 1.15:30 best supported implant function in a cohort of mice receiving the same islet dose and product. The simplicity of our manufacturing approach allows us to easily screen for design specifications that facilitate a balance of islet engraftment and structural stability.

In general, and in the context of islet transplantation, the interface between implants and the immune system is distinct between animal models and transplant sites. While we have conducted our murine studies using immunodeficient strains, we procured naive, immunocompetent NHPs and employed systemic immunosuppression for the transplant studies presented here. Our NHP immunosuppression protocol bore several differences compared to other studies in the literature, including a distinct induction regimen (anti-IgG1κ treatment and TNF

inhibition) compared to Deng *et al*. (antithymocyte globulin and anti-CD20) and Berman *et al*.'s 2016 study (antithymocyte globulin and belatacept).[15,19] We also imposed a stricter limit on blood sirolimus concentrations (15 ng/mL) than Deng *et al*. (20 ng/mL).[19] Regardless of the efficacy of various immunosuppression approaches, these not only pose an intrinsic risk to the islets due to drug toxicity, but also do not guarantee complete knockdown of the immune cell compartments involved in fibrosis and adaptive immunity, which are present in the omentum.[8,36] We also did not investigate the inflammatory response to the cellularized scaffolds, which is likely distinct from the response to acellular implants. Ultimately, our non-encapsulating approach will require an immunomodulatory or tolerogenic therapy, such as use of FasL- or PD-L1-functionalized biomaterials or delivery of nanoparticles to reprogram immune cells: an appealing alternative to encapsulation approaches that prevent integration of the islet implant with surrounding tissue.[18,37-41]

In addition to the immunological differences between animal models, there are important physical and metabolic differences. First, cynomolgus monkeys exhibit bipedal behavior, sitting upright and standing on their hindlimbs, which presents distinct mechanical loads on scaffolds *in vivo* compared to the quadrupedal animals we have previously used: mice and pigs.[21-26] Although our porcine study only assessed islet survival on scaffolds in the omentum, rather than therapeutic efficacy, the methodology is illustrative of the elevated metabolic demands of NHPs relative to pigs.[22] We observed effective islet revascularization in the porcine model when seeding at a density of approximately 15 IEQ/mm^3 on 13 mm diameter scaffolds (approximately 4,000 IEQ/scaffold); in the NHP model, if we use Deng *et al*.'s average of 101,500 IEQ/transplant as a benchmark for full insulin independence, we would need three to four 35 mm diameter scaffolds to transplant that number of islets at the optimal seeding density.[19,22] NHPs have been shown to have increased

insulin requirements compared to humans, with NHP islets lowering blood glucose further than human islets at the same dose (Fig. 1).[42] And, while NHPs generally require a dose in the order of 10,000 IEQ/kg to achieve insulin independence with immunosuppression, a dose of approximately 4,000-5,000 IEQ/kg with immunosuppression is adequate in humans.[7,15,19]

An additional considerations in the NHP model is the amount of time required to achieve islet engraftment, endogenous C-peptide production at normal levels (0.51-2.72 ng/mL), and insulin independence. With the exception of Deng *et al.*'s NHP study, Berman *et al.*'s 2009 and 2016 NHP studies and Stice *et al.*'s 2018 clinical study all demonstrated a fall in endogenous C-peptide levels during the peritransplant period, with a late-term increase beginning, at the earliest, approximately one month post-transplant.[14,15,17,19] While we elected to terminate our NHP pilot studies 4-6 weeks after transplant due to near-complete loss of endogenous C-peptide, there is evidence that our transplants survived throughout each study. Endogenous C-peptide was detected in Animal 1 at day 25 post-transplant, despite having a level of 0 ng/mL the prior week (Fig. 3I), and insulin-positive cells were visible on an explanted scaffold 41 days after transplant, despite Animal 2 having no detectable endogenous C-peptide from days 8-41 (Fig. 3G, J).

6.6 Conclusion

In conclusion, the adaptability of microporous PLG scaffolds for islet transplantation in multiple animal models illustrates potential to improve the translatability of successful mouse studies to bipedal species, including NHPs and, ideally, human T1D patients. We demonstrated tolerability of acellular PLG scaffolds in healthy NHPs, and we saw evidence of islet survival via C-peptide measurements and staining of insulin-positive cells, consistent with evidence in the literature that the diabetic NHP model and omentum transplant site require patient, diligent peritransplant management to mitigate cell stress and establish robust, unassisted glycemic control.

While γ irradiation does necessitate a compensatory increase in the PLG:NaCl ratio, our data suggests that a moderate increase to a 1.15:30 w/w ratio can preserve the structural integrity of the scaffold during seeding and transplantation, without negatively affecting the survival and engraftment of the cells. While further studies are needed to investigate long-term gain of function in islets transplanted on scaffolds and validate the intermediate PLG:NaCl ratio in a large animal model, successful completion of these steps would open the door to testing adjunctive immunomodulatory therapies and cell sources that have the potential to expand the population of eligible transplant recipients.[18,37-39,43,44]

6.7 Methods

6.7.1 Scaffold fabrication and sterilization

Scaffolds were fabricated using a salt porogen leaching method, which we have previously described.[32] The PLG:NaCl ratio was adjusted according to Table 1, with scaffold diameters of 5 mm and 35 mm used for murine and NHP studies, respectively. After leaching for 1.5 hours (5 mm scaffolds) or 3 hours (35 mm), scaffolds were air-dried at room temperature for 2 hours and stored in a desiccator prior to shipment for sterilization. When packaging for sterilization, blunt forceps were used to carefully place scaffolds into sterilization pouches. The pouches were labeled, sealed, and placed into a sturdy cardboard box to prevent damage during shipment and handling. Scaffolds allocated for γ irradiation were sent to Steris Industries and received a dose of 43.80-45.09 kGy, for an exposure time of 522 minutes. After sterilization, sealed pouches were returned to the desiccator before further use of the scaffolds.

Irradiated, 35 mm scaffolds used in NHP studies underwent bacteriology and endotoxin testing to ensure compliance with FDA guidelines for implanted medical devices (<0.5 EU/mL if directly in contact with blood, <20 EU/device if not directly in contact with blood).[33]

Table 6.1: Summary of scaffold conditions included in this study. Variable parameters are listed in each column. The range for PLG weight includes the upper 5% error, since having too little PLG is detrimental to scaffold integrity; the range for NaCl weight includes the lower 5% error.

Irradiated? (Y/N)	Diameter (mm)	PLG:NaCl Ratio (w/w)	PLG Weight (mg)	NaCl Weight (mg)	Experiments Conducted
N	5	1:30	2.5-2.625	71.25-75	NHP/Human Islet Comparison
Y	35	1:30	135-141.75	3,848-4,050	NHP Immunoreactivity, NHP Transplants
Y	35 (punched out)	1.25:30	168.75-177.188	3,848-4,050	Murine Irradiated vs. Non-irradiated
N	35 (punched out)	1.25:30	168.75-177.188	3,848-4,050	Murine Irradiated vs. Non-irradiated
Y	35	1.25:30	153.125-160.781	3,492-3,675	NHP Transplants
Y	5	1.05:30	2.625-2.756	71.25-75	PLG:NaCl Ratio Comparison
Y	5	1.15:30	2.875-3.019	71.25-75	PLG:NaCl Ratio Comparison
Y	5	1.25:30	3.125-3.281	71.25-75	PLG:NaCl Ratio Comparison, µCT, Compression
N	5	1.25:30	3.125-3.281	71.25-75	µCT, Compression

Scaffolds were selected for use based on multiple quality benchmarks, including uniform shape and normal dimensions upon visual inspection, no cracking, no presence of wear debris, and buoyancy in water (lack of buoyancy indicates insufficient salt leaching or collapse of pores).

6.7.2 Islet isolation, shipment, and culture

All animal procedures pertinent to NHPs were performed in accordance with the Guidelines for Care and Use of Laboratory Animals of the University of Illinois-Chicago (UIC, PRO21-198 and PRO19-013) and approved by the Animal Ethics Committee (IACUC) of UIC. NHP islets were isolated from the pancreata of deceased cynomolgus monkeys using a collagenase enzyme (Sigma) and cultured overnight by CellTrans, Inc. Samples of the isolated islets were assessed with a viability stain and glucose stimulated insulin secretion (GSIS) assay at CellTrans, Inc. to confirm function. The day after isolation, the islets were shipped overnight to the University of Michigan, where they were resuspended in CMRL 1066 medium (Corning) supplemented with 10% FBS and 1% ITS. Human islets were obtained from Prodo Laboratories Inc, where they underwent viability and purity testing prior to shipment. Upon receipt, they were cultured in PIM(S) media supplemented with PIM(ABS) and PIM(G) (Prodo Labs, cat nos. PIM-S001GMP, PIM-ABS001GMP, PIM-G001GMP). All islets were cultured for a minimum of three hours at 37°C and 5% CO_2 to recover from transport. We performed a second viability test by staining with fluorescein diacetate (in HBSS) and propidium iodide prior to transplantation.

6.7.3 NSG mouse studies

All murine studies were conducted in accordance with institutional guidelines and protocols (PRO00009714) approved by the University of Michigan IACUC. Naive NOD.Cg-Prkdc^{scid}Il2rg^{tm1Wjl}/Szj (NSG) mice (Jackson Laboratories, cat. no. 005557), 6-8 weeks of age, received intraperitoneal (IP) injections of streptozotocin (STZ) (Sigma, cat. no. S0130) at a dose

of 140 mg/kg to induce diabetes. Blood glucose measurements were taken daily via a tail prick until the day of surgery, following a 4-6 hour fast, using an Accu-Chek glucose meter (Roche Diabetes Care, Inc., Indianapolis, IN). Mice with at least two consecutive fasting blood glucose readings above 350 mg/dL and less than a 20% loss in bodyweight compared to the day of injection were considered candidates for transplantation.

On the day of transplantation, islets were aliquoted into 1.5 mL microcentrifuge tubes as 2,000 IEQ or 1,000 IEQ doses (±20%) and placed on ice for transportation from cell culture to the animal surgical suite. Prior to seeding, all scaffolds were sterilized in 70% ethanol and washed twice in deionized water. Following sterilization and washing, scaffolds were dried on sterile gauze. Islets were seeded onto 5 mm scaffolds by distributing the entire contents of one aliquot onto both sides of the scaffold, using large bore 200 µL pipette tips.

Mice were anesthetized using 2% inhaled isoflurane, and they received a 5 mg/kg dose of carprofen subcutaneously (SQ). The abdomen was shaved and sterilized with betadine and ethanol in triplicate. One incision was made along the lower abdomen, and the epididymal fat pads (EFPs) were isolated. One scaffold was wrapped in each EFP before returning the fat to the scrotum (i.e., a mouse receiving 4,000 IEQ received two scaffolds seeded with 2,000 IEQ each, or a mouse receiving 2,000 IEQ received two scaffolds seeded with 1,000 IEQ each). The incision was closed using sutures on the body wall and staples on the skin.

Fasting blood glucose was measured daily for the first 10 days after transplantation, then three times per week for the duration of the studies. Scaffolds were explanted 3-6 weeks after transplantation. Non-survival explants were conducted by removing the fat pads after euthanasia, and survival explants were conducted following the same surgical procedure as transplantation. Once diabetes was reestablished, survival explant recipients were euthanized.

6.7.4 Implantation of acellular, irradiated scaffolds in NHPs to assess immunoreactivity

Three healthy cynomolgus monkeys (*Macaca fascicularis*) were sedated according to approved IACUC protocols. To prepare the surgical site, the fur was shaved from the xiphoid process to the pubis. The site (per-umbilical and right and left upper quadrants) was then sterilized with betadine and isopropyl alcohol in triplicate.

Two irradiated, blank scaffolds (containing no islets) of 35 mm diameter, fabricated with a 1:30 PLG:NaCl ratio, were gently inserted into a pocket of the bursa omentalis, opened with a single incision, using a spatula. Neither the scaffolds nor the incision were secured with sutures, to avoid additional manipulation of the tissue that could cause fibrotic scarring. Animals were administered intravenous (IV) hydromorphone (0.1 mg/kg) and lidocaine (1.5-3.0 mg/kg/h) during surgery as needed. Bupivicaine (1 mg/kg, SQ) was administered at the end of the procedure before closure.

The bursa omentalis was removed from each recipient 30 days after implantation and examined for signs of fibrosis and degradation of the scaffolds. Scaffold explants were isolated from the adipose tissue and either fixed in formalin for paraffin sectioning or flash frozen in isopentane and embedded in optimal cutting temperature (OCT) compound for cryosectioning. Sectioned tissues were stained for α-smooth muscle actin (α-SMA), a fibroblast marker; CD11b, a marker for neutrophils, monocytes, macrophages, and natural killer cells; and CD8, a marker for cytotoxic T cells. DAPI was used as a nuclear counterstain.

6.7.5 Allogeneic islet transplantation in diabetic NHPs

In four separate pilot studies, a diabetic cynomolgus monkey received an allogeneic islet transplant via irradiated scaffolds implanted in the omentum. Each recipient was administered 100 mg/kg STZ (Teva Parenteral Medicines, Inc., Tel Aviv, Israel) via IV 15-24 days prior to surgery

to induce diabetes. Animals received 150-200 mL of IV saline pre-STZ and 250 mL of IV saline post-STZ. Once diabetes was established, animals received long-acting exogenous insulin via SQ injection (Lantus 100 units/mL, Sanofi, Paris, France) throughout the duration of the study. With each subsequent animal, the insulin regimen was adjusted according to Tables 2-3.

Candidacy for surgery was determined by measuring bodyweight and serum C-peptide before STZ (e.g., days -22, -21, and -16) and after STZ (days -14, -9, -7, -5, and -1). In addition, fasted intravenous dextrose tolerance tests (IVDTTs) were conducted before and after STZ, during which blood glucose and C-peptide were measured at serial timepoints up to 40 minutes after the dextrose challenge. Blood glucose was monitored using either an Accu-Chek glucose meter or the FreeStyle Libre 2 Continuous Glucose Monitor (Abbott Diabetes Care, Alameda, CA), with nonfasting readings taken every morning and evening in addition to those taken during the IVDTTs.

Allogeneic islet transplant recipients were systemically immunosuppressed with tacrolimus (Prograf, Astellas Pharma, Inc., Northbrook, IL) and sirolimus (Rapamune, LC Laboratories, Woburn, MA). Immunosuppression was initiated approximately 1-2 weeks prior to transplantation with starting doses of 0.025 mg/kg tacrolimus and 0.020 mg/kg sirolimus, twice per day. Blood draws were performed two times per week to verify therapeutic concentrations of tacrolimus (4-6 ng/mL, measured by homogeneous particle-enhanced turbidimetric immunoassay) and sirolimus (10-15 ng/mL, measured by chemiluminescent microparticle immunoassay). Basiliximab (Simulect, Novartis, East Hanover, NJ) was administered as follows: 5 mg IV on Day 0, 25 mg IV on Day 14 and Day 28 post-transplant. Etanercept (Enbrel, Amgen, Thousand Oaks, CA) was administered as follows: 50 mg IV on Day 0, then 25 mg SQ on Day 3, Day 7±1, and Day 10±1.

Table 6.2: Summary of insulin regimens used for each NHP transplant. *See Table 6.3.

Animal #	Days Administered (Relative to Tx)	Morning Dose (Units)	Evening Dose (Units)
1	-16 to -6	4	4
	-5 to -1	5	4
	0 to 8 (morning)	Sliding Scale*	Sliding Scale*
	8 (evening) to 21	4	4
	21 to 27	4	3
2	-21 to -1	4	4
	0 to 41	Sliding Scale*	Sliding Scale*
3	-19 to -1	3	3
	0 to 15	2	2
	16 to 33	3	2
4	-13 to 0	4-6	0-6
	0 to 35	Sliding Scale*	Sliding Scale*

Table 6.3: Sliding scales used for post-transplant insulin administration for Animals 1, 2, and 4.

Animal 1		Animal 2		Animal 3	
BG (mg/dL)	Insulin (Units)	BG (mg/dL)	Insulin (Units)	BG (mg/dL)	Insulin (Units)
≤199	0	≤199	0	≤49	0
200-299	2	200-299	2	50-199	4
300-399	4	300-399	3	200-299	6
400-499	6	≥400	4	≥300	8

≥500	8	–	–	–	–

NHP islets were isolated, cultured, aliquoted, and seeded onto 35 mm diameter, irradiated scaffolds following a similar procedure to as in the NSG mouse transplants. For Animal 1, a scaffold was seeded with 33,024 IEQ (5,326 IEQ/kg dose, taken from four donors) using a custom, vacuum-driven seeding device. For Animal 2 (9,409 IEQ/kg, six donors), Animal 3 (34,186 IEQ/kg, eight donors), and Animal 4 (22,083 IEQ/kg, four donors), islets were seeded manually using a large bore pipette tip. Animals 1, 2, and 3 received islets on scaffolds fabricated with a 1:30 w/w PLG:NaCl ratio, and Animal 4 received islets on a scaffold fabricated with a 1.25:30 w/w PLG:NaCl ratio.

On the day of surgery, each transplant recipient was sedated and anesthetized per IACUC protocols and in the same manner as the acellular scaffold transplant, and Meloxicam SR (0.6 mg/kg, SQ) was administered prior to surgery. Under aseptic conditions, a midline incision (6-8 cm) was created using a sterile scalpel blade, before assessment of the intraperitoneal cavity. A 6 cm incision was made in the omentum. The omentum was then held with sterile surgical graspers or forceps while inserting the scaffold in between the layers of the omentum. No additional manipulation was needed to close the omentum incision. The abdominal incisions were closed in 3 layers using 3-0 Vicryl for the abdominal wall and subcutaneous layer, and 4-0 Vicryl for the skin (subcuticular). Buprenorphine (0.2 mg/kg, SQ) was administered immediately post-surgery.

After transplant, blood glucose was monitored twice daily, in the same manner as before transplant. Long-acting exogenous insulin therapy was continued as shown in Tables 2-3. Bodyweight and serum C-peptide were measured on the day of transplant (day 0) and twice per week thereafter.

Each animal was terminated approximately 28-40 days (~4-6 weeks) after transplant. Each monkey was sedated and anesthetized as previously described, administered 500 U/kg heparin via IV injection 10 minutes prior to euthanasia, and euthanized with an overdose of sodium pentobarbital (1 mL/10 lb). Afterward, a necropsy was performed. The entire omentum was removed, with scaffolds being retrieved from Animal 2 for cryosectioning. Tissue sections were stained for insulin and DAPI.

6.7.6 Comparison of non-sterilized and γ irradiated scaffolds with μCT

Acellular scaffolds of 5 mm diameter, fabricated with a 1.25:30 PLG:NaCl ratio and separated into irradiated and non-irradiated conditions, were imaged using a Nanotom M (Phoenix X-ray, Waygate Technologies USA, Houston, TX). Specimens were immobilized inside a plastic tube for scanning. The X-ray tube was fitted with a diamond-coated tungsten target and 0.254 mm aluminum filter and powered to 65 kV and 250 μA. Spot size was set to zero. Imaging was done at 4 μm voxel size using an exposure time of 500 ms, with three frames averaged and one skipped for each rotation. The sample stage rotated through 360 degrees and collected 2,000 images per scan. Image acquisition and reconstruction of raw data were performed using Phoenix Datos|x 2 version 2.6.1 (Phoenix X-ray, Waygate Technologies USA, Houston, TX).

Raw data files for each individual scaffold were imported into ImageJ2 (v. 2.14.0) as z-stacks and cropped to isolate the scaffold material and interior pores, removing the exterior space and plastic tubing used as a fixture. The BoneJ2 plugin was used for image analysis, treating PLG branches within the scaffold similarly to how trabecular bone is treated in osseous specimens.[34,35] Representative, 3D μCT images were developed using the 3D Viewer plugin. Images were segmented into PLG and background using *Plugins→BoneJ→Optimize Threshold*, then porosity was calculated as the ratio of empty space (non-PLG voxels) to total volume using

Plugins→BoneJ→Volume Fraction. Additionally, we calculated the mean thickness of the PLG branches within each scaffold using *Plugins→BoneJ→Trabecular Thickness*. Three scaffolds were imaged for the irradiated and non-irradiated conditions, with measurements of porosity and mean branch thickness done in triplicate, using three distinct regions of interest.

6.7.7 Compressive testing of irradiated and non-irradiated scaffolds

Irradiated and non-irradiated scaffolds were subjected to compressive loading using a Mach-1 Mechanical Testing System (Biomomentum, Inc., Laval, QC, CA) set up on an anti-vibration table. Scaffolds were transferred from sterilization pouches onto a steel compression platen of 9.53 mm diameter and centered to prevent torque during compression. An upper platen of the same diameter was lowered with a 0.005 mm/s ramp rate to establish contact with the sample (a load of 0.1015 N). Upon contact, the platen was raised to reach 2x the load resolution of the load cell, and relative displacement was set to zero. After 30 s to allow for equilibration, the scaffold was compressed between the parallel platens at a displacement rate of 0.005 mm/s until failure or a maximum displacement of 0.5 mm.

Data acquisition was performed using the Mach-1's mating software. For each scaffold, the slope of the force-displacement curve ($\Delta F/\Delta l$) was measured as an average across the linear region of the graph, typically beginning around a displacement of 0.1 mm.

6.7.8 Statistical analysis

All statistical analyses were conducted using Prism 9.1.0 (GraphPad Software, Inc.). Statistical differences were determined using a two-tailed t test, unless otherwise noted. A significance level $\alpha = 0.05$ was used for all studies. Significance is denoted as * $p \leq 0.05$, ** $p \leq 0.01$, *** $p \leq 0.001$, or **** $p \leq 0.0001$. Values are reported as the mean ± standard error of the

mean (SEM), unless otherwise noted. *n* denotes the number of biological replicates (animals) or the number of scaffolds analyzed (characterization studies).

6.8 Acknowledgements

This work was supported by NIH grants 1R01DK121462 and 1R01CA272940-01A1, JDRF, the JDRF Center of Excellence at the University of Michigan, and the Caswell Diabetes Center.

J.L.K. was supported by the National Science Foundation Graduate Research Fellowship under Grant No. DGE-2241144.

6.9 Supplemental information

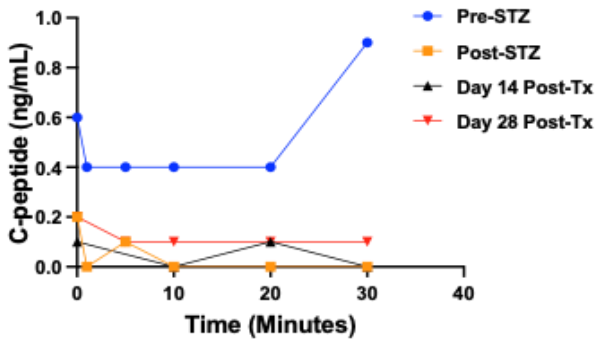


Figure 6.7: Serum C-peptide measurements taken during IVDTTs for Animal 1.

6.10 References

1. Gregory, G. A. *et al.* Global incidence, prevalence, and mortality of type 1 diabetes in 2021 with projection to 2040: A modelling study. *The Lancet Diabetes & Endocrinology* **10,** 741–760 (2022).
2. Hirsch, I. B. Pathogenesis of type 1 diabetes. (2022).
3. Joish, V. N. et al. Estimation of annual health care costs for adults with type 1 diabetes in the United States. Journal of Managed Care & Specialty Pharmacy 26, 311–318 (2020).
4. CGM and time in range. American Diabetes Association (2023). Available at: https://diabetes.org/tools-support/devices-technology/cgm-time-in-range#:~:text=Most%20people%20with%20type%201,Some%20may%20have%20different%20targets. (Accessed: 4th August 2023)
5. Parums, D. V. Editorial: First Regulatory approval for allogeneic pancreatic islet beta cell infusion for adult patients with type 1 diabetes mellitus. *Medical Science Monitor* **29,** (2023).
6. Qi, M. *et al.* Five-year follow-up of patients with type 1 diabetes transplanted with Allogeneic Islets: The UIC experience. *Acta Diabetologica* **51,** 833–843 (2014).
7. Czarnecka, Z., Dadheech, N., Razavy, H., Pawlick, R. & Shapiro, A. M. The current status of Allogenic Islet Cell Transplantation. *Cells* **12,** 2423 (2023).

8. Naziruddin, B. *et al.* Evidence for instant blood-mediated inflammatory reaction in clinical autologous islet transplantation. *American Journal of Transplantation* **14,** 428–437 (2014).
9. Williams, J. *et al.* Over ten-year insulin independence following single allogeneic islet transplant without T-cell depleting antibody induction. *Islets* **10,** 168–174 (2018).
10. A Safety, Tolerability, and Efficacy Study of VX-880 in Participants with Type 1 Diabetes. *ClinicalTrials.gov* (2023). Available at: https://classic.clinicaltrials.gov/ct2/show/NCT04786262?term=VX-880&draw=2&rank=1. (Accessed: 2nd July 2024)
11. A Safety, Tolerability, and Efficacy Study of Sernova's Cell Pouch for Clinical Islet Transplantation. *ClinicalTrials.gov* (2023). Available at: https://clinicaltrials.gov/study/NCT03513939?intr=Sernova%20Cell%20Pouch&rank=1. (Accessed: 2nd July 2024)
12. Brusko, T. M., Russ, H. A. & Stabler, C. L. Strategies for durable β cell replacement in type 1 diabetes. *Science* **373,** 516–522 (2021).
13. Arifin, D. R., Valdeig, S., Anders, R. A., Bulte, J. W. M. & Weiss, C. R. Magnetoencapsulated Human Islets xenotransplanted into swine: A comparison of different transplantation sites. *Xenotransplantation* **23,** 211–221 (2016).
14. Berman, D. M. *et al.* Long-term survival of nonhuman primate islets implanted in an omental pouch on a biodegradable scaffold. *American Journal of Transplantation* **9,** 91– 104 (2009).
15. Berman, D. M. *et al.* Bioengineering the endocrine pancreas: Intraomental islet transplantation within a biologic resorbable scaffold. *Diabetes* **65,** 1350–1361 (2016).
16. Baidal, D. A. *et al.* Bioengineering of an intraabdominal endocrine pancreas. *New England Journal of Medicine* **376,** 1887–1889 (2017).
17. Stice, M. J., Dunn, T. B., Bellin, M. D., Skube, M. E. & Beilman, G. J. Omental pouch technique for combined site islet autotransplantation following total pancreatectomy. *Cell Transplantation* **27,** 1561–1568 (2018).
18. Lei, J. *et al.* FasL microgels induce immune acceptance of islet allografts in nonhuman primates. *Science Advances* **8,** (2022).
19. Deng, H. *et al.* Bioengineered omental transplant site promotes pancreatic islet allografts survival in non-human primates. *Cell Reports Medicine* **4,** 100959 (2023).
20. Hunckler, M. D. & García, A. J. Engineered biomaterials for enhanced function of insulin-secreting β-cell organoids. *Advanced Functional Materials* **30,** (2020).
21. Blomeier, H. *et al.* Polymer Scaffolds as Synthetic Microenvironments for Extrahepatic Islet Transplantation. *Transplantation* (2006) doi:10.1097/01.tp.0000231708.19937.21.
22. Gibly, R. F. *et al.* Extrahepatic islet transplantation with microporous polymer scaffolds in syngeneic mouse and allogeneic porcine models. *Biomaterials* **32,** 9677–9684 (2011).
23. Gibly, R. F., Zhang, X., Lowe, W. L. & Shea, L. D. Porous scaffolds support extrahepatic human islet transplantation, engraftment, and function in mice. *Cell Transplantation* **22,** 811–819 (2013).
24. Kasputis, T. *et al.* Microporous polymer scaffolds for the transplantation of embryonic stem cell derived pancreatic progenitors to a clinically translatable site for the treatment of type I diabetes. *ACS Biomaterials Science & Engineering* (2018). doi:10.1021/acsbiomaterials.7b00912
25. Youngblood, R. L., Sampson, J. P., Lebioda, K. R. & Shea, L. D. Microporous scaffolds support assembly and differentiation of pancreatic progenitors into β-cell clusters. *Acta Biomaterialia* **96,** 111–122 (2019).

26. Bealer, E. *et al.* Extrahepatic transplantation of 3D cultured stem cell-derived islet organoids on microporous scaffolds. *Biomaterials Science* **11,** 3645–3655 (2023).
27. Krug, N., Zarges, J.-C. & Heim, H.-P. Influence of ethylene oxide and gamma irradiation sterilization processes on the properties of poly-L-lactic-acid (PLLA) materials. *Polymers* **15,** 3461 (2023).
28. Montanari, L. *et al.* Gamma irradiation effects on poly(dl-lactictide-co-glycolide) microspheres. *Journal of Controlled Release* **56,** 219–229 (1998).
29. Dorati, R. *et al.* γ-irradiation of PEGd,lPLA and PEG-PLGA multiblock copolymers: I. Effect of irradiation doses. *AAPS PharmSciTech* **9,** (2008).
30. Makadia, H. K. & Siegel, S. J. Poly lactic-co-glycolic acid (PLGA) as biodegradable controlled drug delivery carrier. *Polymers* **3,** 1377–1397 (2011).
31. Keles, H., Naylor, A., Clegg, F. & Sammon, C. Investigation of factors influencing the hydrolytic degradation of single PLGA microparticles. *Polymer Degradation and Stability* **119,** 228–241 (2015).
32. Nof, M. & Shea, L. D. Drug-releasing scaffolds fabricated from drug-loaded microspheres. *Journal of Biomedical Materials Research* **59,** 349–356 (2002).
33. U.S. Food and Drug Administration. Guidance for industry: Pyrogen and endotoxins testing: Questions and answers. *U.S. Food and Drug Administration* (2012). Available at: https://www.fda.gov/regulatory-information/search-fda-guidance-documents/guidance-industry-pyrogen-and-endotoxins-testing-questions-and-answers. (Accessed: 12th March 2024)
34. Doube, M. *et al.* BoneJ: Free and extensible bone image analysis in ImageJ. *Bone* **47,** 1076–1079 (2010).
35. Domander, R., Felder, A. A. & Doube, M. BoneJ2 - refactoring established research software. *Wellcome Open Research* **6,** 37 (2021).
36. Meza-Perez, S. & Randall, T. D. Immunological functions of the omentum. *Trends in Immunology* **38,** 526–536 (2017).
37. Coronel, M. M. *et al.* Immunotherapy via PD-L1-presenting biomaterials leads to long-term Islet graft survival. *Science Advances* **6,** (2020).
38. Li, F. *et al.* FAS ligand-modified scaffolds protect stem cell derived β-cells by modulating immune cell numbers and polarization. *ACS Applied Materials & Interfaces* **15,** 50549–50559 (2022).
39. Li, F. *et al.* Membrane-coated nanoparticles for direct recognition by T cells. *Biotechnology and Bioengineering* **120,** 767–777 (2022).
40. De Toni, T. *et al.* Parallel Evaluation of polyethylene glycol conformal coating and alginate microencapsulation as immunoisolation strategies for pancreatic islet transplantation. *Frontiers in Bioengineering and Biotechnology* **10,** (2022).
41. Bochenek, M. A. *et al.* Alginate encapsulation as long-term immune protection of allogeneic pancreatic islet cells transplanted into the omental bursa of macaques. *Nature Biomedical Engineering* **2,** 810–821 (2018).
42. Casu, A. *et al.* Metabolic aspects of pig-to-monkey (macaca fascicularis) islet transplantation: Implications for translation into clinical practice. *Diabetologia* **51,** 120–129 (2007).
43. Hogrebe, N. J., Augsornworawat, P., Maxwell, K. G., Velazco-Cruz, L. & Millman, J. R. Targeting the cytoskeleton to direct pancreatic differentiation of human pluripotent stem cells. *Nature Biotechnology* **38,** 460–470 (2020).

44. Hogrebe, N. J., Maxwell, K. G., Augsornworawat, P. & Millman, J. R. Generation of insulin-producing pancreatic β cells from multiple human stem cell lines. *Nature Protocols* **16,** 4109–4143 (2021).

Chapter 7 Conclusion and Future Directions

7.1 Summary of findings and significance

The work in this dissertation demonstrates the prognostic and therapeutic potential of polymer scaffolds in type 1 diabetes (T1D). The increasing incidence od T1D necessitates advancements in prevention, as well as cell replacement therapies for the existing patient population. In this work, we addressed both sides of this clinical need, with polymeric scaffolds acting as a disease monitor when transplanted subcutaneously and acellularly, and acting as a protective delivery platform when seeded with cells and transplanted into the epididymal fat pads. Additionally, we demonstrate an engineering approach to improve the quality of cells being delivered, utilizing a metabolic network reconstruction to model *in vitro* treatment of stem cell derived islets (sc-islets).

In chapters three and four we demonstrate the utility of poly(e-caprolactone) (PCL) scaffolds as an immunological niche (IN) for T1D monitoring. In order to effectively prevent disease progression, the disease time course needs to be well understood. The current stage designation of T1D includes dysglycemia as a marker for stage 2, which precedes clinical diagnosis, or stage 3. In chapter three we show that the IN delineates healthy from diseased groups in two murine T1D models, and in chapter four we show that longitudinal monitoring further elucidates risk and progressor status. These findings improve on current monitoring standards, as the signature identifying -7 week versus -5 weeks from symptom onset happens prior to dysglycemia. This signature could act as an additional staging tool, with autoantibody positivity and -7 week signature scores corresponding to a stage 1a, and the -5 week signature score

corresponding to a still asymptomatic, but more progressed stage 1b. This distinction could be used to time immunotherapy treatment without relying on dysglycemia, which may preserve a greater portion of the native islets. The generation of a signature to distinguish progressors from non-progressors also has the potential to improve monitoring for disease. As autoantibody positivity does not progress to symptomatic disease in all patients, being able to identify that sub-population at an earlier time would lessen the burden of continuous monitoring for people who don't need it.

In chapter five, we develop a metabolic network model capable high throughput screening of factors to improve maturation of sc-islets. The metabolic immaturity of current sc-islets requires an *in vivo* maturation period following *in vitro* culture, which delays therapeutic efficacy of these cells at a time when they are also under stress from the immune reaction to transplant. The field needs a metabolically mature cell source with comparable efficacy to native islets, but large library screens of drug or genetic targeting agents is infeasible in cultures that are time and resource intensive. Our metabolic network reconstruction captures the metabolic flux discrepancies between mature and sc-islets, and has been validated against *in vitro* treatments. We identified a new target for metabolic maturation, NMNAT3, via a 443 gene knock-in screen, and a pilot *in vitro study* of this target suggests that sc-islets treated based on our modeling results demonstrate improved ATP metabolism. Developing a functional metabolic model will expedite the development of more mature sc-islets by identifying the best targets for treatment.

In chapter six, we demonstrate tunability of microporous polymer scaffolds for use in islet transplantation. Current protocols for islet transplantation use portal vein injection as the delivery method. This approach leads to an immediate inflammatory response which results in significant cell death, as well as irretrievability of the transplanted material. In our studies, we demonstrate

that acellular irradiated scaffolds have a minimal immune response in an immune competent non-human primate model, and that restoration of euglycemia in immune deficient mice differs based on polymer to salt ratio. These studies offer a framework for manufacturing considerations in translatability of scaffolds for islet delivery. The added irradiation step needed to meet sterility requirements for NHP studies had unexpected effects on transplant efficacy. These results demonstrate the need for tunability in cell delivery platforms to meet the needs of various models.

Taken together, the results of this dissertation demonstrate the abilities of microporous polymer scaffolds as a platform to enhance disease monitoring and treatment of T1D. Investigating uses in both treatment and monitoring demonstrate the scaffolds capacity for impact in both the at-risk and active disease populations.

7.2 Future directions

7.2.1 Gene signatures to inform immunotherapy administration

A treatment study to identify the signature at the optimal timing of treatment is needed to establish signature genes as biomarkers for treatment administration. Current treatments have a window of effectiveness, in which the autoimmune response is present, and the treatment acts to attenuate the response, but it is not so progressed that there is not a sufficient islet mass to preserve function. Our gene signatures precede dysglycemia, which decreases the risk of losing a critical islet mass from waiting too long, but this earlier indicator for treatment does have the risk of being too early. Additional work needs to be done to identify the earliest time point at which treatment based on the progressor signature effectively prevents disease progression.

In addition to treatment timing with existing immunotherapies, treatment studies targeting the signature genes may identify new therapies for disease prevention. Of particular interest is Erdr1, which has a roll T cell and NK cell activation and macrophage polarization and is

upregulated in the -5 week progressor signature. Mechanistic studies into whether this gene has potential as an immunomodulatory target could lead to novel immunotherapies that attenuate disease onset by targeting immune cell activation rather than depletion.

7.2.2 Non-progressor signature as targets for T1D prevention

Similarly to how the progression signature may offer insights into mechanisms for delaying disease onset, the non-progressor signature should be studied to determine if targeting these gene offers a protective effect to the at-risk population. A study targeting F2rl1 receptors on immune cells could be conducted to determine if systemic depletion of F2rl1 activity is disease protective, or if losing the protective effect on β cells locally leaves cells vulnerable to alternative stressors. Sox11 as a potentially regenerative target could also be investigated as a therapeutic in patients who received treatment after developing dysglycemia. In this case, the existing immunotherapy approaches would still be used to delay disease progression, but Sox11 treatment of the remaining cells could promote a regenerative phenotype to compensate for the cells lost pre-treatment.

7.2.3 Early differentiation interventions in metabolic network models

These studies focused on modeling the maturation of our final differentiation product, sc-islets. The main factors governing stages 1-5 of differentiation are designed to direct sc-islets down the β cell lineage. It is possible that in addition to directing cell identity, addition of metabolic factors at early stages could result in more metabolically mature sc-islets. Screening for metabolic maturation factors at early time points has the added challenge of ensuring any treatments do not reduce differentiation efficiency. To account for this, stage specific modeling needs to account for both metabolic, and cell identity factors when evaluating treatment efficacy for improving sc-islet outcomes.

7.2.4 Modeling of metabolic stress conditions

Future studies should develop metabolic models for islets in stressed conditions. This could be done by collecting transcriptomic data for sc-islets from hyperglycemic *in vitro* cultures, sc- or mature islets from the early stages of transplantation, or NOD mouse islets in the early stages of insulitis, to model the metabolic states of type 2 diabetes, transplant alloimmunity, and autoimmunity respectively. Each of these metabolic reconstructions would model a condition relevant to cell replacement therapy or disease prevention, and would serve as a screening tool for interventions to improve metabolic function under stress.

7.2.5 Metabolic network analysis in other disease models

While cellular metabolism is essential to the maturation and function of mature islets, metabolic dysregulation is not specific to islets or T1D. Implementing metabolic network modeling in other disease models has the ability to inform metabolic targeting to improve impaired metabolism, as is the case with sc-islets, or to deplete metabolic function of harmful cells. FK866 for example, shows potential for improving sc-islet metabolism in our models, but it was originally identified as a cancer therapy from its ability to induce apoptosis by depleting NAD^+ reserves in cancer cells. There are many disease models, autoimmune and otherwise, that could benefit from metabolic targeting. Disease specific metabolic reconstructions offer a strategy for high throughput screening of treatment models, without having to experimentally investigate all options.

Over 8 million people globally live with Type 1 Diabetes (T1D) with incidence on the rise. Despite advancements in glucose management with the invention of insulin pumps and continuous glucose monitors, burden of care and complication risk remain high. Promising treatments for both prevention and cell replacement have been developed, but improvements are needed to improve efficacy and maintenance of long-term euglycemia.